

Genetic architecture of craniofacial shape in the house mouse: a genetic and morphological perspective

Dissertation

zur Erlangung des Doktorgrades
der Mathematisch-Naturwissenschaftlichen Fakultät
der Christian-Albrechts-Universität zu Kiel

vorgelegt von

Luisa Fernanda Pallares Amaya

Plön, June, 2015

| | |
|-----------------------------|------------------------------|
| Erstgutachter: | Prof. Dr. Diethard Tautz |
| Zweitgutachter: | Prof. Dr. Thomas C. G. Bosch |
| Tag der mündlichen Prüfung: | 27.08.2015 |
| Zum Druck genehmigt: | 27.08.2015 |

gez. Prof. Dr. Wolfgang Duschl (Dekan)

Contents

| | |
|--|----|
| Summary of the dissertation | 6 |
| Zusammenfassung der Dissertation | 7 |
| Introduction | 9 |
| A genetic theory of adaptation | 9 |
| A theory of morphological evolution..... | 10 |
| The vertebrate cranium | 12 |
| Developmental origin of the craniofacial skeleton..... | 13 |
| Types of ossification..... | 13 |
| Genetic vs non-genetic determination of cranial shape | 14 |
| Morphometrics | 15 |
| Traditional morphometrics | 15 |
| Geometric morphometrics | 16 |
| Genetics of craniofacial shape | 17 |
| Genetic architecture of adaptive morphological differences..... | 18 |
| Lessons from humans | 19 |
| The mouse..... | 19 |
| Evolutionary history..... | 20 |
| Genetic basis of craniofacial variation in the mouse..... | 21 |
| The mandible | 21 |
| The skull | 22 |
| Overview of the dissertation | 24 |
| Chapter One..... | 25 |
| Use of a natural hybrid zone for genome-wide association mapping of craniofacial traits in the house mouse | 25 |
| Introduction | 25 |
| Methods..... | 27 |
| Ethical statement | 27 |
| Mapping population | 27 |
| Shape phenotyping | 28 |
| Size | 29 |

| | |
|--|----|
| Genotyping..... | 29 |
| Association mapping..... | 30 |
| Permutations | 30 |
| LD analysis..... | 31 |
| Chromosomal partitioning of variance | 31 |
| Regression of shape on genetic admixture | 32 |
| Morphological differences between house mouse subspecies | 32 |
| Data..... | 32 |
| Results..... | 33 |
| Phenotypic variation | 33 |
| Genetic architecture | 34 |
| Genomic regions associated with shape | 35 |
| Discussion..... | 40 |
| Natural hybrid zone | 40 |
| Genetic architecture of craniofacial shape variation | 41 |
| Candidate genes..... | 44 |
| Conclusions | 45 |
| Supplementary Figures | 46 |
| Supplementary Tables | 51 |
| Chapter two | 54 |
| Mapping of craniofacial traits in outbred mice identifies major developmental genes involved in craniofacial formation | 54 |
| Introduction | 54 |
| Methods..... | 56 |
| Mapping population | 56 |
| Shape phenotyping | 57 |
| Size phenotyping..... | 58 |
| Genotyping..... | 58 |
| Association mapping..... | 58 |
| Significance of SNP associations | 60 |
| Overlap with previous studies | 60 |
| Chromosomal partition of the variance..... | 60 |

| | |
|---|-----|
| Results..... | 61 |
| Heritability of individual PCs..... | 61 |
| Heritability of craniofacial shape and size..... | 63 |
| Genomic regions associated with craniofacial size and shape..... | 63 |
| Chromosomal partition of the variance..... | 65 |
| Candidate genes..... | 67 |
| Discussion..... | 67 |
| The genetic architecture of craniofacial traits..... | 69 |
| Heritability of morphological traits..... | 70 |
| Candidate genes..... | 71 |
| Conclusion..... | 72 |
| Supplementary Figures..... | 74 |
| Supplementary Tables..... | 82 |
| Chapter Three..... | 87 |
| Morphological transitions along a hybridization gradient: implications for the genetic architecture of shape variation..... | 87 |
| Introduction..... | 87 |
| Methods..... | 88 |
| Mouse samples..... | 88 |
| Phenotype..... | 88 |
| Hybrid groups..... | 89 |
| Size differences..... | 89 |
| Shape differences between <i>M. m. musculus</i> and <i>M. m. domesticus</i> | 90 |
| Shape transition along the hybrid gradient..... | 90 |
| Shape differences between hybrid groups..... | 91 |
| Results..... | 91 |
| Size differences..... | 91 |
| Shape differences between <i>musculus</i> and <i>domesticus</i> | 93 |
| Shape transition along the hybrid gradient..... | 93 |
| Shape differences between groups..... | 98 |
| Discussion..... | 99 |
| Size..... | 100 |

| | |
|---|-----|
| Shape..... | 100 |
| Phenotypic transition as a scenario for complex traits' evolution | 101 |
| Conclusion..... | 102 |
| Contributions to the thesis | 105 |
| Perspectives | 106 |
| Acknowledgements..... | 107 |
| References | 109 |
| Curriculum Vitae | 123 |
| Affidavit..... | 124 |

Summary of the dissertation

Morphological diversity in nature is astounding. A remarkable example of such diversity is the vertebrate cranium. This structure is developmentally, anatomically, and functionally integrated with the many other tissues and sensory systems of the head. Because of this, it is under strong constraints to achieve an adult form (size and shape) compatible with the functional requirements of the individual. The genetic basis of craniofacial diversity has been traditionally studied from a macro-evolutionary perspective (i.e. at the between-species level), with special focus on adaptive radiation and domestication.

The work presented in this thesis is an attempt to understand the genetic basis of craniofacial shape variation in the house mouse. By using between-subspecies and within population variation, I address the question from a micro-evolutionary perspective. In this thesis I also explore the genetic architecture of the traits (i.e. number, effect size, and genomic distribution of the causal loci), and the extent to which phenotypic variation can be explained by genetic variation – i.e. heritability of the traits.

The first two chapters of this thesis are the first genome-wide approximation to the genetic architecture of craniofacial shape and size in mice. I combine highly recombinant mouse populations –wild hybrid mice and outbred lab mice- with dense marker coverage of the genome to map the loci underlying phenotypic variation. I identify genes previously known to be involved in craniofacial formation, and provide a list of genomic regions that contain new candidate genes for craniofacial development. Regarding the genetic architecture, I show that craniofacial traits are highly polygenic and highly heritable, with many loci of very small effect distributed uniformly along the genome.

The last chapter of the thesis is an assessment of the morphological transition associated with the degree of admixture between two subspecies of the house mouse, *Mus musculus musculus* and *Mus musculus domesticus*. I show that craniofacial shape changes, but not size changes, are correlated with the level of admixture. The transition from *M. m. musculus* to *M. m. domesticus* is continuous, such mode would be expected from a trait with polygenic architecture, and therefore these results are in line with the genetic results obtained in previous chapters.

Overall the work presented in this thesis is the first genome-wide analyses of the genetic basis and genetic architecture of craniofacial shape variation in the house mouse. It is also the first time shape variation is explored in a close-to-natural context; previous work used crosses between inbred

mouse strains. Therefore, the results reported here are directly relevant to the understanding of complex traits evolution.

Zusammenfassung der Dissertation

Es ist erstaunlich, wie vielfältig Morphologie in der Natur vertreten ist. Ein beeindruckendes Beispiel dieser Diversität stellt der Schädel von Wirbeltieren dar. Der Schädel bildet sowohl entwicklungsbiologisch, anatomisch und funktional zusammen mit vielen anderen Geweben und Sinnesorganen den Kopf eines Organismus. Daher liegt ein bestimmter Rahmen zu Grunde, in dem der Schädel in Größe und Form variieren darf, jedoch stets voll kompatibel mit seiner Funktion im adulten Individuum sein muss. Ursprünglich wurde die Diversität des Schädels und des Gesichts aus einer zwischen-artlichen Perspektive betrachtet. Ein spezieller Fokus lag dabei auf adaptiver Radiation und Domestikation.

Die vorliegende Arbeit beschäftigt sich mit Fragen zur genetischen Grundlage der Schädelmorphologie aus der micro-evolutionären Perspektive, d.h. zwischen Hausmäusen zweier Unterarten auch verschiedenen Populationen der gleichen Unterart. Zudem untersuche ich die „genetische Architektur“ einiger Merkmale, wie Anzahl, Effektgröße und Verteilung der für die Variation mit verantwortlichen Genorte im Genom. Ein weiterer Aspekt ist das Ausmaß, in wiefern phänotypische Variation durch genetische Variation erklärt werden kann (Vererbbarkeit von bestimmten Merkmalen).

Die ersten zwei Kapitel dieser Dissertation ist die erste genomweite Untersuchung zur genetischen Architektur der Schädelvariation in Mäusen. Um die Genorte ausfindig zu machen, die für die phänotypische Variation verantwortlich sind, habe ich mit hoch rekombinanten Mauspopulationen gearbeitet (wilde Hybridmäuse und ausgezüchtete Labormäuse). Die dichte Verteilung der Marker im Genom ist dafür unerlässlich. Einige in meiner Arbeit gefundenen Gene sind bereits bekannt dafür, dass sie eine Rolle spielen bei der Formierung von Schädeln. Zudem konnte ich eine Liste mit weiteren sehr viel versprechende, bisher unbekanntem genomische Regionen aufstellen, die eine in die Entwicklung des Schädels involviert sind. In Bezug auf die Größe, Art und Verteilung der verantwortlichen Genregionen im Genom lässt sich sagen, dass die Merkmale der Schädelknochen durch viele verschiedene Gene beeinflusst wird, also sehr polygen ist. Darüberhinaus sind die Effekte

stark vererbbar Die identifizierten Gene liegen jedoch nicht alle in einem Gencluster, vielmehr treten verantwortliche Gene sehr häufig im Genom auf und liegen dort gleichförmig verteilt vor.

Das letzte Kapitel dieser Arbeit befasst sich mit der Veränderung von morphologischer Variation mit dem Grad von genetischer Durchmischung zweier Hausmausunterarten (*Mus musculus musculus* und *Mus musculus domesticus*). Ich konnte zeigen, dass die Form der Schädelknochen mit dem Grad der Durchmischung beider Unterarten, korreliert. Ein Größenunterschied der Schädelknochen konnte nicht festgestellt werden. Der Übergang von *M. m. musculus* zu *M. m. domesticus* ist kontinuierlich, was für ein polygenisches Merkmal zu erwarten ist. Somit bestätigen diese Ergebnisse, was ich bereits in Kapitel 1 und 2 dieser Arbeit postuliert habe.

Alles in Allem beschreibt diese Dissertation zum aller ersten Mal allgemeine Merkmale der genetischen Grundlagen zur Schädelmorphologie in Hausmäusen auf genomweiter Ebene, d.h. welche Regionen sind verantwortlich für die Variation der Schädelform, wie viele dieser Regionen gibt es, wo liegen sie und wie groß ist ihr jeweiliger Effekt. Darüberhinaus untersucht diese Arbeit die Frage nach Formvariation in einem sehr natürlichen Kontext durch die Nutzung von wilden bzw. ausgezuchteten Mäusen, wohingegen vorhergegangene Studien sich auf Variation zwischen verschiedenen Inzuchtstämmen konzentrierten. Die aus dieser Dissertation hervorgegangenen Ergebnisse sind daher direkt relevant, für das Verständnis zur Evolution komplexer Merkmale.

“(…) whilst this planet has gone cycling on according to the fixed law of gravity,
from so simple a beginning endless forms most beautiful and most wonderful
have been, and are being, evolved”
(Darwin 1859).

The morphological diversity of animals and plants has always amazed and puzzled biologists. However, it is still only poorly understood how such diversity evolves.

In the last decades new methods for the study of shape have been developed, broadening the possibilities of a real understanding of morphological form. Now it is possible to go beyond unidimensional measures of form like length, width, and height, and use multidimensional measurements that adequately characterize the shape of complex structures.

The combination of new ways of measuring shape and new methods in quantitative genetics and genomics has changed the way morphological variation is studied. Now that we can go beyond descriptive morphology, we can hopefully begin to understand the genetic basis of morphological diversity.

A genetic theory of adaptation

Differences in morphological shape have been traditionally understood from an adaptationist perspective. There is no consensus surrounding the way in which adaptation proceeds, in particular regarding the effect sizes that new mutations have in the phenotype (Orr 2005a).

Throughout the end of the 19th century and beginning of the 20th Mendelians and biometricians were the first to discuss whether loci of big effect (Mendelians) or small effect (biometricians) were responsible for phenotypic variation. The infinitesimal model proposed by Fisher in 1918 brought the discussion to an initial end. The model showed how continuous variation could be explained by an infinite number of Mendelian-segregating loci; however, such loci would have each very small effects on the phenotype (reviewed in Rockman 2012).

Although the infinitesimal model explained the underlying genetic architecture of continuous traits, the problem of how phenotypic evolution could occur was still in the air. In 1930, Fisher showed with his geometric model that mutations of small effect were less likely to cause deleterious effects in the organism than mutations of intermediate or big effect. However, when the effect of drift was considered, the scenario changed. In 1983, Kimura showed that *de novo* mutations of intermediate or big phenotypic effect were less likely to be lost by drift than mutations of small effect.

The results of Fisher's geometric model and Kimura's estimations were used by Allen Orr (1998) to propose the distribution of effect sizes that underlies adaptation. Few mutations of large effect will be fixed in the first stages of adaptation, and then many mutations of small effect will follow, refining the adaptive trait. Such an exponential model of size effects underlying adaptation is widely accepted today, and empirical data seem to support it (reviewed in Rockman 2012 and Orr 2005b).

However, the support that empirical evidence gives to the exponential model has recently been questioned (Martin & Orgogozo 2013; Rockman 2012; Stern & Orgogozo 2008). The available data is dominated by candidate gene studies, and findings typically represent classic Mendelian genes, resulting in the identification of large effect loci underlying phenotypic changes. From a more conceptual perspective, the universality of the model was criticized because it only considers scenarios where adaptation originates from new mutations (Rockman 2012). Recent data indicates that the exponential model does not hold when highly complex traits and evolution from standing variation are considered (reviewed in Rockman 2012).

Hence, the formulation of a general theory of adaptation requires not only that more data are collected (Orr 2005a; Orr & Coyne 1992), but also that phenotypic traits with diverse genetic architectures and evolutionary histories are considered.

A theory of morphological evolution

The pursuit of a theory of morphological evolution has focused on predictability. Can the genetic changes resulting in morphological diversity be predicted? Along this line, evolutionary developmental biologists have proposed the cis-regulatory theory of morphological evolution. It states that morphological evolution is more likely to be due to changes in regulatory elements – enhancers- than to changes in the coding sequence of the genes (Carroll 2000; Carroll 2008; Stern 2000; Wray 2007).

This theory was historically fuelled by two key discoveries: the surprising similarity between protein coding genes of distantly related organisms (Jacob & Monod 1961; King & Wilson 1975), and the discovery of the Hox genes and their role in the development of extremely different animal forms (reviewed in Carroll 2005).

The arguments supporting the cis-regulatory theory of morphological evolution are: (1) gene regulation is responsible for phenotypic differences in tissues and organs of multicellular organisms, (2) changes in gene expression are often correlated with phenotypic changes, (3) coding sequences are highly conserved between taxa, (4) cis-regulatory sequence evolution is more flexible than changes in coding sequences, (5) the size of non-coding regions in the genome are much larger than coding regions, and therefore the mutational target size is larger in the former, (6) cis-regulatory mutations have fewer pleiotropic effects than coding mutations, and (7) many cis-regulatory mutations have been found causing morphological changes (reviewed in Stern & Orgogozo 2008).

Recently, the analysis of empirical data showed first, that other types of structural variation in the genome and other types of regulatory elements (other than enhancers) are also involved in morphological evolution (Alonso & Wilkins 2005; Fondon & Garner 2004), and second, that such empirical evidence does not strongly support the claims of the cis-regulatory theory. There seems to be enough evidence for cis-regulatory as well as for coding changes as causal of morphological evolution (Hoekstra & Coyne 2007; Stern & Orgogozo 2008). However, it should be acknowledged that the available data is highly biased towards candidate gene approaches and towards reports of coding changes because they are easier to identify than regulatory changes (Stern & Orgogozo 2008).

However, when the question was approached from a taxonomic perspective and the data for within and between species was analyzed independently, a clearer scenario arose. Morphological differences between species or between higher taxonomic levels are associated predominantly with cis-regulatory changes; however within-species differences are mostly due to coding changes (Stern & Orgogozo 2008; Stern & Orgogozo 2009). Interestingly, this would indicate that the genetic changes underlying macroevolution are not the same underlying microevolution. Only a very specific type of genetic variation generating morphological diversity within species is selected over long evolutionary time scales (Stern & Orgogozo 2008; Stern & Orgogozo 2009).

Building on these patterns, a refined theory of morphological evolution has been proposed (Gompel & Prud'homme 2009; Martin & Orgogozo 2013; Stern 2013; Stern & Orgogozo 2009). Although it includes some of the ideas from the cis-regulatory theory, it also incorporates the concept of gene

networks and parameters derived from population genetics. This theory proposes that given a large population size, natural selection will prefer mutations happening in the regulatory region of genes located in a bottleneck position within a gene network. A bottleneck means that upstream signals converge in a specific gene before being distributed to downstream effector genes. Because mutations in these genes will generate very specific phenotypic changes, therefore reducing pleiotropy, such genes will be “hot-spots” for morphological evolution. However, under a scenario with small population size or under strong selection (e.g. within populations), the predictability of the genetic location of morphologically relevant mutations is lost.

It seems that the genetic bases of morphological evolution are to some extent predictable. However, it should be noticed that the current theories are restricted to evolution due to *de novo* mutations, and empirical data are biased towards simple phenotypes (Martin & Orgogozo 2013). A new framework will have to be developed for highly polymorphic traits that most probably evolve from standing genetic variation without fixation of any particular haplotype.

The vertebrate cranium

One of the most striking examples of morphological diversity and complexity is the vertebrate cranium. This structure is developmentally, anatomically, and functionally integrated with the many other tissues and sensory systems of the head, and therefore it is under strong constraints to achieve an adult form (size and shape) compatible with the functional requirements of the individual. At the same time, it is one of the most diverse morphological structures in vertebrates. Throughout this dissertation, I will use the cranium of the house mouse as a model for complex traits.

The phylogenetic origin of the cranium goes back to the origin of vertebrates approximately 500 million years ago. Together with the vertebral column, these two structures are used to define in general terms what a vertebrate is (Shimeld & Holland 2000). From a developmental perspective, the two main vertebrate innovations are the neural crest (NC) and the epidermal placodes. The NC is a population of migratory cells that make up most of the mesenchyme tissue from which the cranium develops. The epidermal placodes are thickenings of ectoderm that form the sensory organs of the head (Green *et al.* 2015; Shimeld & Holland 2000). As it is evident, the two main developmental innovations are tightly linked to the morphological innovations.

Developmental origin of the craniofacial skeleton

The cranium is the most complex bony structure of the vertebrate body. Not only it is made of many independent parts of different embryonic origin, but it is made of tissues that are not found in other places of the body, like dermal bone and secondary cartilage (Helms & Schneider 2003; Thorogood 1993).

Regarding the embryonic origin, cranial bones originate either from mesoderm or from ectoderm, contrasting with the other parts of the skeleton that are exclusively mesodermal. The evolutionary origin of ectodermal bone is associated with the origin of the neural crest cells (NCCs) and therefore with the origin of vertebrates. NCCs are a population of cells that originate during the formation of the neural tube development and then migrate towards the trunk and the head of the embryo around embryonic day 7.5-8.5 (Green *et al.* 2015; Kaufman & Bard 1999). The cells migrating towards the head are known as cranial crest cells and are the only NCCs able to form bone and cartilage (Helms & Schneider 2003; Santagati & Rijli 2003). The anterior part of the skull (viscerocranium) and the mandible are neural-crest-derived structures. The bones forming the base and back of the skull derive from mesoderm. Interestingly these parts of the skull, as well as the mandible are more recent than the viscerocranium, they were acquired later in evolutionary time (Gans & Northcutt 1983).

Types of ossification

Cranial bones are also particular because their ossification can be endochondral or intramembranous. All the other bones of the body have endochondral ossification, with the exception of the knee (Abzhanov *et al.* 2007). Interestingly, cranial bones cluster in two modules depending on the type of ossification and not on their developmental origin, and such modularity is thought to constrain the evolvability of cranial development (Koyabu *et al.* 2014).

The base of the skull has endochondral ossification, while the superior and anterior parts as well as the mandible are dermal bones, meaning they have intramembranous ossification. During endochondral ossification a cartilage template is initially formed and eventually replaced by bone (reviewed in Longand Ornitz 2013), while dermal bones ossify directly from mesenchyme, without a cartilaginous template (Abzhanov *et al.* 2007; Franz-Odenaal 2011).

Irrespective of the type of ossification, the steps required for bone formation are well understood (reviewed in Franz-Odenaal 2011), and the genes controlling such steps are known (Franz-Odenaal 2011; Green *et al.* 2015; Long & Ornitz 2013). However, although the general developmental processes underlying the formation of the skull and the mandible are understood, it is not yet known how their three-dimensional shape is determined.

Genetic vs non-genetic determination of cranial shape

Intuition might tell us that bone tissue, which supports the body, protects the organs, and serves as attachment point for the muscles, should be a static tissue, a tissue that remains unchanged once the desired structural properties are reached. Yet, bone is a very dynamic tissue.

At birth most of the craniofacial bones are completely ossified with exception of the cranial base that, at this point, is mainly cartilage and ossifies postnatally. However, these bones keep growing for weeks after birth, and once they reach their final size and shape, a process called remodeling – new bone deposition and old bone resorption- continues during the life of the organism. Bone remodeling is responsible for bone homeostasis and repair (Hadjidakis & Androulakis 2006; Raggatt & Partridge 2010).

The malleability of bone tissue has been used for some authors as an argument to propose that the determination of craniofacial bone shape is mainly controlled by environmental effects such as pre and postnatal mechanical forces and signaling from surrounding tissues during development (Herring 1993). In this context bone shape is considered an environmentally-controlled phenotype. In an attempt to disentangle the effect of environmental and genetic factors on the shape of the mouse mandible, Boelland Tautz (2011) measured the effect of age, size, diet, and raising conditions (laboratory or wild). They found that the summed effect of all such environmental factors does not mask the genetic signal behind the phenotype.

It is known that the shape of bone structures involved in active behaviors like feeding (e.g. mandible) are influenced by environmental components, but it is also known that craniofacial shape is highly heritable (see section 4 of this introduction). The latter indicates that there is enough genetic variance for morphological evolution to occur, and therefore, if the environmental effects are adequately accounted for, it should be possible to identify the genetic components underlying bone shape variation.

Morphometrics

In 1993, Rohlf and Marcus defined the field of morphometrics as: “Concerned with methods for the description and statistical analysis of shape variation within and among samples of organisms and of the analysis of shape change as a result of growth, experimental treatment or evolution. Morphometric methods are needed whenever one needs to describe and to compare shapes of organisms or of particular structures”.

Traditional morphometrics

The first attempts to quantify variation in morphology are traced back to the morphometricians at the beginning of the 20th century. The study of shrimps and crabs proportions by Karl Pearson and W.F.R. Weldon pushed them to develop statistical tools, such as the correlation coefficient, to understand such data (Reyment 1996). During most of the 1900s the methods used to quantify the variation in form are known as traditional morphometrics, or multivariate morphometrics. This approach relies on multiple linear measurements of the structure of interests, e.g. width, length, and height, and the correlation between them (Adams *et al.* 2004; Adams *et al.* 2013). In the 1930s, several methods to analyze multivariate data were developed: principal components and canonical correlation, discriminant functions, Hotelling’s T^2 distribution, and in general the analysis of variance by Ronald Fisher (Adams *et al.* 2004; Reyment 1996). With these advances in statistics new types of questions were able to be answered.

In 1941, Darcy Thompson finished the definitive version of “On Growth and Form”, originally published in 1917. With this book he stated that a complete understanding of biological form requires a rigorous mathematical and physical approach (Reyment 1996). A very influential part of his work is the idea of the transformation grids. Using this qualitative tool –the mathematics for it came much later- he showed how an organism can be described by the deformation of another (Mitteroecker & Gunz 2009).

A major inconvenience of using traditional morphometrics is that distances and ratios of distances do not capture the geometry of the structure, and therefore the visualization of the changes in form was not possible. The results of morphometrics analysis were typically represented as tables, and in the best scenario depicted in scatter plots, e.g. principal component plots (Rohlf & Marcus 1993)

Geometric morphometrics

A “revolution” in morphometrics came about in the late 1980’s when methods that took into account the geometry of the structure were developed (Rohlf & Marcus 1993). The morphological studies shifted from using linear measurement to using landmarks and outlines (Adams *et al.* 2004), and the new field of geometric morphometrics (GM) was born.

The advantages of GM methods compared to traditional morphometrics rely on the preservation of the geometry of the structure across all the statistical analyses by using a coordinate system. This allowed the visualization of the changes in shape. Besides, the use of outlines and landmarks doesn’t require an *a priori* selection of variables that should be measured as it is in traditional morphometrics; the results of GM analysis will reveal which regions of the structure drive the changes in the form (Rohlf & Marcus 1993).

Another development that contributed to the establishment of GM was the rigorous mathematical and statistical framework to study shape developed by Kendall (Adams *et al.* 2004). From such framework derives the (mathematical) definition of shape: shape is defined as “all the geometric information that remains when location, scale and rotational effects are filtered out from an object” (Kendall 1977).

The form of a structure is the information associated with shape and size. In geometric morphometrics size and shape are usually analyzed independently. Size in GM is known as centroid size, and corresponds to the square root of the sum of the squared distance between the landmarks and the centroid.

Geometric morphometric methods

Two ways of capturing the geometry of an object are widely used in GM, defining outlines (2D) or surfaces (3D), and defining landmarks. Landmarks are points that can be recognized in all the individuals included in the analysis, their meaning can relate to homologous, mechanical, developmental, or positional criteria, besides others.

The most widespread and more understood geometric approach is the Procrustes method (Bookstein 1996; Mitteroecker & Gunz 2009). It takes the raw landmark coordinates and removes

the non-shape information like position, size, and orientation. The general Procrustes analysis –GPA consist on (1) translating the landmark configurations of all individuals to the same position by superimposing the centroids; (2) scaling the landmark configurations to a same value of centroid size, usually one; (3) rotating the configurations until the minimum distance between landmarks on all configurations is reached (Mitteroecker & Gunz 2009; Zelditch *et al.* 2012).

The coordinates resulting after the GPA are called Procrustes coordinates, and the differences in these coordinates between individuals represent differences in shape. The Procrustes coordinates are used for subsequent statistical analysis like principal components and canonical variate analysis.

Geometric morphometrics today

Today, more than 20 years after the “revolution”, geometric morphometrics is a mature field. These decades of GM research have allowed a deeper understanding of biological shape and with the development of new statistical tools, the diversity of questions that GM can address increase constantly. Currently, it is possible to address aspects of shape like allometry, asymmetry, and modularity in a rigorous quantitative way (Adams *et al.* 2013).

GM tools have been brought to fields like systematics, developmental biology, and quantitative genetics, resulting in a better understanding of shape from an evolutionary perspective (Adams *et al.* 2013; Klingenberg 2010).

Genetics of craniofacial shape

Plenty of genes have been associated with the formation of the skull and the mandible. For example, 883 protein coding genes are reported in the MGI database of mammalian phenotypes as having craniofacial phenotypes (Eppig *et al.* 2015). This knowledge comes predominantly from loss-of-function studies or from disease-related phenotypes, especially from humans and mice. The observed phenotypes are usually drastic, e.g. the complete loss of certain bones, or the absence of the head. Given the high complexity of these structures it is not surprising that many genes are involved in their development. However, these approaches fall short when trying to understand which genes are involved in the fine-tuning of the shape of the skull and the mandible.

The nature of the studies mentioned above makes it hard to know if such genes play a role in a natural variation context, and therefore whether they are relevant to an evolutionary study. The drastic craniofacial phenotypes associated with the loss of one gene are most probably not present in natural population because they will be accompanied by an equally drastic reduction in fitness.

Some approaches to study shape variation in more realistic –natural- scenarios have been explored recently (Boell *et al.* 2013). The proposal is that the study of phenotypes caused by gene-dosage differences instead of null knock-out gets us closer to a natural scenario. Other approaches come from the fields of developmental biology, quantitative genetics, and genomics.

Genetic architecture of adaptive morphological differences

Some species are models for the study of craniofacial variation due to their historical and ecological context (e.g. Darwin finches, and cichlids or sticklebacks, respectively). Others are models given their association with humans (e.g. domesticated dogs), or for being models for the study of human phenotypes (mice and dogs). Recently, the study of non-disease related craniofacial variation in humans has received great attention.

Darwin finches are a model for diversification of morphological shape, in particular of beak shape. From developmental studies (Abzhanov *et al.* 2006; Abzhanov *et al.* 2004; Mallarino & Abzhanov 2012), and recently from genome-wide scans (Lamichhaney *et al.* 2015), it is known that the beak, a relatively simple structure, has a polygenic architecture. At least 15 genomic regions were associated with beak diversity between pairs of species with different shape (Lamichhaney *et al.* 2015).

Sticklebacks are fish models for body shape variation due to changes in habitat. The study of lake and river ecotypes revealed around 5 quantitative trait loci –QTL- that explain much of the variation associated with craniofacial shape differences (Jamniczky *et al.* 2015; Kimmel *et al.* 2005). Cichlids are another fish group extensively explored due to their history of adaptive radiation and convergent morphological evolution. Using crosses between morphological distinct species, Albertson and colleagues (2003) identified 26 QTLs underlying craniofacial shape differences (20 more QTLs were identified for linear measurements) with effect sizes ranging between 5 and 20%.

Studies of domesticated dogs have identified 26 genomic regions associated with linear measurements of the skull and 7 associated with mandible (Boyko *et al.* 2010). The effect size of the QTLs is high, with the first couple of QTLs explaining most of the phenotypic variation. Using

geometric morphometrics, five QTLs were correlated with brachycephalic shape in dogs (Schoenebeck *et al.* 2012).

The studies mentioned above focused on highly morphological divergent pairs of species in an attempt to understand the genetic basis of adaptive phenotypes. They are typical examples of adaptive radiation and domestication, and therefore only cover evolutionary scenarios characterized by strong selection and drift. The results from these studies suggest oligogenic architecture for craniofacial traits, i.e., a moderate number of loci with moderate or high effects on the phenotype.

Lessons from humans

In the last five years, the interest for exploring the genetic basis of non-disease-related facial variation in humans has increased. Our micro-evolutionary perspective on the genetics of craniofacial shape variation comes exclusively from these studies.

In 2011, a genome-wide association study (GWAS) using almost 10,000 individuals identified 5 loci associated with facial morphology in Europeans (Liu *et al.* 2012). The fact that such a big study was not able to identify more regions hints to a very complex genetic architecture underlying facial variation. Other studies explored the same question identifying also very small number of genes (Boehringer *et al.* 2011; Claes *et al.* 2014; Paternoster *et al.* 2012).

The heritability of craniofacial traits has also been explored in humans. Using linear measurements of the skull and mandible of the Hallstadt population, heritability of individual measurements ranged from 0.19-0.43 (Martínez-Abadías *et al.* 2009). Using a Korean population and combining multiple linear measurements of the face, the heritability ranged from 0.45-0.55 (Kim *et al.* 2013). These results show that craniofacial shape in humans have high amounts of genetic variation and therefore high evolutionary potential.

The house mouse

Mus musculus is a taxonomic group containing three main subspecies colloquially known as the house mouse: *Mus musculus domesticus*, *Mus musculus musculus*, and *Mus musculus castaneus*, and two recently recognized subspecies *Mus musculus gentilulus*, and *Mus musculus molossinus* (Auffray

& Britton-Davidian 2012). The three main subspecies diverged in the Iranian region around 0.5 million years ago (Hardouin *et al.* 2015). The current geographical distribution locates *M. m. castaneus* in the south and east of Asia; *M. m. musculus* in north Asia and Eastern Europe; and *M. m. domesticus* in Western and Southern Europe and some regions of the North and West of Africa.

The Eastern and Western European subspecies overlap in the middle of Europe and form a hybrid zone that runs from Denmark to the Black sea (reviewed in Baird & Macholán 2012). This hybrid zone is considered a tension zone that keeps its stability by migration-selection balance. The population of hybrid mice has been previously studied regarding morphological patterns (Alibert *et al.* 1994; Auffray *et al.* 1996b; Mikula *et al.* 2010a; Mikula & Macholán 2008), microbial and parasite load (Baird *et al.* 2012; Wang *et al.* 2015), reproductive isolation (Payseur *et al.* 2004; Teeter *et al.* 2008; Turner & Harr 2014; Turner *et al.* 2012), and behavior (Bimova *et al.* 2011; Latour *et al.* 2013). The general agreement is that hybrids are less fit than the pure subspecies, which results in the stability of the hybrid zone.

The house mouse group is conservative regarding morphological shape. To the naked eye the different subspecies might look very similar (Auffray & Britton-Davidian 2012); however the differences in craniofacial shape are enough to distinguish them. The craniofacial differences between populations and subspecies of the house mouse have been extensively studied using traditional and geometric morphometrics (Boell & Tautz 2011; Gerasimov *et al.* 1990; Macholán 2006; Siahsarvie *et al.* 2012).

Evolutionary history of the house mouse

The house mouse is generalist, although when living next to humans it feeds preferentially on grains. This type of diet makes it very difficult to measure or even to speculate about the evolutionary sources that resulted in different craniofacial morphologies in the subspecies.

Some studies have addressed this question from different perspectives. Renaudand Auffray (2010) explored the morphological changes associated with insular evolution. They concluded that although some of the variation corresponds to plastic responses and allometry, the main morphological variation in mandible shape could be attributed to adaptation to new diets. Boelland Tautz (2011) showed evidence for higher similarity in mandible shape between old populations of mice than between more recent populations. The same pattern was shown by Siahsarvie *et al.* (2012). These results indicate that differences in mandible shape cannot be attributed to neutral evolution, but it

remains to be clarified how much of this variation is due to drift or to local adaptation. It was shown that commensalism did not involve a convergent mandible shape in the three subspecies of the house mouse (Siahsarvie *et al.* 2012), and therefore, if local adaptation is to be claimed, detailed studies on the local ecology of each subspecies are needed.

Genetic basis of craniofacial variation in the mouse

In 1991, Atchley and Hall proposed the mouse mandible as a model for the study of complex morphological structures (Atchley & Hall 1991). From then onwards, the studies on this structure multiplied, and today it is a well established model for the study of the development, genetics, and evolution of complex structures, in particular of morphological complexity (Klingenberg & Navarro 2012). Studies of the skull, on the contrary, have lagged behind due to its more complex structure compared to the mandible. The latter can be adequately approximated by two dimensions, but the skull requires a three-dimensional approach that conveys its complexity. Recently, this has started to change.

A seminal paper on the genetics of mandible shape in mice was published already in 1985 by Atchley and collaborators. The authors used families of outbred mice to approach questions like modularity and integration, maternal effects, and heritability of craniofacial measurements. It took almost a decade until the first studies using actual genomic data (i.e. genomic markers) became available.

The mandible

From 1997 -when the first studies using linkage mapping appeared (i.e. QTL) - until today, at least 10 studies have been published regarding the genetic basis of mandible shape variation in the mouse (Boell *et al.* 2011; Burgio *et al.* 2012a; Cheverud *et al.* 1997; Klingenberg *et al.* 2004; Klingenberg *et al.* 2001; Leamy *et al.* 2008; Leamy *et al.* 2000; Leamy *et al.* 1997).

All the studies that used a QTL approach were based on F2 populations derived from crosses between Large (LG/J) and Small (SM/J) inbred strains (Cheverud *et al.* 1997; Klingenberg *et al.* 2004; Klingenberg *et al.* 2001; Leamy *et al.* 2008; Leamy *et al.* 1997). The only exception is Leamy *et al.* (2000) that used an inbred line derived of wild *Mus musculus castaneus* (Cast/Ei) and a traditional inbred line (M16i). This studies used between 76 and 92 microsatellites, and one of them used 350

SNPs. Burgio *et al.* (2012a) used a congenic approach including a traditional inbred line (B6) and an inbred line derived of wild *Mus spretus* (SEG/Pas), and Boell *et al.* (2011) opted for consomic lines made from B6 and an the wild-derived inbred line PWD/Ph (representing *M. m. musculus*).

Interestingly, some of the previously mentioned studies were not directly focused on the loci underlying mandible shape variation, but addressed more specific questions like the genetic basis of asymmetric shape variation, and shape variation QTLs associated with imprinting. They concluded that asymmetric patterns like directional asymmetry do have a genetic basis while fluctuating asymmetry patterns most probably do not (Leamy *et al.* 2000; Leamy *et al.* 1997). The effect of imprinting is thought to be negligible in mandible shape variation (Leamy *et al.* 2008).

Almost 20 years of research has shown that the genetic architecture of mandible shape variation is not simple. Using linear measurements and geometric morphometrics in two dimensions, between 25 and 37 QTLs have been associated with shape variation, and 12 to 23 with size variation. The mapping resolution, however, does not allow the identification of candidate genes. The percentage of phenotypic variance explained by individual QTLs ranged from 1.6 – 18.3%, indicating a moderate effect size. However, added together, the QTLs identified can account for a big proportion of the total phenotypic variation.

The genetic loci underlying shape variation seem to have moderate pleiotropy, with such effects restricted to different regions of the mandible, but by no means forming completely isolated regions or modules (Burgio *et al.* 2012a; Cheverud *et al.* 1997; Klingenberg *et al.* 2004). It has been claimed that epistasis plays an important role in mandible shape determination (Boell *et al.* 2011).

The skull

Fewer studies have been published regarding the genetic basis of skull variation in mouse. The studies that used a QTL approach were based on F2 crosses between Large (LG/J) and Small (SM/J) inbred lines (Leamy *et al.* 1999; Wolf *et al.* 2005), and in the backcross between B6 and A/J inbred lines (Maga *et al.* 2015). Burgio and collaborators used congenic lines built from B6 and SEG/Pas a wild-derived inbred line (Burgio *et al.* 2009; Burgio *et al.* 2012b).

Using linear measurements (2D) and geometric morphometrics (3D), these studies have identified between 20 and 30 QTLs associated with skull shape variation. The individual effects of the QTLs range from 1-11%, and the added effect can account for between 26% and 40% of the total

phenotypic variation. As well as in the case of the mandible, the mapping resolution does not allow the identification of individual candidate genes. However, Maga *et al.* (2015) used a method to prioritize genes based on gene enrichment tools that use information from disease-related genes. Although this method is arguably far from ideal, they prioritize 16 genes out of the 2,476 genes contained in the QTLs identified by the study.

These studies indicate that the loci underlying skull variation act in a modular way, affecting preferentially some parts of the skull and not others (Leamy *et al.* 1999; Maga *et al.* 2015). They also highlight the role of epistasis in shape determination (Burgio *et al.* 2009; Burgio *et al.* 2012b; Wolf *et al.* 2005).

It is relevant to mention that two common features of the above mentioned studies are: i) low genomic marker resolution (less than 100 microsatellites and 300 to 800 SNPs) and ii) the use of mouse inbred lines (laboratory inbred-lines and wild-derived inbred lines). However, to address craniofacial variation from an evolutionary perspective, it is necessary to use populations which are closer to the natural context (e.g., wild-derived, outbred populations).

Overview of the dissertation

In this dissertation I sought to understand the genetic architecture of craniofacial shape and size variation in the house mouse. The work presented here contributes to the general understanding of the genetic basis and evolution of complex traits.

In the first chapter I present the first genome-wide approximation to the genetic architecture of 3D craniofacial shape and size variation in mice. By using dense marker coverage and a natural hybrid population between *M. m. musculus* and *M. m. domesticus*, I identified, with high resolution, candidate loci and genes involved in craniofacial shape variation. I show that the loci involved in size and shape variation are uniformly distributed along the genome, and the effect that each locus has on the phenotype is very small. In addition, I present the first estimates of heritability for shape and size variation in a natural population of mice. Overall, this chapter shows that the phenotypic differences between subspecies have a polygenic basis, and are not due to loci of large effect.

In the second chapter I use outbred mice to explore the genetic architecture of craniofacial size and shape from a micro-evolutionary perspective. I found that the traits are highly polygenic and highly heritable, showing that within-population variation show the same patterns found in chapter one for between-subspecies variation. Moreover, I identify key candidate genes involved in the determination of skull and mandible shape.

In chapter three I explore how craniofacial morphology changes according to the percentage of admixture between *M. m. musculus* and *M. m. domesticus* genomes. I show that shape changes are correlated with the degree of hybridization and occur in a continuous way from one subspecies to the other. These results are consistent with the highly polygenic architecture found to underlie craniofacial traits, and could be seen as a practical example of the way a complex trait evolves in nature.

Use of a natural hybrid zone for genome-wide association mapping of craniofacial traits in the house mouse

Introduction

Unravelling the genetic basis of organismal form remains one of the major challenges of biological research (Mallarino & Abzhanov 2012; Muller & Newman 2003). Although many efforts have been dedicated to finding genomic regions involved in morphological trait variation and adaptation, very few genes have been identified, and we are only at the beginning of understanding the developmental mechanisms generating variation in natural populations (Barrett & Hoekstra 2011; Mallarino & Abzhanov 2012). Many long standing questions about the genetic basis of morphological adaptation remain unanswered (Orr 2005a): How many loci underlie complex trait variation? What is the distribution of effect sizes of these loci? How do loci interact? Do traits have similar genetic architecture in different taxa?

Morphology can evolve rapidly between populations and species enabling adaptation to environmental changes. In particular, adult morphological traits are an important target of natural selection because they determine how an organism interacts with the environment. In this study we focus on the adult house mouse (*Mus musculus*) craniofacial skeleton, formed by the skull and mandible.

The head is a particularly elaborated part of the vertebrate morphology, which has undergone extensive adaptive change during the diversification of vertebrates, but is expected to be under stabilizing selection within species. Craniofacial evolution has been intensively studied due to the high prevalence of craniofacial defects in humans and because the head was a key innovation in the evolution of vertebrates (Wilkie & Morris-Kay 2001). However, there are currently few insights into the developmental processes and genetic pathways that regulate craniofacial shape formation because the complexity of craniofacial phenotypic characters cannot be adequately understood

using classical genetic approaches. For example mutagenesis screens are unlikely to detect many important variants determining morphology in the adult because they are also essential for early embryonic development. The study of gene dosage effects may provide one solution to this problem (Boell et al. 2013), but it requires further validation. In an alternative approach, Attanasio *et al.* (2013) have used genomic analyses and transgenic reporter gene constructs to suggest that craniofacial shape can be modified by possibly thousands of tissue-specific enhancers of developmental genes.

Most of the currently available information on mouse craniofacial features concerns the mandible; it represents a well-established model for the study of morphological shape and its underlying genetics (Atchley & Hall 1991; Klingenberg & Navarro 2012), and has a relatively simple anatomical complexity compared to the skull. Craniofacial differences between populations and subspecies of house mice have been widely studied (Boell & Tautz 2011; Gerasimov *et al.* 1990; Macholán 2006; Siahsarvie *et al.* 2012), but so far the phenotypic differences have not been linked to the underlying gene(s). Further, it remains unclear how much variation in morphology is due to local adaptation vs. neutral drift. Results from multiple studies suggest that craniofacial morphology is under directional and/or stabilizing selection (Boell & Tautz 2011; Renaud & Auffray 2010; Siahsarvie *et al.* 2012), but the generalist diet of the house mouse makes it difficult to infer the selective pressures that might have caused the differences in shape among populations and subspecies of the *Mus musculus* group.

Genetic mapping studies – quantitative trait locus (QTL) and genome-wide association studies (GWAS) – are the most common methods for identifying genes involved in complex traits. The incorporation of geometric morphometrics has enabled the application of genetic mapping approaches to craniofacial bone formation and shape determination. It has also allowed the quantification of small between-individual characteristic of natural populations and therefore the detection of subtle phenotypic effects (Klingenberg 2010). Using QTL mapping, many genomic regions have been associated with variation of skull and mandible shape in mice (Cheverud *et al.* 1997; Klingenberg *et al.* 2004; Klingenberg *et al.* 2001; Leamy *et al.* 2000; Leamy *et al.* 1997; Leamy *et al.* 1999; Wolf *et al.* 2005). In humans, recent GWAS and candidate-gene studies have identified several genes involved in non-disease related facial variation in human populations (Boehringer *et al.* 2011; Claes *et al.* 2014; Liu *et al.* 2012; Paternoster *et al.* 2012).

Traditional QTL designs have limited mapping resolution, and the phenotypic and genomic variation in traditional laboratory strains represents a small proportion of natural variation in house mice (Yang *et al.* 2011b). In a first attempt to overcome some of these limitations Burgio and colleagues developed interspecific congenic strains using *Mus musculus* and *Mus spretus*, and mapped skull and

mandible shape in mice (Burgio *et al.* 2009; Burgio *et al.* 2012a; Burgio *et al.* 2012b; Burgio *et al.* 2007). Currently, mouse populations with better characteristics for fine mapping are being evaluated, e.g. the Collaborative Cross (CTC 2004) and commercial outbred lines (Yalcin *et al.* 2010).

Genetic mapping in wild populations has been proposed as an alternative to identify loci contributing to natural trait variation (Beraldi *et al.* 2007; Poissant *et al.* 2012; Schielzeth & Husby 2014; Slate 2005; Slate *et al.* 2002). With this approach, samples with larger phenotypic and genetic variation can be studied, and good mapping resolution is predicted, due to the history of recombination, (see (Laurie *et al.* 2007) for specific estimates in mice), provided high density genetic markers are available.

In this study we use a mapping population composed of 178 males derived from a natural hybrid zone to explore the genetic architecture of skull and mandible shape in the house mouse. The same population has been used to map hybrid sterility loci in a parallel study (Turner & Harr 2014). Here we combine 3D geometric morphometrics and association mapping for the first time to study the genetic basis of natural shape variation. This approach results in high mapping resolution - in many cases single-gene level – enabling the identification of candidate genes involved in craniofacial variation. We also show that these traits have a complex genomic architecture consistent with a polygenic model of morphological adaptation.

Methods

Ethical statement

Mice were maintained and handled in accordance to FELASA guidelines and German animal welfare law (Tierschutzgesetz § 11, permit from Veterinärämter Kreis Plön: 1401-144/PLÖ-004697).

Mapping population

Mice were caught across the Bavarian hybrid zone, and brought to the Max Planck Institute for Evolutionary Biology in Plön, Germany (Turner *et al.* 2012). Mating pairs were established using mice that were close neighbors in the wild, i.e. they came from the same or nearby trapping locations. In this way the first generation offspring was produced in a close-to-natural breeding situation. First generation offspring were raised under identical laboratory conditions, minimizing environmentally

induced shape variation. Litters were weaned at 28 days and sacrificed by CO₂ asphyxiation between 9 and 12 weeks of age. 178 male mice were included in the mapping population, including full siblings, half siblings and unrelated individuals. Detailed information about the sampling procedure and breeding can be found in Turner *et al.* (2012).

Shape phenotyping

Heads were scanned with a computer tomograph (micro-CT—vivaCT 40, Scanco, Bruettisellen, Switzerland) and three-dimensional cross-sections of the skull and mandible were generated with a resolution of one cross-section per 0.021mm. 48 three-dimensional landmarks were located in the skull and 14 in each hemi-mandible using the TINA landmarking tool (Schunke *et al.* 2012) (supplementary Table 1.1, Figure 1.1). All further morphometric analyses were performed in MorphoJ (Klingenberg 2011).

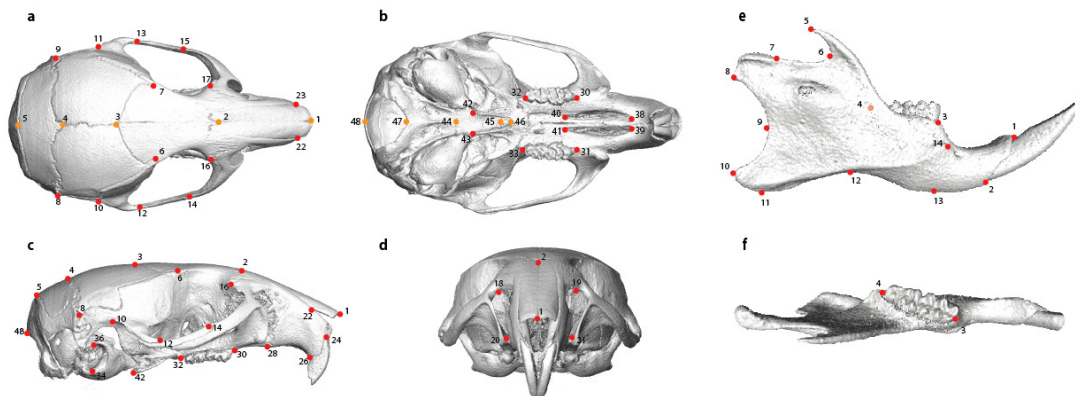


Figure 1.1. Three-dimensional landmarks located in the skull and mandible. Dorsal (a), ventral (b), lateral (c) and frontal view (d) of the skull. In a) and b) paired landmarks (right and left) are drawn in red, midline landmarks are orange and represent the plane of symmetry. In the lateral view of the mandible (e) the landmark 4 is outside the 2D plane and its position is better represented in the dorsal view (f). See suppl. Table 1.1 for the description of the landmarks.

This study is focused on the symmetric component of skull and mandible shape, therefore the raw landmark coordinates of the right and left sides were averaged. Because the skull has a pattern of object symmetry –right and left sides are connected by an internal plane of symmetry- (Klingenberg

et al. 2002; Mardia *et al.* 2000), a mirror image of the skull is generated and overlapped with the original; the average of the two images is a perfectly symmetric structure and corresponds to the symmetric component of shape (Klingenberg *et al.* 2002). The mandible has a matching symmetry pattern –right and left sides are physically independent from each other–, therefore a simple average of sides was used.

A generalized Procrustes analysis (GPA) was performed on skull and mandible averaged landmark coordinates. Since the age of the mice ranged from 62 to 86 days when phenotyped, a regression of shape vs age (days) was performed to remove shape variation due to age differences. 1.8% of the skull shape variation was explained by age (10,000 permutations, $p=0.0002$), and 3.1% of mandible variation ($p=0.03$). The residuals of the regression were used in a principal component analysis (PCA) and PC scores were used as phenotypes in the mapping.

Size

Centroid size (CS) is the standard measure of size in geometric morphometrics and is estimated as the square root of the sum of the squared distances of a set of landmarks from their centre of gravity or centroid (Zelditch *et al.* 2012). Using MorphoJ, mandible CS was calculated as the average of right and left hemimandibles CS. Skull CS was calculated using all the landmarks from the right and left side (Klingenberg *et al.* 2002).

Genotyping

DNA was extracted from liver, spleen, or ear samples using salt extraction or DNeasy kits (Qiagen, Hilden, Germany). The mice were genotyped by Atlas Biolabs (Berlin, Germany) using the Mouse Diversity Genotyping Array (Affymetrix, Santa Clara, CA) (Yang *et al.* 2009). Genotypes at 584,729 SNPs were called using the apt-probeset-genotype software provided by Affymetrix using standard settings. VINOs (variable intensity oligonucleotides) were identified using the MouseDivGeno algorithm and removed from the dataset (53,148 SNPs). SNPs with observed heterozygosity > 0.9 (18,120 SNPs) were removed. SNPs with $\geq 5\%$ missing data or minor allele frequency $< 5\%$ were removed. To avoid redundancy and gain power in the mapping analysis, all SNPs in perfect linkage disequilibrium with other SNPs ($LD=1$) were removed. A total of 145,378 SNPs were eventually used. The X chromosome was not analyzed in this study.

Association mapping

The SNPs that passed the quality control and the PC axes that explained more than 1% of the variation in each dataset (Suppl. Table 1.2) were used for association mapping.

The univariate linear mixed model (LMM) implemented in genome-wide efficient mixed-model association-GEMMA (Zhou & Stephens 2012) was used to perform the association mapping. This method uses a variance component model where the effect of an allele is modelled as a main effect, while population structure and relatedness among samples (estimated by a kinship matrix) are taken into account by means of variance components of random polygenic effects. The centered kinship matrix was calculated in GEMMA using all LD-pruned SNPs.

The effect size of significant SNPs was calculated in the following way $(\beta^2 * \text{var}(x))/\text{var}(y)$ where $\text{var}(x)$ is the variance of the genotype at the focal SNPs, and $\text{var}(y)$ is the variance of the phenotype. β is reported for each SNP in the LMM output.

To estimate the genome-wide parameters PVE and PGE, we used the Bayesian sparse model (BSLMM) implemented in GEMMA (Zhou *et al.* 2013). In contrast with the LMM model that assumes that every genetic variant affects the phenotype, the BSLMM is flexible, allowing also the possibility that only a small proportion of the variants have some effect. As a result, BSLMM performs better for several genetic architectures and performs similarly to LMM when the genetic architecture of the trait is indeed highly polygenic (Zhou *et al.* 2013). Because the architecture of the phenotypes studied here is unknown, we used BSLMM for genome-wide heritability estimates. The results reported here were generated using the option `-bslmm 1` (linear BSLMM) and 5 million sampling steps with 500K burn-in steps. We performed additional analyses for 10 and 50 million steps using a subsample of the data to confirm the accuracy of the Bayesian estimates (data not shown).

Permutations

The genome wide significance threshold was defined by permutation. The way in which the craniofacial phenotype is handled in this study, that is, its decomposition in principal components, necessitates a high number of tests. That is, 21 tests for skull shape (20 PCs and 1 for size), and 20 for mandible shape (19 PCs and 1 for size). To account for multiple testing due to the number of SNPs and also for the number of phenotypes mapped, we performed the mapping analysis for 10,000 permuted datasets. For each repetition, all phenotypes were randomized among individuals,

keeping the genotypes unaltered to preserve genetic structure. For each permutation, the best p-value across all phenotypes was reported and the 95% quantile of the distribution of p-values was used as genome wide significance threshold (Suppl. Fig. 3). This yielded a p-value of 9.4×10^{-7} for skull and 8.1×10^{-7} for mandible. Bonferroni correction yields a p-value of 1.6×10^{-8} for skull and 1.8×10^{-8} for mandible. However, since Bonferroni correction is considered overly conservative in mapping studies, we focus the discussion on the regions identified using the permutation-based threshold.

LD analysis

Each pair of significant SNPs was tested for genotypic linkage disequilibrium by calculating the squared correlation estimator r^2 . To estimate the interval associated with each significant SNP from the LD-pruned data, we report significant regions defined by the position of the most distant downstream and upstream SNP showing a minimum $r^2 = 0.8$ to the significant SNP. PLINK 1.07 (Purcell *et al.* 2007) was used for the r^2 calculations. Gene annotation for significant SNPs and regions was performed using the UCSC Genome Browser (Kent *et al.* 2002) and UCSC Annotation data (Karolchik *et al.* 2014).

In addition to studies previously reporting QTL related to craniofacial formation (cited in Table 1.1), we used the MGI database to search for phenotypes associated with genes in significant GWAS regions (Eppig *et al.* 2012). The QTLs reported in Leamy *et al.* (1999) do not include confidence intervals, thus we assumed overlap when our regions were within 10 Mb from peak markers (see Table 1.2).

Chromosomal partitioning of variance

Partitioning of the total variance among individual chromosomes was performed in the GCTA software (Yang *et al.* 2011c). GCTA performs a restricted maximum likelihood analysis to calculate the variance explained by each chromosome while controlling for the effect of the others, this means that relatedness and population structure is accounted for (option `--reml --mgrm`). Due to the small number of mice used in this study, it was not possible to fit all 19 autosomes at the same time. Individual analyses were run for each chromosome including the first 10 principal components derived from the kinship matrix as covariates (option `--reml --grm --qcovar`). Resulting per-

chromosome estimates are inflated due to relatedness among individuals; hence the sum of all chromosomes effects exceeds the heritability estimates for each phenotype. However, because overestimation is uniformly spread across the genome (Yang *et al.* 2011d), the relative effects of chromosome are informative even though absolute estimates are error-prone. We calculated the relative contribution of each chromosome by dividing individual values over the total variation explained (Figure 1.4).

Regression of shape on genetic admixture

To explore the pattern of change in craniofacial morphology through the hybrid zone, a multivariate regression was performed between skull and mandible shape and hybrid index (% *M. m. musculus* ancestry, Turner *et al.* (2012)). Shape vectors were obtained in MorphoJ following the generalized Procrustes fit and multivariate regression was performed in MorphoJ.

11 wild caught mice from the *M. m. musculus* extreme of the hybrid zone and 19 from the *M. m. domesticus* side were also included in the regression. These mice were not environmentally controlled; therefore they differ in age, sex, and other environmental factors.

Morphological differences between house mouse subspecies

10 mice from the Cologne/Bonn region in Germany (*M. m. domesticus*) and 15 from Kazakhstan (*M. m. musculus*) were used to illustrate the craniofacial shape differences between the two subspecies of mice (Figure 1.2). The mice were sacrificed by CO₂ asphyxiation at non-matched ages. These mice are part of the wild colonies kept in the Max Plank Institute for Evolutionary Biology in Plön, Germany. Phenotypes were measured as described above for hybrid mice, with a slightly different set of landmarks (44 for the skull and 13 for the mandible - see Figure 1.1). Differences between the mean shapes of the two subspecies were calculated using the discriminant function implemented in MorphoJ.

Data

The phenotype data, the LD-pruned and the original SNP data, as well as kinship matrix are available at DRYAD: doi: 10.5061/dryad.bt848.

Results

Phenotypic variation

M. m. musculus and *M. m. domesticus* show subtle differences in skull and mandible shape, however these differences can be precisely quantified using geometric morphometrics. *M. m. domesticus* is characterized by a relatively flat skull vault and a broader back of the cranium. Its frontal bone is longer and wider, making the middle of the cranium more robust compared to *M. m. musculus*. The ascending ramus of the mandible is more robust and compact in *M. m. domesticus*. The coronoid process is much more pronounced in *M. m. musculus* and the angle between the condyle and the angular process is wider. From a posterior view it is evident that the buccal-lingual contrast is more marked in *M. m. domesticus*, with *M. m. musculus* having a relatively straight disposition (Figure 1.2).

The animals used in this study were first-generation offspring of mice captured in a natural hybrid zone in Bavaria (Turner et al. 2012). Skull morphology measurements were based on computer tomography scans and 3D landmarks (Figure 1.1).

Regression of shape vectors on individual measures of genetic admixture (see Methods) showed that most hybrid phenotypes are intermediate between pure subspecies' phenotypes (inferred from individuals with >80% genomic makeup from one subspecies; Suppl. Figure 1.1).

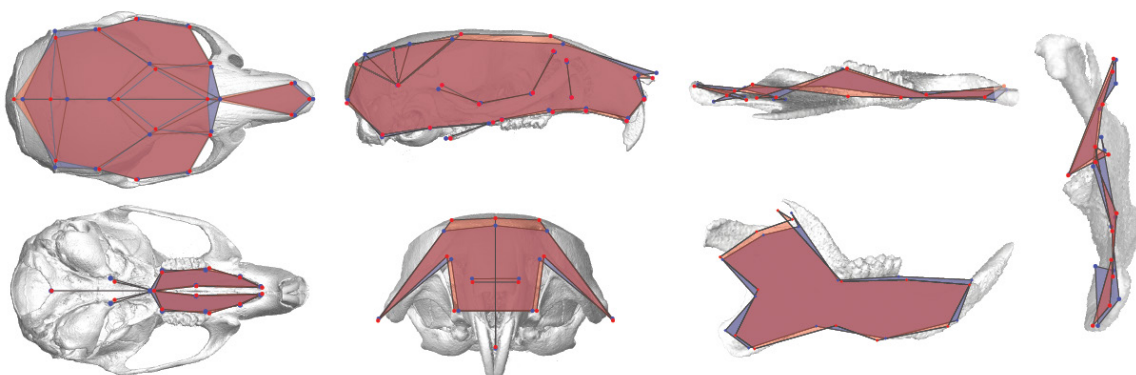


Figure 1.2. Shape differences between the two subspecies of *Mus musculus* that encounter each other in the European mouse hybrid zone, *M. m. musculus* (eastern European) and *M. m. domesticus* (western European). Blue, mean shape of *M. m. domesticus*. Red, mean shape of *M. m. musculus*. Differences are scaled by 2x. Wild derived mice from the German region of Cologne/Bonn were used to represent the *M. m. domesticus* subspecies, and mice from Kazakhstan to represent the *M. m. musculus* subspecies. The underlying skull and mandible images are provided for orientation and do not directly represent the landmarks.

These results suggest that transgressive phenotypes, i.e. hybrid phenotypes outside the pure subspecies range of shape, are not of special relevance for the craniofacial morphology in this population. Inclusion of wild caught, not environmentally-controlled mice from the extremes of the hybrid zone into the regression did not alter the pattern substantially (Suppl. Figure 1.1), showing that indeed, the first generation lab-bred hybrids represent the full range of phenotypic transition between the subspecies.

Genetic architecture

We analyzed skull and mandible separately. Right and left sides of the structures were averaged, and corrected for age differences using a multivariate regression of shape vs age. On each of the dataset, we performed a generalized Procrustes analysis (GPA) of the raw landmark coordinates, followed by a principal component analysis (PCA) to reduce the dimensionality of the data and make it suitable for the association analysis.

All PC axes explaining at least 1% of the phenotypic variation were included in the mapping: 20 axes for skull explaining 86% of the total observed shape variation, and 18 axes for mandible explaining 92% of the variation (Suppl. Table 1.2). The PC scores were used as individual phenotypes. The complex genetic relatedness of the mapping population was accounted for by using the linear mixed model implemented in GEMMA (Suppl. Fig. 1.4).

No significant genetic associations were found for skull or mandible size (centroid size measurement).

To estimate to which extent the shape changes associated with each PC axis have a genetic basis, we calculated the 'chip heritability' of each PC. The 'chip heritability' -from now on PVE, to match the GEMMA output- is the percent of phenotypic variation explained by all the SNPs used in the mapping. We find a strong genetic signal in most of the PCs, with 25 of the 38 PCs having PVE values above 50% (Suppl. Table 1.2). The total PVE estimate for skull and mandible shape suggests that ~64% of the phenotypic variation has a genetic basis. For size, the estimate reaches ~72% (Suppl. Table 1.2).

Most of the chip heritability can be attributed to SNPs of small effect, also known as polygenic effect. However, there are SNPs with effect size above the polygenic level. The percentage of phenotypic variation explained by the latter (from now on PGE) was estimated. ~30-37% of shape and size

variation is explained by such “large effect” SNPs (Suppl. Table 1.2), leaving a large proportion of the variation to be explained by loci with small effect. PGE values, however, should not be over interpreted due to the relatively high error estimates (Supp. Table 1.2).

We calculated the proportion of variation explained by each chromosome and tested for a correlation between this parameter and chromosomal length. A positive correlation was found for mandible and skull shape; i.e., the longer the chromosome, the more variation it explains (Figure 1.4), suggesting a more or less random distribution of major and minor effect loci across the chromosomes.

Genomic regions associated with shape

We identified significant associations for 6 of the 20 PC axes included for skull, and for 8 of the 18 PC axes for mandible (see Suppl. Table 1.2). The skull and mandible shape traits that showed association with genetic variant(s) are depicted in Suppl. Figure 1.5 and Suppl. Fig 1.6. Following the genome-wide significance threshold of $p < 8 \times 10^{-7}$ defined through permutations (see Methods and Suppl. Fig. 1.3), a total of 27 SNPs showed significant associations with skull and 16 SNPs with mandible shape variation (Table 1.1, Figure 1.3). 28% of these SNPs fall inside genic regions.

Together, the group of SNPs identified in this study explains 13% of the total variation in skull shape in the mapping population, and 7% of the mandible variation (Table 1.1). The biggest effect is caused by the SNP associated with skull PC1, which is the major axis of shape variation in the hybrid population. The distribution of effect sizes is shown in Figure 1.5.

We tested for long-range linkage disequilibrium (LD) between pairs of significant SNPs. We did not find any significant linkage between physically distant SNPs, suggesting the associations found in this population are not confounded by diffuse or long range LD. LD blocks were calculated for each focal SNP, first using $r^2 \geq 0.2$, with the purpose of exploring the maximum block size showing any linkage. The median size was 1.8 Mb (max = 1.99 Mb, min = 0.97 Mb). Using a more meaningful threshold of $r^2 \geq 0.8$, the median size of the regions was 0.15 Mb.

After grouping the SNPs based on LD ($r^2 \geq 0.8$), a total of 19 genomic regions associated with craniofacial traits were defined (Table 1.2). The phenotypic effect of the genotypes for the significant regions is shown in Suppl. Fig. 1.2. For all SNPs, phenotypic means for heterozygous individuals were intermediate between the means of the homozygous classes, suggesting most effects are additive.

Nine genomic regions were associated with skull shape. Regions 6 and 9 contain some SNPs that are not in strong linkage, but are still relatively close together (~0.5 to 2Mb apart), and therefore were combined into single regions. Mandible shape was associated with 10 genomic regions. The median size of the regions was 148 kb (min = 8.7 kb, max = 5,013 kb). For several significant SNPs, there were no highly linked SNPs in the dataset; hence the inferred significant intervals are one bp in length. We did not include these intervals in median estimates of mapping resolution. However, when evaluating potential candidate genes, we included 150 kb intervals (median for other regions) around each of these SNPs.

The significant regions identified in this study overlap with previous QTL studies of skull and mandible shape in mice. For the sake of precision, we did not include studies for which QTL intervals were reported only in cM, but only those with precise intervals reported in bp. Four of the 9 regions associated with skull shape overlap with the results of Burgio *et al.* (2009), who used interspecific recombinant congenic strains (IRCS) between C57BL/6 and *Mus spretus* to explore the genetic basis of skull shape. Six of the 10 regions associated with mandible shape overlap with regions in Burgio *et al.* (2012a) and/or with Leamy *et al.* (2008), who used IRCS and a F3 SM/J – LG/J crosses to explore mandible variation, respectively.

Table 1.1. Significant SNPs associated with mandible and skull shape variation. The percentage of phenotypic variation explained by each SNP is shown.

| Phen | Chr | Pos | SNP | p-value | MAF | Gene | %var | %var total |
|-----------------|-----|-----------|-------------|-----------------------|------|---------|------|------------|
| Skull | | | | | | | | |
| PC1 | 17 | 30615222 | JAX00435677 | 3.6x10 ⁻⁷ | 0.24 | Btbd9 | 33.8 | 5.59 |
| PC2 | 10 | 61542659 | JAX00290754 | 4.1x10 ⁻⁷ | 0.38 | . | 18.3 | 2.21 |
| PC10 | 5 | 50372456 | JAX00129855 | 2.8x10 ⁻⁷ | 0.08 | Gpr125 | 17.2 | 0.50 |
| PC13 | 6 | 148560348 | JAX00148139 | 3.8x10 ⁻⁷ | 0.24 | Gm6313 | 1.8 | 0.04 |
| PC14 | 5 | 62659428 | JAX00584067 | 3.2x10 ⁻⁷ | 0.11 | . | 14.7 | 0.27 |
| PC18 | 1 | 111842009 | JAX00007979 | 9.7x10 ⁻⁷ | 0.26 | . | 12.6 | 0.16 |
| | 1 | 113192684 | JAX00262739 | 6.0x10 ⁻⁷ | 0.30 | . | 13.1 | 0.17 |
| | 1 | 113521976 | JAX00008104 | 6.9x10 ⁻⁷ | 0.30 | . | 13.1 | 0.17 |
| | 1 | 114504925 | JAX00262960 | 4.5x10 ⁻⁷ | 0.30 | . | 13.4 | 0.17 |
| | 1 | 114521206 | JAX00262964 | 7.0x10 ⁻⁷ | 0.29 | . | 12.9 | 0.17 |
| | 1 | 114573977 | JAX00262971 | 2.6x10 ⁻⁷ | 0.29 | . | 13.9 | 0.18 |
| | 1 | 114667409 | JAX00262998 | 2.4x10 ⁻⁹ | 0.33 | . | 18.4 | 0.24 |
| | 1 | 114720894 | JAX00263006 | 3.5x10 ⁻⁸ | 0.32 | . | 15.7 | 0.20 |
| | 1 | 115459643 | JAX00008250 | 3.9x10 ⁻⁷ | 0.30 | . | 13.5 | 0.17 |
| | 8 | 90136634 | JAX00164479 | 4.3x10 ⁻⁷ | 0.20 | . | 13.4 | 0.17 |
| | 8 | 91911137 | JAX00164612 | 8.7x10 ⁻¹¹ | 0.21 | . | 21.0 | 0.27 |
| | 8 | 93693782 | JAX00676020 | 3.9x10 ⁻⁷ | 0.28 | . | 13.5 | 0.17 |
| | 8 | 93900937 | JAX00676081 | 3.1x10 ⁻⁷ | 0.33 | Fto | 13.9 | 0.18 |
| | 8 | 93918262 | JAX00676089 | 1.5x10 ⁻⁷ | 0.33 | Fto | 14.7 | 0.19 |
| | 8 | 94057678 | JAX00676176 | 4.8x10 ⁻⁷ | 0.32 | Fto | 13.4 | 0.17 |
| | 8 | 94413228 | JAX00164799 | 1.5x10 ⁻⁷ | 0.28 | . | 14.4 | 0.19 |
| | 8 | 95015417 | JAX00676516 | 9.6x10 ⁻⁷ | 0.26 | . | 12.7 | 0.16 |
| | 11 | 51316312 | JAX00027368 | 1.3x10 ⁻⁸ | 0.12 | Col23a1 | 16.6 | 0.21 |
| | 17 | 17491991 | JAX0073985 | 2.1x10 ⁻⁸ | 0.37 | . | 16.6 | 0.21 |
| | 17 | 17500615 | JAX00432709 | 1.8x10 ⁻⁸ | 0.36 | . | 16.9 | 0.22 |
| | 17 | 17500690 | JAX00432710 | 7.0x10 ⁻⁸ | 0.32 | . | 15.3 | 0.20 |
| | | | | | | | | 12.6* |
| Mandible | | | | | | | | |
| PC3 | 3 | 125400219 | JAX00536726 | 9.9x10 ⁻⁷ | 0.09 | Ndst4 | 13.7 | 1.14 |
| PC7 | 11 | 58409394 | JAX00312338 | 9.7x10 ⁻⁷ | 0.12 | . | 21.2 | 0.96 |
| PC7 | 11 | 96437460 | JAX00319199 | 3.4x10 ⁻⁸ | 0.12 | Skap1 | 16.6 | 0.75 |
| PC11 | 15 | 31358406 | JAX00060457 | 6.0x10 ⁻⁷ | 0.26 | . | 17.6 | 0.50 |
| PC11 | 15 | 31371834 | JAX0039778 | 1.2x10 ⁻⁸ | 0.23 | Ropn1l | 19.9 | 0.57 |
| PC12 | 15 | 31407662 | JAX00060460 | 6.4x10 ⁻⁷ | 0.24 | March6 | 17.1 | 0.49 |
| | 8 | 52637099 | JAX00668547 | 1.9x10 ⁻⁷ | 0.09 | . | 15.7 | 0.32 |
| PC12 | 17 | 94874936 | JAX0079706 | 9.7x10 ⁻⁹ | 0.25 | . | 17.6 | 0.36 |
| PC13 | 17 | 94994750 | JAX0079715 | 7.8x10 ⁻⁸ | 0.38 | . | 15.9 | 0.33 |
| | 2 | 76287988 | JAX00493638 | 7.7x10 ⁻⁷ | 0.33 | Osbp16 | 18.7 | 0.37 |
| PC15 | 3 | 106920129 | JAX00111463 | 9.1x10 ⁻⁷ | 0.46 | . | 12.8 | 0.22 |
| PC15 | 3 | 106922140 | JAX00533242 | 6.2x10 ⁻⁷ | 0.46 | . | 13.1 | 0.23 |
| PC16 | 3 | 106925166 | JAX00533253 | 6.3x10 ⁻⁸ | 0.47 | . | 15.5 | 0.27 |
| | 3 | 106930043 | JAX00111464 | 6.8x10 ⁻⁷ | 0.46 | . | 13.0 | 0.23 |
| | 16 | 85292313 | JAX0071995 | 5.1x10 ⁻⁷ | 0.08 | . | 13.1 | 0.18 |
| PC18 | 17 | 4793878 | JAX00430026 | 2.1x10 ⁻⁷ | 0.36 | . | 20.0 | 0.23 |
| | | | | | | | | 7.14* |

MAF, minimum allele frequency. If the SNP falls in an intragenic region, the gene is shown. %var, variation of each PC explained by the SNP. %var total, variation of the mapping population explained by the SNP, calculated by multiplying %var of the SNP times %var of the PC (values shown in Sup. Table 1.2). *indicates the total phenotypic variation explained by the SNPs identified in this study.

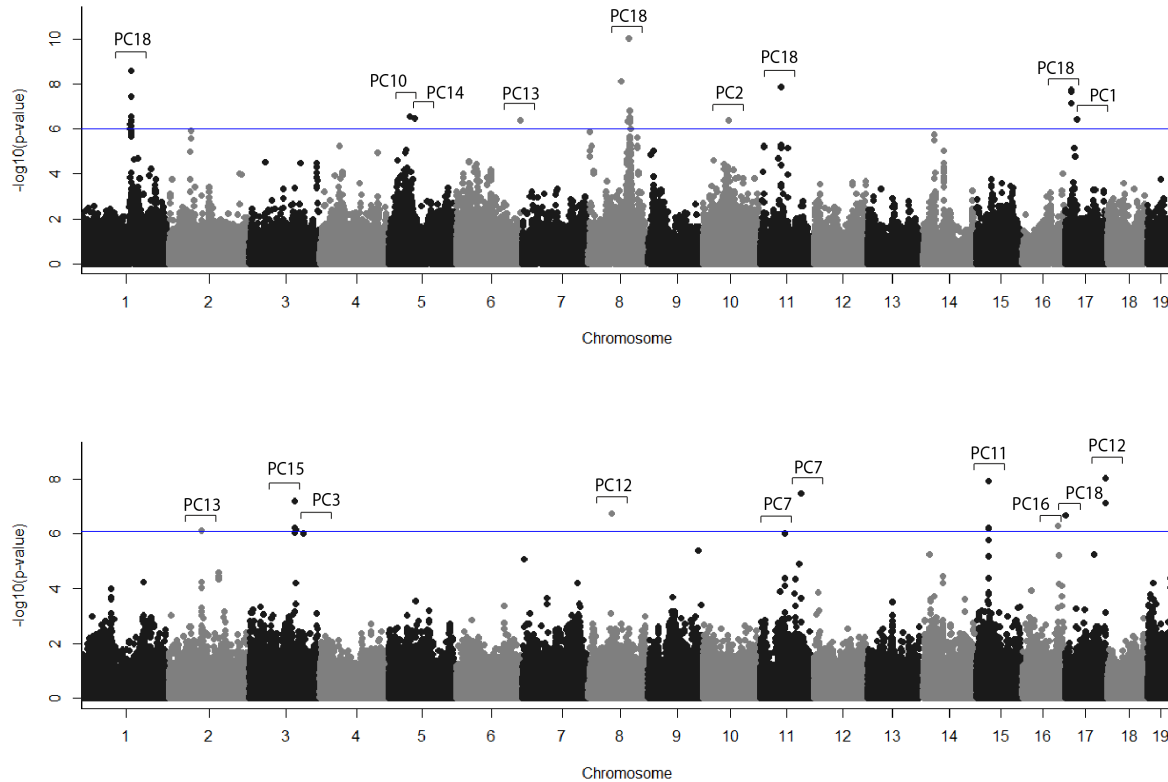


Figure 1.3. Manhattan plots showing the significant associations found for skull shape (top) and mandible shape (bottom). The phenotype (PC axis) associated with each SNP is shown. The blue line indicates the significant threshold used in this study: 9.4×10^{-7} for skull and 8.1×10^{-7} for mandible (see methods). Only one SNP per perfect linkage group (LD=1) is shown (see methods).

12 of the significant SNPs fall in intronic regions of 10 genes (Table 1.1). Among them is *Ndst4*, associated with PC3 of the mandible, which codes for a heparan sulfotransferase, a family of proteins involved in craniofacial formation through the modulation of BMP, Wnt, Shh and FGF signaling, e.g., *Ndst1* (Hu *et al.* 2007; Pallerla *et al.* 2007). The specific role of *Ndst4* in craniofacial formation is not yet known.

Several interesting candidate genes are found inside the significant regions (Table 1.2). *Glo1* (glyoxalase 1, region 1, skull PC1) is involved in osteoclastogenesis, stimulating the maturation of osteoclasts (Kawatani *et al.* 2008). Two members of the cadherin family, *Cdh7* and *Cdh19*, are found in region 6. This family is well known for its function in bone formation through the mediation of cell-cell interactions (Hay *et al.* 2009; Marie & Hay 2013).

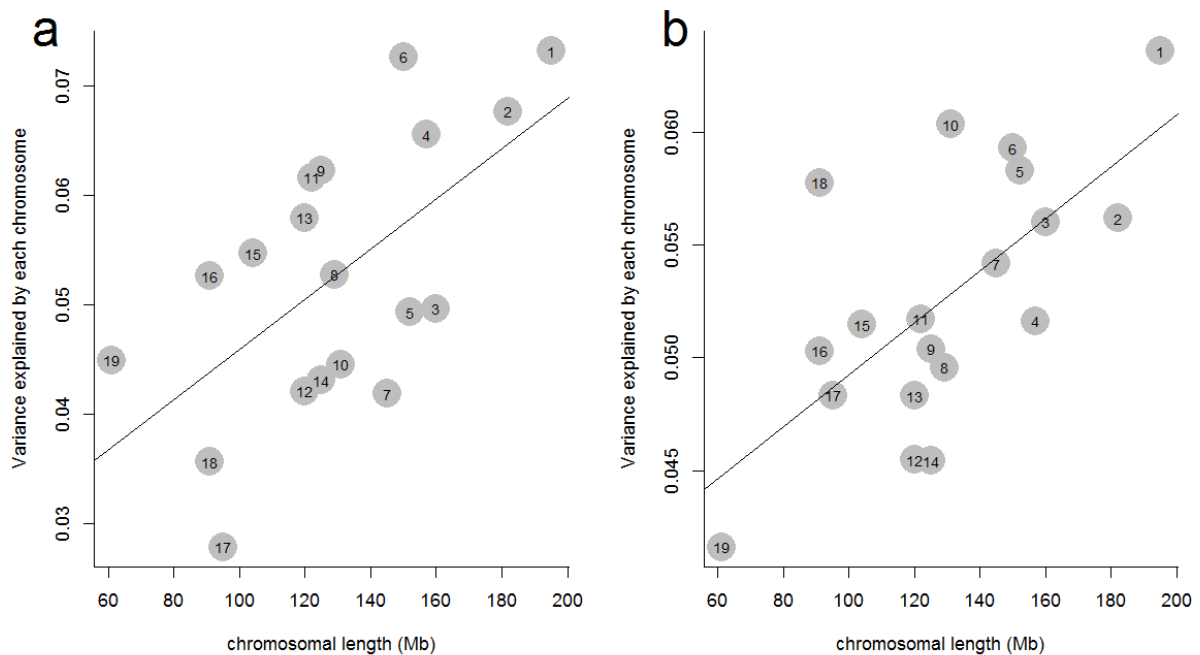


Figure 1.4. Correlation between variance explained and chromosome length for skull (a) and mandible (b). The units of variance explained by chromosome are arbitrary and were adjusted to add up to one. Numbers in the circles represent chromosome number. $R^2=0.33$, $p=0.005$ for skull, and $R^2=0.40$, $p=0.002$ for mandible.

Region 9 comprises several genes, including seven with well-known roles in bone formation. *Irx3* and *Irx5* are part of the iroquois homeobox gene family of transcription regulators. *Irx5* modulates craniofacial development through regulation of neural crest cells (NCC) migration, is co-expressed with *Irx3*, and both interact at the protein level (Bonnard *et al.* 2012). These genes are regulated by *BMP2* and *BMP4*, and are expressed in neural crest cells, embryonic maxillary mesenchymal, and others. Compound knockout mice have craniofacial defects.

Another interesting candidate gene in region 9 is *Nkd1*, which regulates the wnt/ β catenin signaling pathway. *Nkd1* knockouts show a subtle craniofacial phenotype that becomes significant when *Nkd2* is knocked out at the same time (Zhang *et al.* 2007). *Rbl2* shows a similar effect; it has no phenotype, but when knocked out together with *Rbl1*, mice show severe cranium deformations due to abnormal endochondral ossification (Cobrinik *et al.* 1996). *Cyld*, a de-ubiquitinating enzyme regulates the maturation of osteoclasts (Jin *et al.* 2008). *Rpgrip1l* is involved in cilia-mediated *Shh* signaling and knockout mice have craniofacial deformations (Delous *et al.* 2007; Vierkotten *et al.* 2007). And lastly, *Chd9*, a chromatin-remodeling protein, may be involved in transcriptional regulation of

osteoprogenitor cells due to its ability to bind to the regulatory region of critical promoters for osteoblastogenesis including *Bmp4*, *OC*, and others (Shur *et al.* 2006).

The gene *Zfp423*, a transcription factor involved in cerebellar and olfactory development, is also found in this region (Alcaraz *et al.* 2011). Although its role in bone morphogenesis has not been shown yet, it modulates the action of BMP target genes (Masserdotti *et al.* 2010), and knockout mice have a small nasal cavity (Cheng & Reed 2007).

Discussion

Natural hybrid zone

The main logistical challenge of mapping in natural populations of mice is obtaining samples of sufficient size, estimated to be thousands of individuals for quantitative traits similar to human studies (Flint & Eskin 2012; Laurie *et al.* 2007). However, mapping in naturally admixed populations from hybrid zones (between species or sub-species) has benefits that may enable mapping with smaller sample sizes (Buerkle & Lexer 2008; Rieseberg & Buerkle 2002; Slate 2005). Phenotypic variation in hybrid zones includes both intra-subspecific polymorphism and inter-subspecific differences. Because many of the latter causative genetic variants are expected to be fixed within their respective subspecies, they may occur at higher frequency in the hybrid zone than segregating alleles contributing to variation within populations. Further, hybrid zones represent hundreds of generations of intercrossing between differentiated lineages, and therefore, mapping resolution is expected to be high relative to laboratory crosses. Our genome-wide association mapping in the house mouse hybrid zone is thus comparable to mapping in recombinant inbred lines, where a relatively small number of individuals also can yield reliable results (Flint & Eskin 2012).

Hybrid zones that have formed recently or those with large amounts of gene flow from source populations may be less suitable for such association studies. For example, a large influx of pure subspecies chromosomes into the hybrid zone could lead to long range associations between genomic regions from different chromosomes (Rieseberg & Buerkle 2002; Teeter *et al.* 2008). We tested for this potentially confounding effect by measuring LD between the significant SNPs. No association between significant SNPs was found, improving our confidence that the identified regions are not artefacts of unusual population structure.

The phenotype of interest in this study, morphological shape, is known to be susceptible to environmental influences. For example, laboratory studies have shown that diet and age can have plastic effects on the shape of the mouse mandible (Boell & Tautz 2011; Renaud *et al.* 2010). However, genetic effects are usually stronger than environmental effects (Boell & Tautz 2011). Here, we have reduced the influence of environmental effects by breeding wild-caught mice from the hybrid zone for one generation under laboratory conditions and using the first generation offspring of the same gender as mapping population. We have furthermore corrected for any effect on shape of the small variation in age (one month) among individuals.

To avoid spurious associations due to relatedness or population structure, we used a mixed model approach implemented in GEMMA (Zhou & Stephens 2012), which corrects for genetic structure using a kinship matrix derived from the data. This approach has not been tested previously in hybrid populations, however, it seems to have corrected accurately for structure in our sample (Suppl. Figure 1.4).

Genetic architecture of craniofacial shape variation

The significant loci identified in this study were associated with a wide range of PCs, from a PC axis explaining a large amount of the total variation (i.e. PC1 and PC2 in skull, and PC3 in mandible) to PCs explaining as little as ~1% of the variation. This implies that shape changes representing a small amount of the total variation in the population can be explained, at least to some extent, by genetic variants. This is striking, since it is customary to assume that PCs with low variation do not contain much biological information. However, compiling data from two QTL studies for mandible shape in mouse, Boell (2013) found a similar pattern, PCs explaining diverse amounts of variation were associated with QTLs. Moreover, our PVE estimates per PC show that most of them have high chip heritability values (see Suppl. Table 1.2), including some with values above 90%. However, the estimation error is high in some cases, probably due to relatively small sample size (Yang *et al.* 2010), and therefore these values should be interpreted with caution.

We identified 9 genomic regions explaining ~13% of the variation in skull, and 10 explaining ~7% of mandible variation. Based on the PVE estimates, the markers included in this study can explain 64% of total craniofacial variation. We controlled for environmental effects such as age, sex, diet, and age at weaning; we expect that heritability of these traits is lower in nature, where environmental factors play an important role. Nevertheless, the PVE indicates that there are more genetic variants

that were not detected, possibly due to small effect sizes. These results are consistent with a polygenic model of morphological shape, that is, many loci of small effect are responsible for between species variation

We estimated the contribution of individual chromosomes to phenotypic variation, following Yang *et. al.* (2011d) (Figure 1.4). Based on the PVE and PGE estimates, we expect many loci with small effect to affect shape variation. As expected, there is a positive correlation between chromosome length and variation explained. This result provides additional evidence that many genes of small effect underlie shape variation.

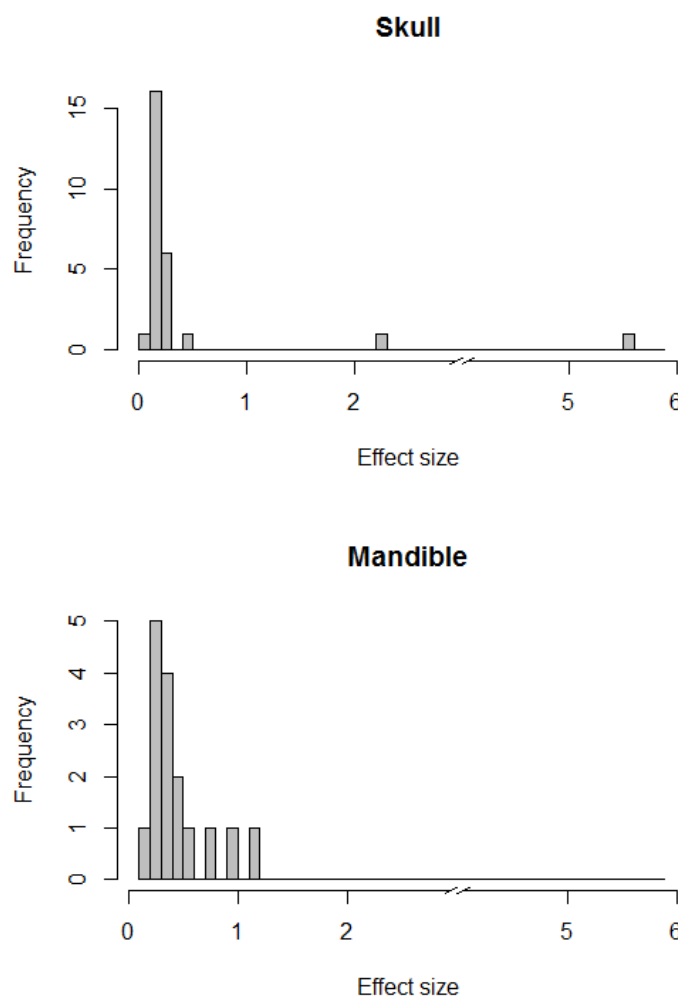


Figure 1.5. Distribution of the effect sizes for mandible and skull shape. Effect size is the percentage of the total phenotypic variation explained by the focal SNP. Note the broken scale to represent one large value in skull.

Table 1.2. Significant regions based on the LD pattern of the significant SNPs.

| Nr | PC | Region | Size(Mb) | Genes | QTL |
|-----------------|------|----------------------------|----------|---|-------------------|
| Skull | | | | | |
| 1 | PC1 | chr17 : 30615222-31231411 | 0.616 | Glo1,Umodl1,Dnah8,Glp1r,Abcg1, Btdb9 | - |
| 2 | PC2 | chr10:61467659-61617659 | [0.15] | Ass1, Neurog3 | - |
| 3 | PC10 | chr5:50297456-50447456 | [0.15] | Gpr125 | - |
| 4 | PC13 | chr6:148485348-148635348 | [0.15] | Gm6313 | 122F [^] |
| 5 | PC14 | chr5 : 62131920-62659428 | 0.528 | G6pd2 | - |
| 6 | PC18 | chr1 : 111842009-115730660 | 3.889* | Dsel,Cdh7,Cdh19 | 66H [^] |
| 7 | PC18 | chr11:51241312-51391312 | [0.15] | Col23a1 | 122D [^] |
| 8 | PC18 | chr17 : 17491991-17500690 | 0.009 | - | - |
| 9 | PC18 | chr8 : 90136634-95150348 | 5.014* | Zfp423,Cnep1r1,Heatr3,Papd5,Adcy7,Brd7, Nkd1 ,Snx20, Nod2,Cyld,Sall1,Tox3,Chd9, Rbl2, Aktip, Rpgrip1l, Fto, Irx3, Irx5 | 122F [^] |
| Mandible | | | | | |
| 10 | PC3 | chr3:125325219-125475219 | [0.15] | Ndst4 | - |
| 11 | PC7 | chr11:58334394-58484394 | [0.15] | Olftr224, 322-325, 328, 330, 2210407C18Rik,Trim58 | 122D+ |
| 12 | PC7 | chr11:96362460-96512460 | [0.15] | Skap1 | SH11.2** |
| 13 | PC11 | chr15 : 31319098-31494802 | 0.176 | Ropn1l, March6 | SH15.1** |
| 14 | PC12 | chr17 : 94874936-94994750 | 0.120 | - | - |
| 15 | PC12 | chr8:52562099-52712099 | [0.15] | - | - |
| 16 | PC13 | chr2 : 76284649-76329794 | 0.045 | Osbp16 | - |
| 17 | PC15 | chr3 : 106920129-106997029 | 0.077 | Kcna10 | SH3.2** |
| 18 | PC16 | chr16:85217313-85367313 | [0.15] | - | 136E+ |
| 19 | PC18 | chr17 : 4741573-4844025 | 0.102 | - | 6C+ |

Regions were defined using a correlation threshold with neighboring SNPs of $r^2=0.8$ (see methods). Only protein-coding genes are shown, based on the UCSC annotation database. The brackets indicate regions where the focal SNP did not show linkage to other SNPs and therefore the region was expanded to the median region size of 0.15Mb (see results). Overlap with previous QTL reported for shape is shown, [^]Burgio et al. 2009, +Burgio et al. 2012, **Leamy et al. 2008. Genes in bold in region 9 are known to display craniofacial phenotypes when mutant (see text).

The effect sizes of individual SNPs estimated in this study range from 0.1% to 5%. With the exception of the single SNP (Region 1) explaining ~5%, the distribution of effect sizes is within the range expected for mouse craniofacial shape variation (Nicolas Navarro, personal communication). A similar range of effects was reported for loci affecting human facial traits (Claes et al. 2014) although loci with very small effects (<1%) were not detected in that study, likely because a specific set of candidate genes with known roles in craniofacial development was interrogated.

We encourage caution when interpreting estimates of effect sizes; values are likely overestimated due to the Beavis effect (Beavis 1998). Recently, Slate (2013) showed that all QTL studies performed in wild and outbred populations have overestimated the QTL effect sizes, giving the false impression that most traits are oligogenic.

On the basis of heritability estimates and comparison with previous QTL studies of skull and mandible shape (Klingenberg *et al.* (2004) – 33 mandible QTLs, Leamy *et al.* (2008) – 36 mandible

QTLs, Leamy *et al.* (Leamy *et al.* 1999) – 26 skull QTLs), we expect the number of loci reported here is an underestimate of the total number underlying craniofacial shape variation in nature.

Candidate genes

Some of the genomic regions identified here overlap with previously identified QTL for craniofacial phenotypes (Table 1.2). However, because no previous studies have reached gene-level resolution, it is unclear whether overlap with previous QTL studies is due to the same underlying causative genes.

The inferences on the identified candidate genes are mostly derived from knockout studies. However, such studies have limited power to reveal functions of regulatory or signaling genes involved in multiple developmental processes, because many processes involved in bone shape specification occur late in development. Moreover, most standard phenotyping approaches of knockout mice do not involve the refined morphometric procedures that we have applied here and phenotypes might therefore have been missed. For example, a pilot study showed that subtle morphological phenotypes can be detected in mice heterozygous for mutations in developmental regulator genes (Boell *et al.* 2013).

Nevertheless, some genes identified here have craniofacial and skeletal phenotypes, representing strong candidates. Future studies, using more subtle approaches to manipulate these and other candidate genes derived from GWAS studies, will show if these indeed affect the anticipated phenotype.

Craniofacial morphology evolves rapidly between populations and species. Much of this evolution appears to reflect responses to the species' ecology (Boell & Tautz 2011). On the other hand, many genes influencing shape variation are highly conserved, implying that the pathways involved in craniofacial shape development may be generally conserved. Variation and rapid divergence in morphology, then, likely arises from finer details of developmental processes. The results of Attanasio *et al.* (2013) suggest that regulation by distant enhancers plays an important role in determining shape development. This may explain why some significant intervals identified here are in regions without annotated genes (Table 1.1). In addition, for intervals with candidate genes, causative mutations affecting the regulation of these or other genes should be considered in addition to mutations in coding sequence.

Region 9 encompasses a cluster of genes with known craniofacial phenotypes or roles in regulatory signaling pathways for craniofacial development. Part of this region, including the genes *Aktip*,

Rpgrip1, *Fto*, *Irx3*, *Irx5*, and *Irx6*, is deleted in *Fused toes* mice (Peters *et al.* 2002), which are characterized by neural tube defects, left-right asymmetry, polydactyly, and craniofacial defects, among other phenotypes. Experiments aimed at identifying the causative gene for this region have revealed that at least three of the genes (*Rpgrip1*, *Irx3*, *Irx5*) have individual effects on craniofacial phenotypes (Bonnard *et al.* 2012). In humans, a duplication including homologs of mouse genes in region 9 (*Rbl2*, *Aktip*, *Rpgrip1*, *Fto*) is associated with dysmorphic faces and other phenotypes (Stratakis *et al.* 2000). Region 9 contains three additional genes with well-known roles in craniofacial development (*Nkd1*, *Cyld*, *Chd9*), and the transcription factor *Zfp423*, a known regulator of BMP signaling with a complex role in brain morphogenesis that might also affect the skull (Alcaraz *et al.* 2011). Taken together, this evidence indicates region 9 may represent a hotspot of genes involved in craniofacial bone formation and shape variation.

The overlap with previous QTL studies (see results) shows that the approach taken here offers the possibility of resolving previously mapped regions, but also enables the discovery of new variants that are likely not variable among classical laboratory strains.

Conclusions

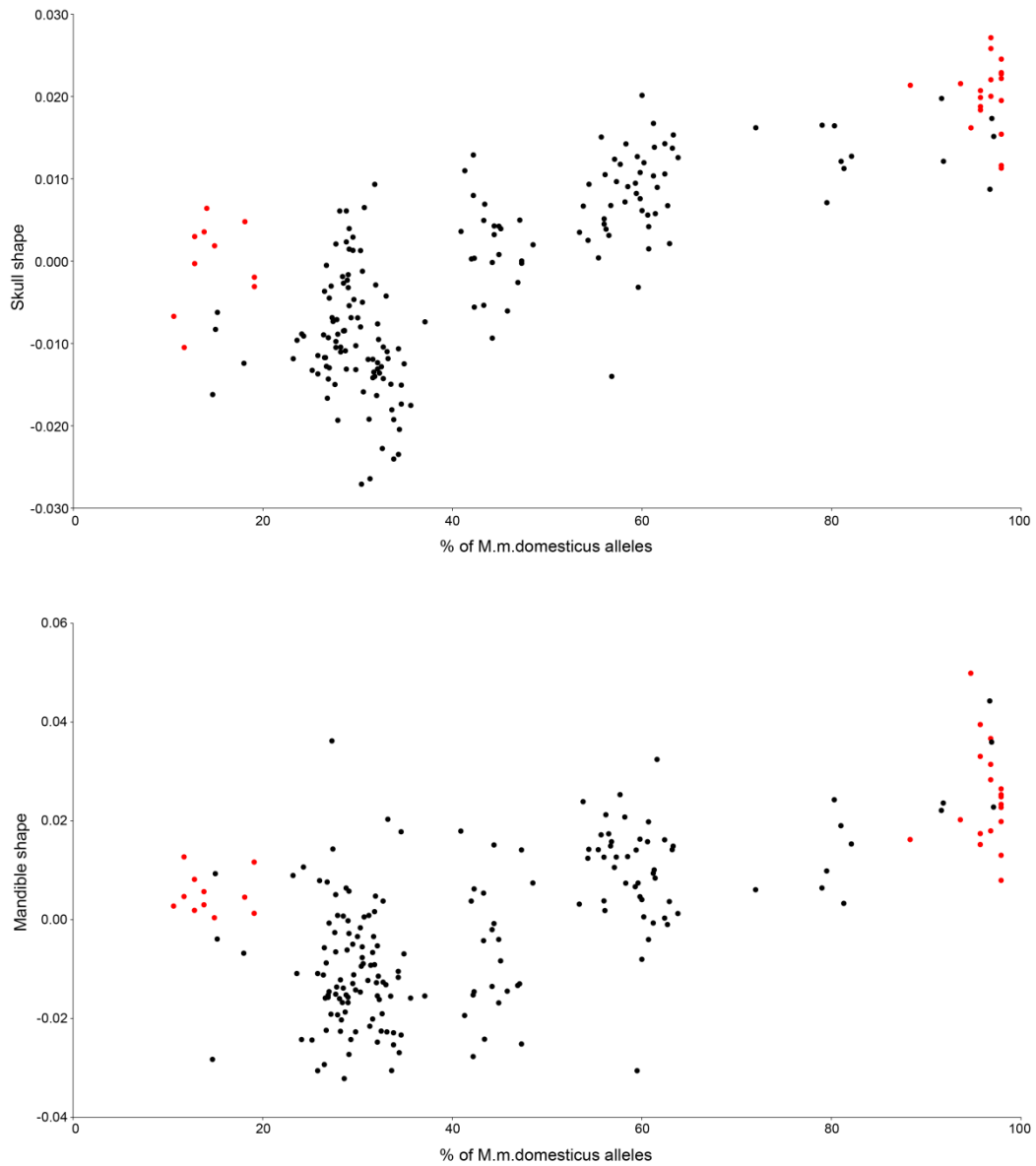
This study has achieved three main goals. First, we identified loci involved in craniofacial shape variation in wild mice. Several of these genes are strong candidates for future investigations of developmental pathways for craniofacial morphology. Moreover, because we focused on naturally occurring variation in a hybrid population between emerging species, these loci may also elucidate the evolutionary dynamics of shape diversification.

Second, we find support for a polygenic architecture underlying craniofacial morphology in mice, and generate the first estimates of craniofacial shape heritability based on a dense SNP coverage of the genome.

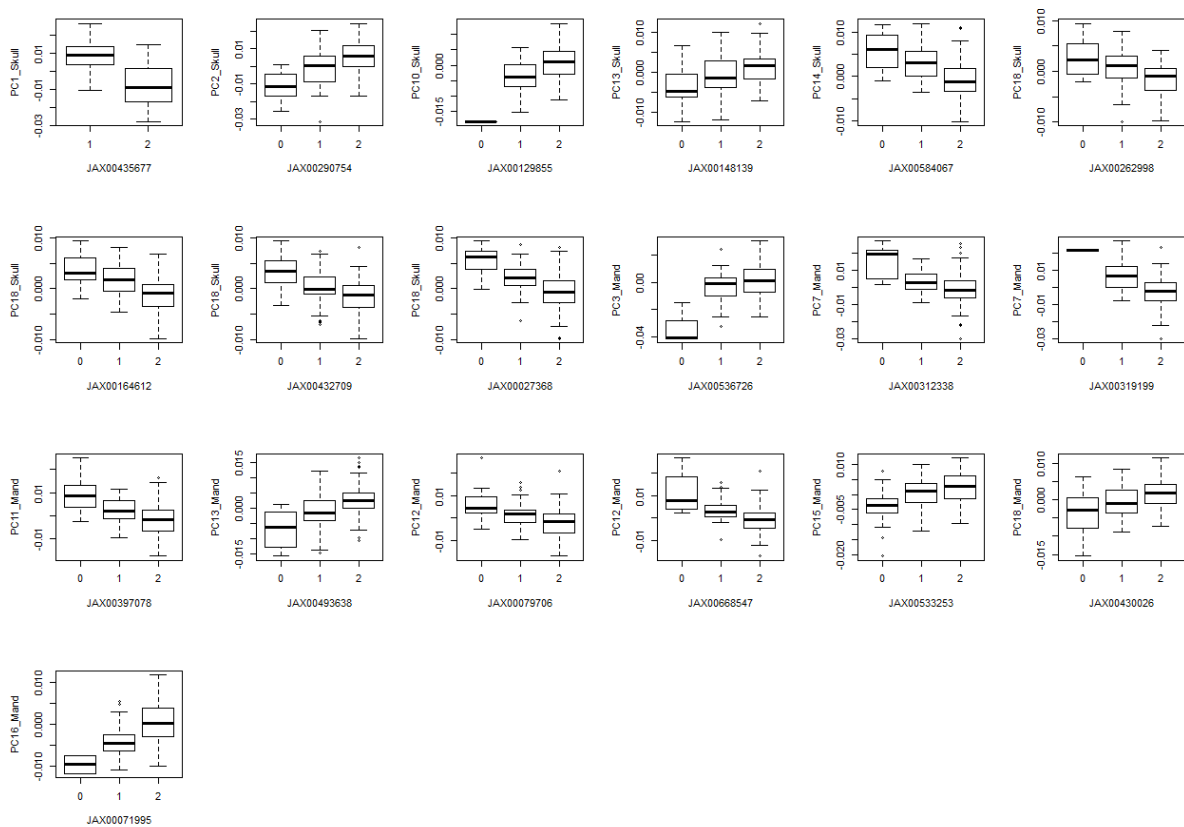
Third, we have shown the feasibility of using natural hybrid zones for exploring the genetic basis of complex traits. In a parallel study, the same mapping population was successfully used to map genes and gene interactions involved in reproductive isolation (Turner & Harr 2014). Natural hybrid zones exist for many animal and plant species and have long been recognized as a potentially powerful mapping resource. Our results encourage the use of such natural systems for future mapping studies.

Supplementary Figures

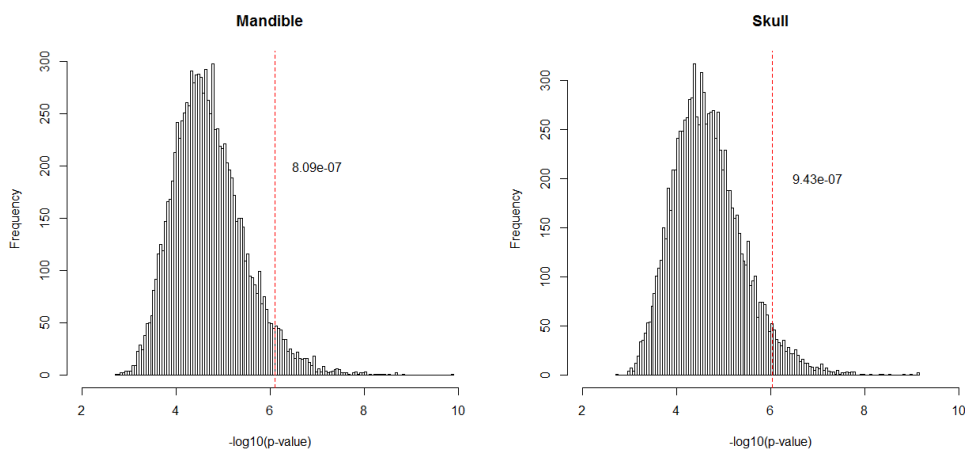
Supplementary Figure 1.1. Regression of shape scores versus percentage of *M. m. domesticus* alleles in the respective animal for the skull and the mandible. The smooth transition suggests that most phenotypic values are intermediate between the phenotypes of the subspecies, as represented by the animals from both ends of the hybrid zone. Red dots are wild caught mice without any control for environmentally-related shape variation.



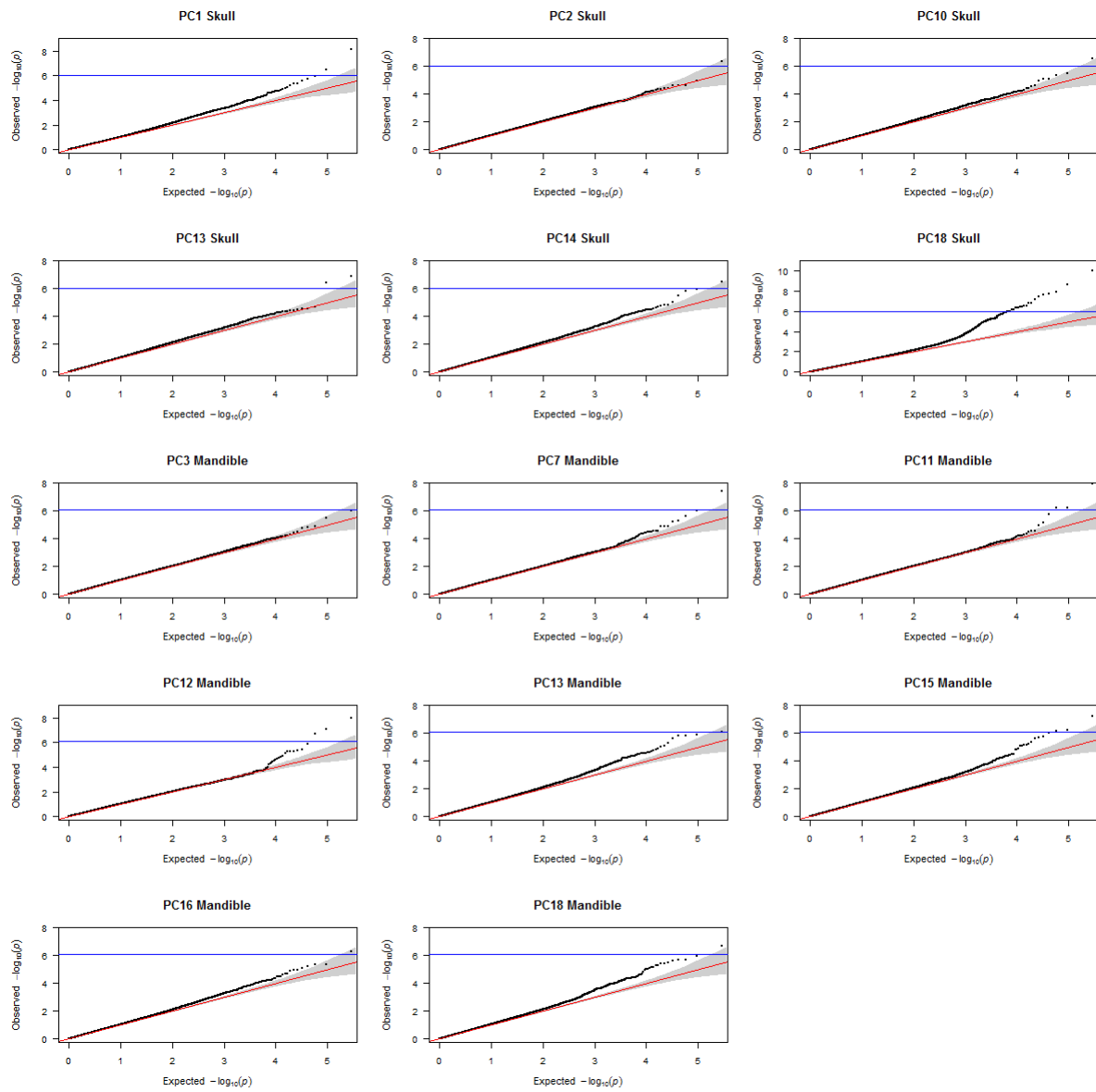
Supplementary Figure 1.2. Phenotypic effect of the significant SNPs. Only the SNP with the best p-value per interval is shown. 0 and 2, homozygote for the two alleles. 1 heterozygote.



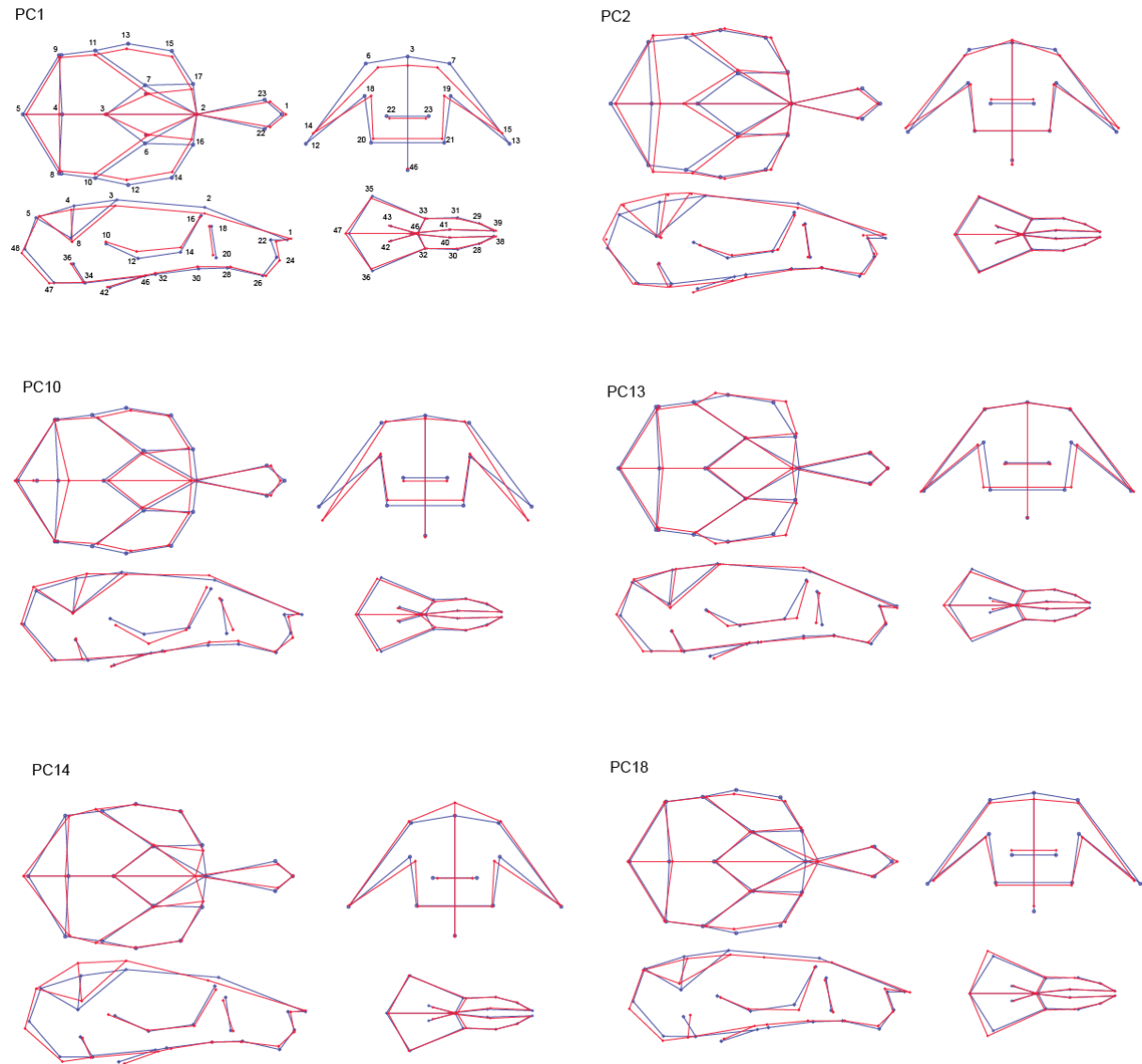
Supplementary Figure 1.3. Distribution of the best p-values of 10,000 permutations for mandible and skull. The 21 skull phenotypes (20 PC axes and 1 centroid size) were permuted and the best p-value obtained out of the 21 phenotypes was recorded, giving a total of 10,000 p-values in the 10,000 permutation rounds. The same procedure was performed with the mandible data. The 0.95 quantile indicated by the dotted line was used as the genome wide significance threshold.



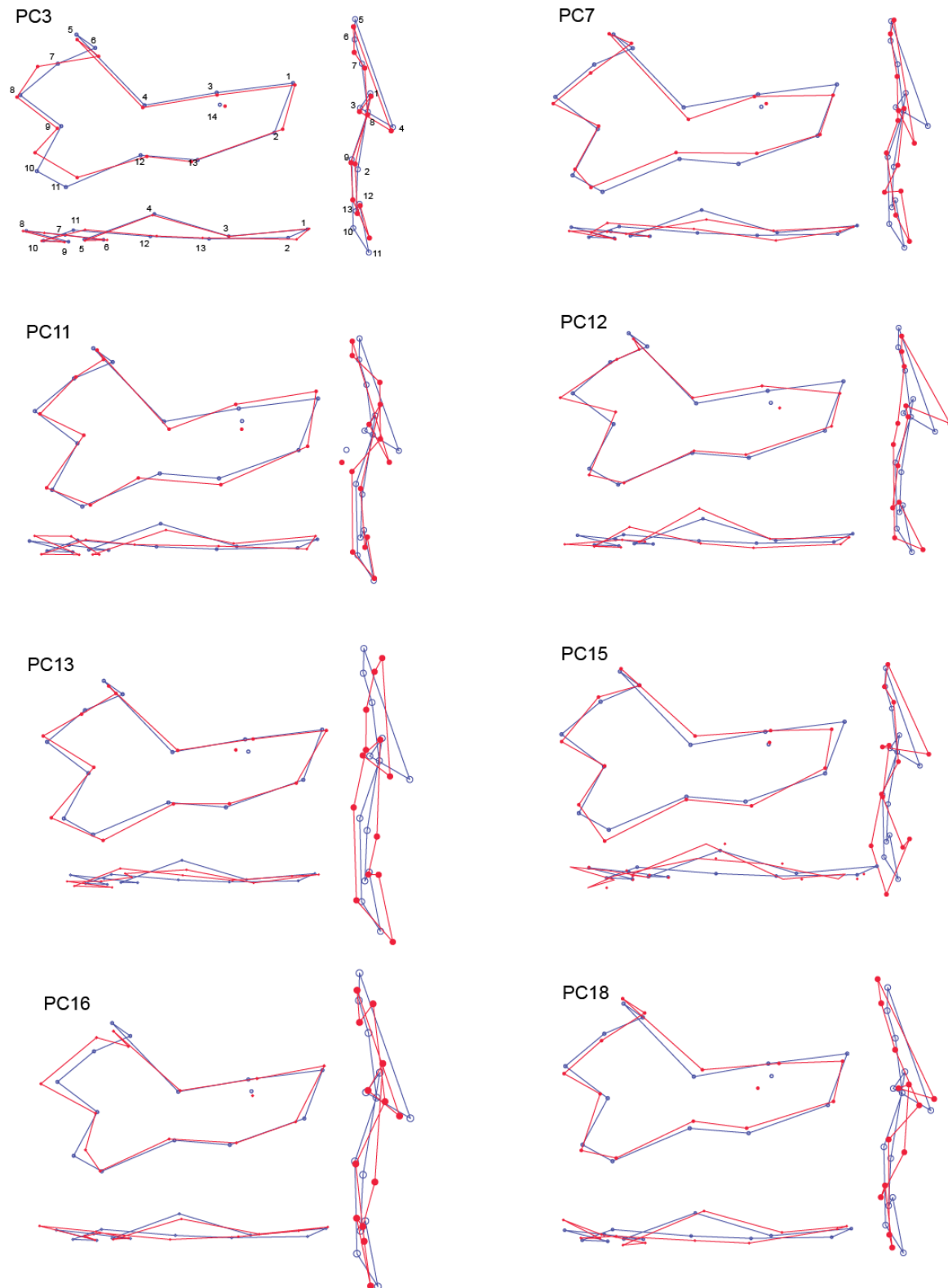
Supplementary Figure 1.4. QQ plots of the phenotypes (principal components) that showed significant association with the markers.



Supplementary Figure 1.5. Principal component axes significantly associated with genomic loci. The associated skull shape changes are shown. Blue, mean shape. Red, positive values of the PC axis. Scale factor, 0.06 units of Procrustes distance.



Supplementary Figure 1.6. Principal component axes significantly associated with genomic loci. The associated mandible shape changes are shown. Blue, mean shape. Red, positive values of the PC axis. Scale factor, 0.1 units of Procrustes distance.



Supplementary Tables

Supplementary Table 1.1 (part I). Description of the landmarks used in skull and mandible. See Figure 2 for a representation within the structures.

| Landmark | Description |
|--------------|---|
| Skull | |
| 1 | Nasal bones most anterior suture |
| 2 | Nasal bones most posterior suture |
| 3 | Frontal bones most posterior suture |
| 4 | Parietal bones most posterior suture |
| 5 | Interparietal bone most posterior point on the median line |
| 6 | Right side, most anterior point of the suture between frontal and parietal bones |
| 7 | Left side, most anterior point of the suture between frontal and parietal bones |
| 8 | Right side, intersection between parietal, occipital and squamosal bones |
| 9 | Left side, intersection between parietal, occipital and squamosal bones |
| 10 | Right, most posterior junction of squamosal bone and the zygomatic process of the squamosal bone |
| 11 | Left, most posterior junction of squamosal bone and the zygomatic process of the squamosal bone |
| 12 | Right side, most anterior suture of the zygomatic process of the squamosal bone and jugal bone |
| 13 | Left side, most anterior suture of the zygomatic process of the squamosal bone and jugal bone |
| 14 | Right side, most anterior suture of jugal bone and the zygomatic process of the maxillary bone |
| 15 | Left side, most anterior suture of jugal bone and the zygomatic process of the maxillary bone |
| 16 | Right side, intersection of the frontal, lacrimal and the zygomatic process of the maxillary bone |
| 17 | Left side, intersection of the frontal, lacrimal and the zygomatic process of the maxillary bone |
| 18 | Right infraorbital foramen most superior point |
| 19 | Left infraorbital foramen most superior point |
| 20 | Right infraorbital foramen most inferior point |
| 21 | Left infraorbital foramen most inferior point |
| 22 | Right premaxilla-right nasal bone most anterior point of suture |
| 23 | Left premaxilla-left nasal bone most anterior point of suture |
| 24 | Most superior point of the right incisor alveolus |
| 25 | Most superior edge of the left incisor alveolus |
| 26 | Most inferior point of the right incisor alveolus |
| 27 | Most inferior point of the left incisor alveolus |
| 28 | Right premaxilla-maxilla most ventral junction |
| 29 | Left premaxilla-maxilla most ventral junction |
| 30 | Most anterior point of the right first molar alveolus |
| 31 | Most anterior point of the left first molar alveolus |
| 32 | Most posterior point of the right third molar alveolus |
| 33 | Most posterior point of the left third molar alveolus |
| 34 | Most inferior point of the right external acoustic meatus |
| 35 | Most inferior point of the left external acoustic meatus |
| 36 | Most superior point of the right external acoustic meatus |
| 37 | Most superior point of the left external acoustic meatus |
| 38 | Most anterior point of the right anterior palatine foramen |
| 39 | Most anterior point of the left anterior palatine foramen |
| 40 | Most posterior point of the right anterior palatine foramen |
| 41 | Most posterior point of the left anterior palatine foramen |
| 42 | Right pterygoid process, most posterior point |
| 43 | Left pterygoid process, most posterior point |
| 44 | Median-line point of the suture between occipital and basisphenoid bones |
| 45 | Median-line point of the suture between basisphenoid and presphenoid bones |
| 46 | Most posterior point of the suture between palatine bones |
| 47 | Foramen magnum most anterior point, Basion |
| 48 | Foramen magnum most posterior point, Bregma |

Supplementary Table 1.1 (part II). Description of the landmarks used in skull and mandible. See Figure 2 for a representation within the structures.

| Landmark | Description |
|-----------------|---|
| Mandible | |
| 1 | Most superior point of the incisor alveolus |
| 2 | Most inferior point of the incisor alveolus |
| 3 | Most anterior point of the first molar alveolus |
| 4 | Most posterior point of the third molar alveolus |
| 5 | Most posterior tip of the coronoid process |
| 6 | Most anterior concave point of coronoid process |
| 7 | Most anterior point of the articular surface of the condyle |
| 8 | Most posterior tip of the condyle |
| 9 | Most anterior concave point between condyle and angular process |
| 10 | Most posterior tip of angular process |
| 11 | Most inferior point of angular process |
| 12 | Ascending ramus dorsal-most ventral point |
| 13 | Alveolar region most inferior point |
| 14 | Most anterior point of the masseteric muscle insertion into the alveolar region |

Supplementary Table 1.2. Principal components included in the mapping. The percentage of the total variation that can be explained by all the SNPs used in the mapping is shown (pve) for PCs and for centroid size.

| Skull | | | | | | |
|------------------------|------|------|------|---------|------|---------|
| PC | %var | %cum | pve | sd(pve) | pge | sd(pge) |
| PC1* | 16.6 | 16.6 | 0.93 | 0.06 | 0.57 | 0.3 |
| PC2* | 12.1 | 28.6 | 0.73 | 0.08 | 0.33 | 0.29 |
| PC3 | 7.7 | 36.3 | 0.93 | 0.06 | 0.36 | 0.28 |
| PC4 | 6.6 | 42.9 | 0.9 | 0.06 | 0.62 | 0.26 |
| PC5 | 5.9 | 48.8 | 0.79 | 0.09 | 0.33 | 0.29 |
| PC6 | 5.3 | 54.1 | 0.57 | 0.14 | 0.43 | 0.28 |
| PC7 | 4.4 | 58.6 | 0.78 | 0.11 | 0.39 | 0.29 |
| PC8 | 3.9 | 62.5 | 0.58 | 0.12 | 0.38 | 0.28 |
| PC9 | 3.4 | 65.9 | 0.69 | 0.1 | 0.4 | 0.28 |
| PC10* | 2.9 | 68.8 | 0.73 | 0.11 | 0.37 | 0.27 |
| PC11 | 2.5 | 71.3 | 0.69 | 0.12 | 0.37 | 0.28 |
| PC12 | 2.4 | 73.7 | 0.54 | 0.11 | 0.49 | 0.3 |
| PC13* | 2.3 | 75.9 | 0.53 | 0.15 | 0.4 | 0.28 |
| PC14* | 1.9 | 77.8 | 0.43 | 0.15 | 0.41 | 0.29 |
| PC15 | 1.7 | 79.5 | 0.68 | 0.12 | 0.49 | 0.28 |
| PC16 | 1.5 | 81.1 | 0.68 | 0.17 | 0.4 | 0.27 |
| PC17 | 1.3 | 82.4 | 0.34 | 0.14 | 0.44 | 0.29 |
| PC18* | 1.3 | 83.7 | 0.36 | 0.13 | 0.53 | 0.3 |
| PC19 | 1.1 | 84.8 | 0.38 | 0.14 | 0.42 | 0.29 |
| PC20 | 1 | 85.8 | 0.42 | 0.21 | 0.41 | 0.27 |
| pve of total variation | | | 64.2 | | 37.5 | |

| Mandible | | | | | | |
|------------------------|------|------|------|---------|------|---------|
| PC | %var | %cum | pve | sd(pve) | pge | sd(pge) |
| PC1 | 21.6 | 21.6 | 0.91 | 0.07 | 0.44 | 0.29 |
| PC2 | 12.8 | 34.5 | 0.89 | 0.06 | 0.21 | 0.25 |
| PC3* | 8.3 | 42.8 | 0.57 | 0.13 | 0.39 | 0.28 |
| PC4 | 7.6 | 50.4 | 0.74 | 0.09 | 0.34 | 0.29 |
| PC5 | 6.5 | 56.9 | 0.5 | 0.15 | 0.35 | 0.27 |
| PC6 | 5.5 | 62.4 | 0.92 | 0.07 | 0.24 | 0.24 |
| PC7* | 4.5 | 67 | 0.5 | 0.12 | 0.37 | 0.29 |
| PC8 | 3.7 | 70.7 | 0.65 | 0.11 | 0.33 | 0.27 |
| PC9 | 3.6 | 74.3 | 0.46 | 0.11 | 0.43 | 0.29 |
| PC10 | 3 | 77.2 | 0.38 | 0.13 | 0.4 | 0.28 |
| PC11* | 2.8 | 80.1 | 0.5 | 0.13 | 0.37 | 0.28 |
| PC12* | 2.1 | 82.1 | 0.36 | 0.12 | 0.34 | 0.28 |
| PC13* | 2 | 84.1 | 0.46 | 0.16 | 0.48 | 0.29 |
| PC14 | 1.8 | 85.9 | 0.68 | 0.11 | 0.33 | 0.27 |
| PC15* | 1.7 | 87.7 | 0.44 | 0.15 | 0.44 | 0.28 |
| PC16* | 1.4 | 89 | 0.43 | 0.18 | 0.4 | 0.28 |
| PC17 | 1.4 | 90.4 | 0.44 | 0.14 | 0.4 | 0.28 |
| PC18* | 1.2 | 91.5 | 0.41 | 0.14 | 0.46 | 0.3 |
| pve of total variation | | | 63.9 | | 33 | |

| | | | | | |
|---------------|--|----|----|----|----|
| Centroid Size | | 75 | 16 | 37 | 27 |
|---------------|--|----|----|----|----|

| | | | | |
|---------------|----|----|----|----|
| Centroid Size | 72 | 16 | 33 | 25 |
|---------------|----|----|----|----|

*indicates the PCs with significant associations. %var, percentage of total phenotypic variation explained by each PC. %cum, cumulative variation. Pve, proportion (from 0 to 1) of the variation in each PC explained by all the SNPs used in the mapping (“chip heritability”). Pve of total variation, percentage of the total phenotypic variation in the mapping population explained by all the SNPs used in the mapping, $\sum_1^n(pve * \%var)$, n= number of PCs. Pge, proportion (from 0 to 1) of the variation in each PC that can be explained by SNPs of large effect. Sd, standard deviation. Pve and pge values were calculated using the BSLMM model from GEMMA.

Mapping of craniofacial traits in outbred mice identifies major developmental genes involved in craniofacial formation

Introduction

Understanding the evolutionary processes that have generated and maintained the morphological diversity in nature is a long standing goal in biology. And how the three dimensional shape of a structure such as the cranium is generated is still a largely unresolved problem in developmental biology. To approach these questions, we need to understand the genetic architecture underlying morphological differences. Among the crucial basic questions to address this problem are how many and which genes underlie morphological variation, as well how big is their individual effect on the phenotype

Craniofacial shape in vertebrates is a particularly challenging problem regarding morphological diversity, and is of special interest for evolution and adaptation to new environments. The fact that the cranial and mandible bones have to be perfectly integrated with the brain and sensory systems, as well as with the respiratory and digestive systems, makes this structure a prime example of both high integration and high evolvability.

Several experimental approaches have previously explored aspects of the genetic basis of craniofacial variation in animals, e.g. in Darwin finches (Abzhanov *et al.* 2006; Abzhanov *et al.* 2004; Lamichhaney *et al.* 2015), in cichlids (Albertson *et al.* 2003; Albertson *et al.* 2005), in dogs (Boyko *et al.* 2010; Schoenebeck *et al.* 2012; Schoenebeck & Ostrander 2013), and in mice (Attanasio *et al.* 2013; Boell *et al.* 2011; Burgio *et al.* 2009; Klingenberg *et al.* 2004; Leamy *et al.* 1997; Maga *et al.* 2015; Pallares *et al.* 2014). The work has been fueled by the developments in geometric morphometrics, which provides the tools and concepts to measure and compare subtle shape variation (Klingenberg 2010). In human craniofacial shape studies, the interest has also shifted from the study of phenotypes related to diseases to the exploration of non-disease-related natural facial variation (Boehringer *et al.* 2011; Claes *et al.* 2014; Liu *et al.* 2012; Paternoster *et al.* 2012).

Early work in mice has focused on the mandible, which is a well-established model for the study of complex traits since mandible shape can be approximated in two dimensions (Atchley & Hall 1991; Klingenberg & Navarro 2012). Several QTL studies have explored mandible shape variation in 2D and have identified several genomic regions underlying variation mostly between inbred lines of mice. The skull has been less studied due to its high complexity and the requirements for an appropriate phenotyping (2D vs 3D), but recently Burgio *et al.* (2009), Pallares *et al.* (2014), and Maga *et al.* (2015) have undertaken the task of identifying the genomic regions underlying 3D skull variation in mice. In our previous study (Pallares *et al.* 2014) we used natural recombinants from a hybrid zone between the house mouse subspecies for a genome-wide associations study (GWAS), based on using the axes from a principal component analysis (PCA) as phenotypes for mapping. This allowed the identification of candidate regions with much higher resolution than conventional QTL studies (Maga *et al.* (2015)).

GWAS approaches not only improve the mapping resolution but, together with the new tools developed to analyze such data, also allow asking and answering new types of questions. Most of these new developments come from the extensive studies of the genetic basis of human height. Most importantly, it was shown that by decomposing the total genetic variance into individual chromosomes it is possible to assess the polygenicity of a trait (Yang *et al.* 2011d). Yang *et al.* (2011d) showed that the genetic variance for human height scales with chromosomal length, indicating that the trait is highly polygenic with individual loci having very small effect on the phenotype. By simultaneously modeling the effect of all the SNPs used in a GWAS, instead of looking only for individual effects, it is possible to estimate the variance in the trait explained by the SNPs (Yang *et al.* 2010). This estimate is known as “SNP heritability” or “chip heritability” (Wray *et al.* 2013) and has helped to reframe the problem of the “missing heritability” in studies of human height (Wood *et al.* 2014; Yang *et al.* 2010), where only a small proportion of height heritability could be accounted for with the genome-wide significant loci identified by GWAS. These tools can now be applied to other organisms and other types of complex traits. Recently they have been used for the study of morphological traits in mice (Pallares *et al.* 2014), great tit (Robinson *et al.* 2013), and soay sheep (Béréanos *et al.* 2015), revealing the highly polygenic nature of craniofacial shape, wing length, and mandible length, respectively.

However, the utility of mapping studies to the understanding of the evolution of complex traits has been questioned (Donnelly 2008; Rockman 2012). Regarding complex traits, it was claimed that the identification, if possible in the first place, of thousands of variants involved in the trait could obscure any biological interpretation (Donnelly 2008), and even the identification of such variants

was considered an almost impossible task (Rockman 2012). But it has now been shown that data derived from GWAS of complex traits such as human height, may help indeed to reveal previously unknown genes and networks of genes underlying complex traits, even in the situation where a quasi-infinitesimal architecture is the norm (Lango Allen *et al.* 2010; Wood *et al.* 2014).

Previous studies in mice addressed the question of shape variability in inbred lines, in interspecific congenic strains or wild hybrid mice. Here, we approach the question from a micro-evolutionary perspective by analyzing within-population shape variation. The relevance of studying phenotypic variation at the within-population level has been well acknowledged (Nunes *et al.* 2013). Unlike the study of variation between far distant species, information at the population level allows the assessment of the mechanistic basis that generate phenotypic variation (Nunes *et al.* 2013).

We use here a population of “Carworth Farms White” CFW outbred mice. Its suitability for genome-wide mapping was previously described (Yalcin *et al.* 2010). Importantly, the mice used in this study do not show evidence of widespread population stratification or cryptic relatedness. The high number of recombination events in the history of this population has resulted in small linkage blocks, which, together with the above mentioned factors, result in high mapping resolution (Yalcin *et al.* 2010).

Methods

Mapping population

Male mice from the CFW mouse colony maintained by Charles River Laboratories were used to perform a genome-wide association mapping. On their arrival to the University of Chicago, the mice were subjected to behavioral and physiological tests during 2011 and 2012 (results from these tests will be published elsewhere). At the end of these experiments, the mice were sacrificed and their heads were stored in ethanol. The average age at the time of sacrifice was 13 weeks (ranging from 12 to 14 weeks). All procedures were approved by the University of Chicago Institutional Animal Care and Use Committee (IACUC) in accordance with National Institute of Health guidelines for the care and use of laboratory animals. The measurements of the skull and mandible were done for 710 individuals between 2013 and 2014 at the Max Planck Institute for Evolutionary Biology in Plön, Germany.

Shape phenotyping

Mouse heads were scanned using a computer tomograph (micro-CT—vivaCT 40; Scanco, Bruettisellen, Switzerland) at a resolution of 48 cross-sections per millimeter. 44 three-dimensional landmarks were located in the skull and 13 in each hemimandible using the TINA landmarking tool (Schunke *et al.* 2012) (suppl. Table 2.1 and suppl. Figure 2.1). The semi-automatic landmark annotation extension implemented in the TINA landmarking tool was used to reduce digitation error and to speed up the phenotyping process (Bromiley *et al.* 2014). All further morphometric analyses were performed using MorphoJ (Klingenberg 2011). The raw 3D landmark coordinates obtained in TINA tool were exported to MorphoJ. The symmetric component of the mandible and skull were obtained following Klingenberg *et al.* (2002). In short, right and left hemimandibles were averaged; a mirror image of the skull was generated and overlapped with the original, the average of these two images was used for following analyses. The averaged landmark coordinates were used in a generalized Procrustes analysis (GPA). This analysis eliminates the variation due to size, location, and orientation of the specimens, and generates a new dataset that only contains shape variation. The new landmark coordinates generated after the GPA are called Procrustes coordinates. The Procrustes coordinates were used in a principal component analysis (PCA) and the PC scores were used as phenotypes in the mapping. The differences in age, spanning 2 weeks, did not correlate significantly with shape variation and were therefore not used as covariate.

CFW mice exhibit abnormal bone mineral density (BMD), representing excessive bone mineralization. A qualitative analysis of mice with high BMD showed obvious differences in the mandible, and moderate ones in the skull compared to mice with normal BMD. We have therefore explored the covariation of BMD with shape measurements, separately for the skull and the mandible.

For the skull, we found only a small correlation between BMD and shape ($r^2=1.4\%$, $p < 0.001$, based on 10,000 permutations). No individual PC axis captured the shape differences due to BMD. BMD was therefore not used as covariate for skull trait mapping to avoid reducing the mapping power.

For the mandible, there was a higher correlation between shape and BMD ($r^2 = 6\%$, $p < 0.001$, based on 10,000 permutations), with the effect of BMD explaining 29% of the variation in the first principal component, but with no strong effect in other PCs. The residuals of the multivariate regression of mandible shape vs BMD were therefore used in a principal component analysis (PCA), and PC scores were used as phenotypes in the mapping.

Size phenotyping

The standard measure of size in geometric morphometrics is the centroid size (CS) and this was used for mapping. It is estimated as the square root of the sum of the squared distances of a set of landmarks from the center of gravity or centroid (Zelditch *et al.* 2012). The CS for mandible was calculated as the average of the CS of right and left hemimandible. The skull CS is calculated using all landmarks from right and left sides (Klingenberg *et al.* 2002). All calculations were done in MorphoJ.

Genotyping

The mice were genotyped using a genotyping-by-sequencing (GBS) approach, rendering a set of 92,374 SNPs, of which 14% (13,450) are private to this population (details will be published elsewhere). In short, GBS libraries were prepared by digesting genomic DNA with the restriction enzyme PstI and annealing oligonucleotide adapters to the resulting overhangs. Samples were multiplexed 5 per lane, and sequenced on an Illumina HiSeq 2500 sequencer using single-end 100-bp reads. By focusing the sequencing effort on the PstI restriction sites, we obtained high coverage at a subset of genomic loci. The 100-bp single-end reads were aligned to the Mouse Reference Assembly 38 from the NCBI database (mm10) using bwa (Li & Durbin 2009). We used GATK (McKenna *et al.* 2010; Van der Auwera *et al.* 2013) to discover variants and call genotypes. For the Variant Quality Score Recalibration (VQSR) step, we calibrated variant discovery against (1) whole-genome sequencing (WGS) data that we ascertained from a small set of CFW mice, (2) SNPs and indels from the Wellcome Trust Sanger Mouse Genome project (Keane *et al.* 2011), and SNPs available in dbSNP release 137. We used IMPUTE2 (Howie *et al.* 2009) to impute low-confidence genotypes, or genotypes that were not called in some mice. A small number of SNPs for which a large proportion of the genotypes were imputed with low certainty were discarded from the study; SNPs with MAF > 0.02 were included in the mapping.

Association mapping

710 mice were used for the mapping of skull traits –shape and size, and 590 mice for mandible traits. Due to the correlation between BMD and mandible shape, only the 590 mice with BMD phenotype

were included in the mapping of mandible shape and size. After quality control, around 80,000 SNPs were included in the mapping.

The principal component axes (PCs) explaining at least 1% of the total phenotypic variation in the mapping population were included in the mapping: 22 PCs representing 84% of skull shape variation, and 21 PCs representing 94% of mandible shape variation. Each PC axis was mapped separately. To map size variation, the centroid size of mandible and skull was used.

We used the linear mixed model (LMM) implemented in GEMMA (Zhou & Stephens 2012) to map the phenotypes, and at the same time to correct for the residual population structure that might still be present in the mapping population. Although the mice are not siblings or half-siblings, some level of p-value inflation was detected when running the mapping without accounting for population structure (not shown). The support for a given SNP was based on the p-value calculated from the likelihood-ratio test in GEMMA.

Proximal contamination is a term coined to represent the loss in power to detect a QTL when the causal marker is included in the calculations of the kinship matrix (Cheng *et al.* 2013; Listgarten *et al.* 2012). To address this problem we used the 'leave one chromosome out' (LOCO) approach in which each chromosome is analyzed using a kinship matrix that does not include any SNPs on the chromosome being scanned (Parker *et al.* 2014).

The heritability of skull and mandible shape and size were estimated with the LMM implemented in GEMMA. We showed previously that craniofacial shape and size are highly polygenic traits (Pallares *et al.* 2014), and therefore LMM and the Bayesian model perform similarly (data not shown). The estimates of heritability correspond to the percentage of phenotypic variation that can be explained with the SNPs used in the mapping; this estimate is known as "SNP heritability" (Wray *et al.* 2013). The total heritability of craniofacial shape was calculated as the weighted sum over all PCs. The weight is given by the percentage of total phenotypic variation explained by each PC (suppl. Table 2.2 and 2.3). The 95% confidence interval was calculated in the same way, but using the 95% lower and upper heritability estimates per PC. The effect size of significant SNPs was calculated using the R^2 value from the *lm()* in R (R-Core-Team 2013).

Significance of SNP associations

A genome-wide significant threshold was calculated for each of the phenotypes used in the mapping (43 PCs and centroid size). The individual phenotypes were permuted 1,000 times and the distribution of minimum p-values was calculated. The significance threshold was defined as 95% of the null distribution. The average 95th percentile for all phenotypes was 8.9×10^{-7} ($-\log(p)$ of 6.04, ranging from 5.97 to 6.16). This average value is used in Figure 2.1, but the exact threshold per phenotype was used to define the significant associations.

The LD pattern around the significant SNPs was used to define the significant regions. A correlation value $r^2 \geq 0.8$ between the focal SNP (most significant SNP) and the neighboring SNPs was used as delimiter. Genes falling in such regions were explored using the MGI database (Eppig *et al.* 2012) and a literature research to search for suitable candidates.

Overlap with previous studies

The overlap with previous studies was calculated by defining 500Kb and 1Mb windows around the best SNP of each of the 31 significant regions identified in this study. The window size was chosen based on the mean size of the significant regions (0.89Mb - see above for the way the regions were defined). Once the “true” overlap was determined, 31 genomic regions of 500Kb and 1Mb were randomly chosen from the genome and the overlap with previous studies was re-calculated. This was repeated 1,000 times to exclude the possibility that the global pattern of overlap was due to chance (suppl. Figure 2.3).

Chromosomal partition of the variance

The proportion of phenotypic variation explained by each chromosome was calculated using the restricted maximum-likelihood analysis implemented in GCTA (Yang *et al.* 2011). The first 10 principal components of the kinship matrix were included as covariates. An individual REML analysis was done for each chromosome (option `-reml -grm -qcovar`). Due to the small sample size of this study (~700 mice) it is not possible to fit all the chromosomes at the same time, this results in an inflation of the individual chromosomal estimates. We therefore used the relative (dividing by the

variation explain by all chromosomes together) and not the absolute contribution of each chromosome to the total phenotypic variation.

Because principal components (PCs) were used as phenotypes, additional calculations were needed to estimate the chromosomal contribution to the global phenotypes –skull and mandible shape. The additive variance per chromosome per PC was multiplied by the percentage of phenotypic variation represented by that PC. Finally, the values for each chromosome were summed across all PCs.

Results

We performed a genome-wide association mapping for skull and mandible shape (Figure 2.1) as well as size. Shape is represented by a multivariate vector of 132 dimensions (y, x, z coordinates of 44 landmarks) for skull, and 39 dimensions for mandible (y, x, z coordinates of 13 landmarks). To make the data suitable for GWAS analyses, a principal component analysis (PCA) was done and the dimensionality of shape data was reduced by using only a subset of principal component axes (PCs) as phenotypes in the mapping.

Skull shape variation was mapped using 22 PCs representing 84% of the total variation in the mapping population. The mapping of mandible shape was done with 21 PCs representing 94% of the total mandible shape variation.

Heritability of individual PCs

The heritability of individual principal component axes was calculated using the LMM implemented in GEMMA (suppl. Tables 2.2 and 2.3). The heritability estimate corresponds to the percentage of phenotypic variance explained by all SNPs used in the mapping, known as “SNP heritability” (Wray *et al.* 2013). Only one out of 21 PCs for mandible and one out of 22 PCs in skull had heritability lower than 20%. 5 PCs show heritability higher than 60%. There is a weak but significant correlation between the percentage of phenotypic variation explained by each PC and its heritability estimates (Figure 2.2).

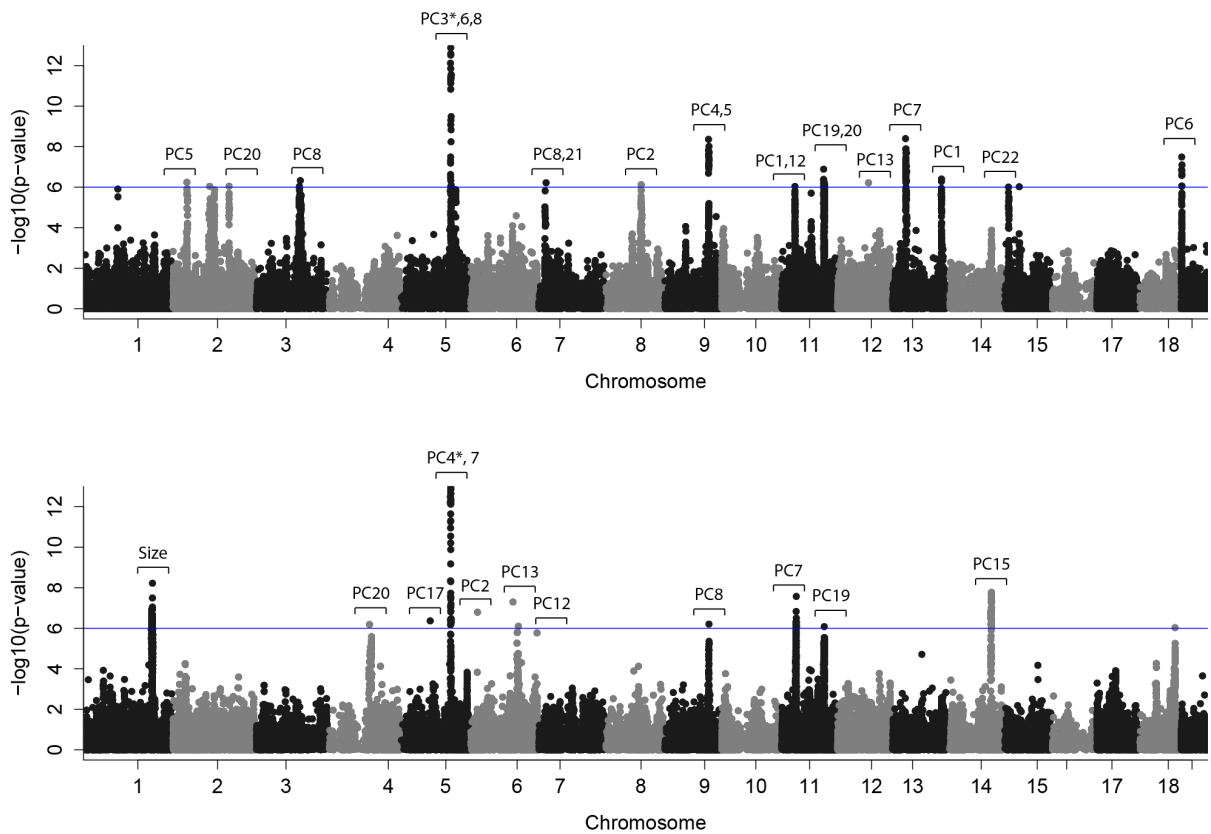


Figure 2.1. Manhattan plot showing the significant associations for mandible and skull. The associated phenotype (PC axes or centroid size) is shown for each QTL. The blue line represents a global significant threshold of $1e-6$ (LOD=6), but the threshold varies depending on the specific PC (average LOD=6.05, min=5.95, max=6.16). SNPs near the blue line without label didn't cross the significant threshold for the specific phenotype. * To improve visualization, the real LOD score is not shown; PC4* LOD=26.6, PC3* LOD=14.8.

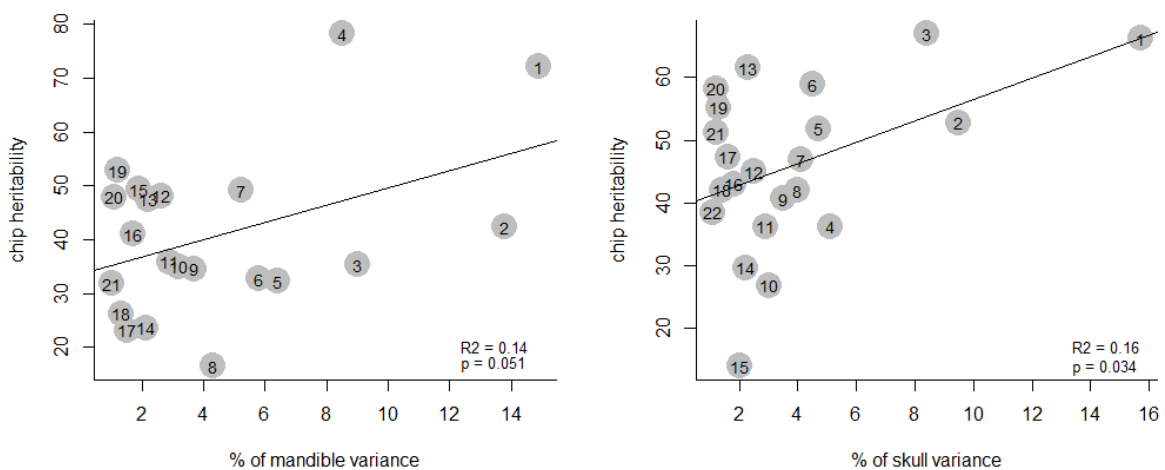


Figure 2.2. Relationship between the SNP heritability of the PC axes and the percentage of total phenotypic variation accounted by the PC axes. The numbers in the plot indicate the PC axis.

Heritability of craniofacial shape and size

Combining the estimates of individual PCs, the SNP heritability of mandible and skull shape was estimated (see Methods). The 80K SNPs used in the mapping explain 43.6% (95% confidence interval 23.6 - 63.6) of mandible variation and 42.4% (27.1 - 58.6) of skull variation. Mandible size has a SNP heritability of 36.4% (16.4 – 56.4) and skull size of 35.4 (15 – 55.8).

Genomic regions associated with craniofacial size and shape

Based on the LD patterns, the SNPs crossing the permutation-derived significance threshold of 8.9×10^{-7} were grouped in 30 regions; 19 regions associated with skull shape (Table 2.1) and 11 with mandible shape (Table 2.2). One region was significantly associated with mandible size. No association was found for skull size (centroid size CS). 22 out of the 31 significant regions overlap with previous studies (See Table 2.1 and Table 2.2).

13 out of the 22 PCs used to map skull shape, and 10 out of the 20 PCs used in the mapping of mandible shape showed a significant association with one or more genomic regions (see Table 2.1 and 2.2, Figure 2.1). The phenotypic variance represented by the associated PCs ranges from high (e.g. PC1skull – 15.8%, PC2mand – 13.8%) to low (e.g. PC20skull – 1.24%, PC20mand –1.1%). Suppl. Figures 4-9 show the skull and mandible shapes associated with the significant PC.

In many cases multiple QTLs were found in the same chromosome (chr2, 5, 6, 11, 13), but associated with different phenotypes (PC axes) (Figure 2.1). More interestingly, five QTLs were associated with more than one phenotype; two of them were associated with traits from skull and mandible (chr5 and chr9).

The 19 QTLs identified for skull shape explain 3.9% of skull variation. The 11 QTLs for mandible shape explain 2.2% of mandible variation. The effect size of individual SNPs ranges from 0.02 to 1.13% of the total phenotypic variation (Table 2.1 and 2.2, Figure 2.5). The single QTL found for mandible size explains 4.1% of size variation.

Table 2.1. Significant SNPs associated with skull shape. The most significant SNP per region, its position, p-value, and the percentage of total skull shape variation accounted by the SNP (%var) are shown.

| Region | Skull | Chr | Pos | SNP | p-value | %varPC | %varSkull | Candidate genes |
|-------------|-------|-----|-----------|-----------------|----------|--------|-----------|--------------------|
| 1 | PC1 | 11 | 32367260 | rs258942042 | 9.13E-07 | 1.91 | 0.30 | Sh3pxd2b |
| 2†* | PC1 | 13 | 110231696 | rs245694506 | 3.93E-07 | 3.86 | 0.61 | Rab3c, Plk2, Pde4d |
| 3 | PC2 | 8 | 80889309 | rs228570244 | 7.54E-07 | 3.03 | 0.29 | Gab1, Inpp4b |
| 4** | PC3 | 5 | 111328046 | rs33702397 | 2.18E-27 | 13.46 | 1.13 | Mn1 |
| 5†** | PC4 | 9 | 99713529 | rs30491142 | 9.69E-09 | 3.94 | 0.20 | Cldn18 |
| 6** | PC5 | 2 | 33284278 | rs27194486 | 5.74E-07 | 3.01 | 0.14 | Lmx1b |
| 7†** | PC5 | 9 | 98588137 | rs13466556 | 4.35E-09 | 4.61 | 0.22 | Foxl2 |
| 8* | PC6 | 5 | 111626960 | rs254983846 | 1.53E-08 | 2.92 | 0.13 | Mn1 |
| 9* | PC6 | 19 | 4165856 | rs37378594 | 3.24E-08 | 3.25 | 0.14 | - |
| 10†* | PC7 | 13 | 31734894 | cfw-13-31734894 | 4.00E-09 | 4.37 | 0.18 | Foxf2, Foxc1 |
| 11†* | PC8 | 3 | 98931976 | rs30352013 | 4.71E-07 | 2.48 | 0.10 | Tbx15 |
| 12* | PC8 | 5 | 110918274 | rs227631022 | 2.63E-09 | 4.12 | 0.16 | Mn1 |
| 13 | PC8 | 7 | 18801571 | rs217020288 | 6.02E-07 | 2.57 | 0.10 | - |
| 14 | PC12 | 11 | 32423285 | rs26862534 | 9.48E-07 | 2.45 | 0.06 | Sh3pxd2b |
| 15* | PC13 | 12 | 70834268 | rs49300701 | 6.03E-07 | 1.96 | 0.05 | |
| 16* | PC19 | 11 | 95634099 | rs26992385 | 8.83E-07 | 2.23 | 0.03 | - |
| 17 | PC20 | 2 | 83096089 | rs46747509 | 9.08E-07 | 2.44 | 0.03 | Itgav |
| 18* | PC20 | 11 | 94881746 | rs50079241 | 1.29E-07 | 3.00 | 0.04 | Col1a1, Dlx3 |
| 19* | PC22* | 15 | 11384042 | rs31584944 | 9.85E-07 | 2.79 | 0.03 | Npr3 |

PC, principal component axis. %varPC is the percentage of variation in the PC explained by the SNP. %varSkull was calculated by multiplying the %varPC with the percentage of the total phenotypic variance associated with the PC. The candidate genes were identified based on their role in bone morphogenesis (see methods).

† Regions that overlap with Maga *et al* 2015

* Regions that overlap with Attanasio *et al* 2014 using a window of 500Kb around the focal SNP

** Regions that overlap with Attanasio *et al* 2014 using a window of 1Mb around the focal SNP

Table 2.2. Significant SNPs associated with mandible shape. The most significant SNP per region, its position, p-value, and the percentage of total skull shape variation accounted by the SNP (%var) are shown.

| Region | Mandible | Chr | Pos | SNP | p-value | %varPC | %varMand | Candidate genes |
|--------|----------|-----|-----------|----------------|----------|--------|----------|-----------------|
| 1 | PC2 | 6 | 17952652 | rs33584134 | 1.61E-07 | 3.84 | 0.53 | - |
| 2* | PC4 | 5 | 111018365 | rs33217671 | 1.66E-15 | 8.34 | 0.71 | Mn1 |
| 3* | PC7 | 5 | 111426493 | rs33614268 | 7.63E-10 | 4.75 | 0.25 | Mn1 |
| 4* | PC7 | 11 | 35295119 | rs28219152 | 2.66E-08 | 4.77 | 0.25 | |
| 5†** | PC8 | 9 | 99595168 | rs29977169 | 6.18E-07 | 2.45 | 0.10 | Cldn18 |
| 6 | PC12 | 6 | 107312800 | rs36343125 | 7.93E-07 | 4.11 | 0.11 | - |
| 7 | PC13 | 6 | 95544081 | cfw-6-95544081 | 5.02E-08 | 3.78 | 0.08 | Suclg2 |
| 8 | PC15 | 14 | 98935309 | rs237064333 | 1.68E-08 | 3.65 | 0.07 | Klf5 |
| 9* | PC17 | 5 | 66618981 | cfw-5-66618981 | 4.30E-07 | 2.41 | 0.04 | - |
| 10‡** | PC19 | 11 | 96261688 | rs233696367 | 8.25E-07 | 2.93 | 0.03 | Hoxb cluster |
| 11† | PC20 | 4 | 90510654 | rs221759350 | 6.48E-07 | 2.13 | 0.02 | - |
| 12* | CS | 1 | 153481175 | rs32618422 | 5.96E-09 | 4.09 | 0.04 | |

PC, principal component axis. CS, centroid size. %varPC is the percentage of variation in the PC explained by the SNP. %varMand was calculated by multiplying the %varPC with the percentage of the total phenotypic variance associated with the PC. The candidate genes were identified based on their role in bone morphogenesis (see methods).

† Regions that overlap with Maga *et al* 2015

‡ Region that overlap with Pallares *et al* 2014

* Regions that overlap with Attanasio *et al* 2014 using a window of 500Kb around the focal SNP

** Regions that overlap with Attanasio *et al* 2014 using a window of 1Mb around the focal SNP

Chromosomal partition of the variance

Partitioning the variance across all chromosomes shows almost all of them contribute to shape variation (Figure 2.3). Accordingly, we find also a correlation with chromosome size, but this is significant only for mandible shape (Figure 2.3b). A positive correlation between chromosomal contribution and length indicates that the genomic distribution of the loci involved in the phenotype is more or less random. It also indicates that the trait is influenced by many loci of small effect. In our previous study we found a highly significant correlation for both, mandible and skull shape (Pallares *et al.* 2014). The weaker correlation in the present study is likely due to lower and somewhat uneven marker coverage, which is in itself not strongly correlated with chromosome length (suppl. Figure 2.2). In particular, chromosome 16 is underrepresented with respect to marker coverage; the fact that this chromosome contributes only very little to the phenotypic variance (Figure 2.3) may be due to this technical reason.

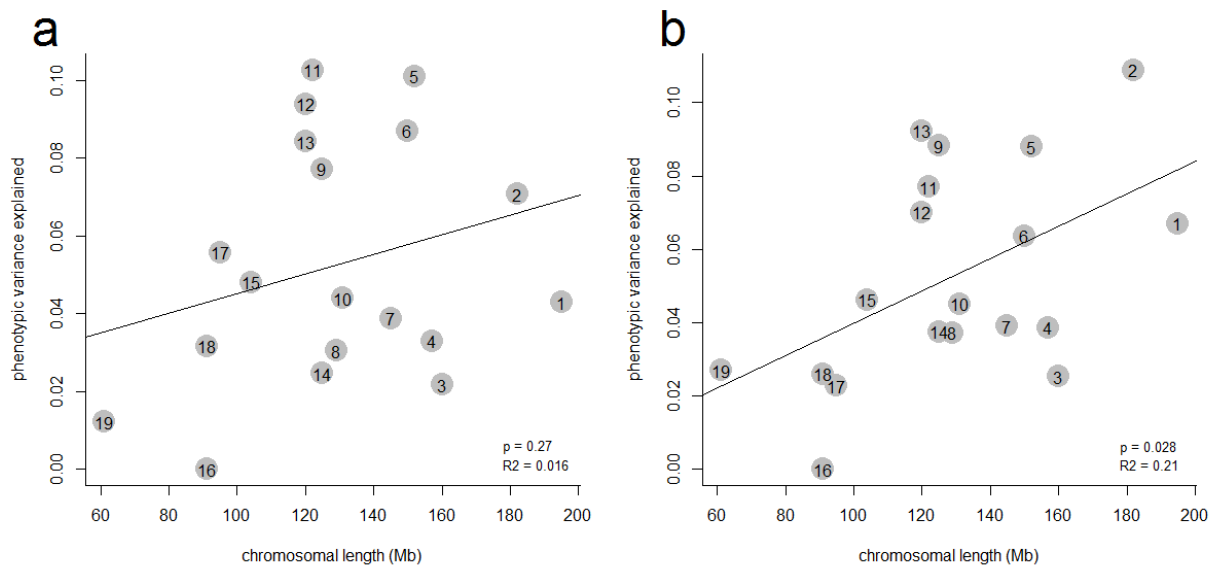


Figure 2.3. Chromosomal partition of the variance. The contribution of each chromosome to (a) skull and (b) mandible shape variation and its correlation with the length of the chromosome is shown.

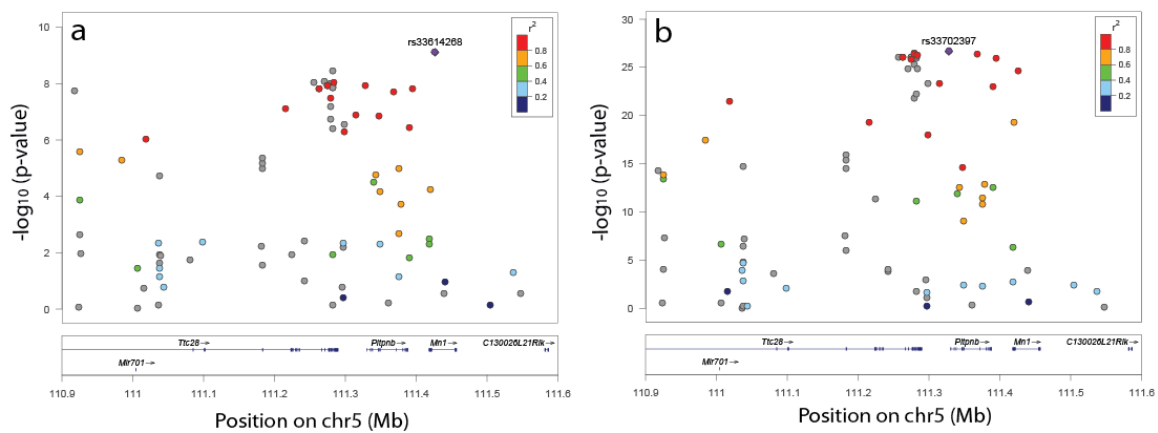


Figure 2.4. Regional plot of the associations signal for PC7-mandible (a) and PC3-skull (b). Both phenotypes are associated with the same genomic region.

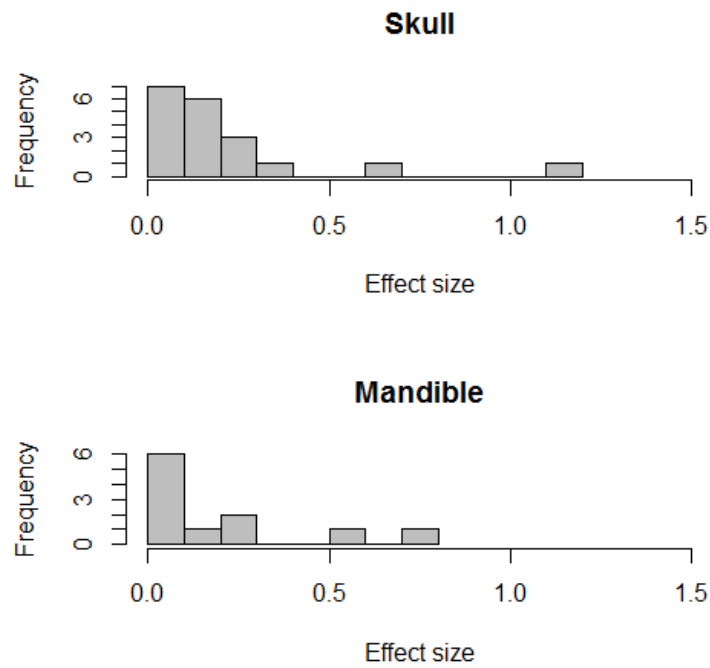


Figure 2.5. Effect size of the best SNPs (most significant) associated with skull and mandible shape.

Candidate genes

The 30 QTLs associated with craniofacial shape harbor 136 protein coding genes (suppl. Tables 2.4 and 2.5). For most of the regions clear candidate genes could be identified based on previously reported craniofacial phenotypes or role in bone morphogenesis. Table 2.3 lists the functional information available for these genes, most of which are transcription factors or known regulators of developmental signaling cascades.

Discussion

The number of regions identified in this study, together with the excellent mapping resolution achieved show the suitability of the CFW outbred population of mice for genome-wide mapping of variants involved in morphological variation. The data also provide essential clues into the genetic architecture and heritability of the trait.

Table 2.3. Functional information for the involvement of the candidate genes in craniofacial phenotypes

| Gene | Biochemical function | Developmental function | Mutant phenotype | Human disease association |
|-----------------|---|---|--|---|
| Cldn18 | structural component of tight junctions | expressed in osteoblasts (Wongdee <i>et al.</i> 2008) and regulates bone resorption and osteoclast differentiation via the RANKL signaling pathway (Alshbool & Mohan 2014) | decreased total body bone mineral density, trabecular bone volume, and cortical thickness (Linares <i>et al.</i> 2012) | |
| Col1a1 | extracellular matrix protein | main component of connective tissues | shows decreased bone volume/tissue volume and reduced trabecular number; exhibits mechanically weak, brittle, fracture-prone bones (Chen <i>et al.</i> 2014) | <i>osteogenesis imperfecta</i> , a human syndrome characterized by bone fragility; subjects also show craniofacial alterations and deficient osteogenesis (Basel & Steiner 2009; Cheung <i>et al.</i> 2011) |
| Dlx3 | transcription factor with homeobox domain | regulates adult bone mass and remodeling (Duverger <i>et al.</i> 2013; Isaac <i>et al.</i> 2014) | branchial arch specification and craniofacial defects (Depew <i>et al.</i> 2005; Duverger <i>et al.</i> 2013) | tricho-dento-osseous syndrome (TDO) in humans, characterized by increased bone mineral density, craniofacial defects, and abnormal teeth and hair (Price <i>et al.</i> 1998) |
| Foxc1 | transcription factor with forkhead domain | interacts with BMP signaling and Msx2 to control calvarial bones osteogenesis (Mirzayans <i>et al.</i> 2012; Rice <i>et al.</i> 2003; Sun <i>et al.</i> 2013) and with Fgf8 to regulate the patterning of the mammalian jaw (Inman <i>et al.</i> 2013) | congenital hydrocephalus with the calvaria bones absent (Kume <i>et al.</i> 1998) | Axenfeld-Rieger syndrome, includes among other defects abnormalities in teeth and jaw (Mears <i>et al.</i> 1998) |
| Foxl2 | transcription factor with forkhead domain | among other functions, is also active in cranial neural crest cells and cranial mesodermal cells (Heude <i>et al.</i> 2015) | muscular and skeletal craniofacial malformations (Heude <i>et al.</i> 2015; Shi <i>et al.</i> 2014) | blepharophimosis, ptosis, epicanthus inversus syndrome (BPES) characterized by eyelid and craniofacial malformations and ovarian failure (Crisponi <i>et al.</i> 2001) |
| Gab1 | adaptor molecule with pleckstrin domain | involved in intracellular signaling cascades of EGFR and FGFR and cytokine receptors (Itoh <i>et al.</i> 2000); regulates osteoblast maturation and mineralization in long bones in mice (Weng <i>et al.</i> 2010) | embryonic lethal (Itoh <i>et al.</i> 2000); specific disruption of Gab1 expression in osteoblasts leads to decreased trabecular bone mass with a reduced bone formation rate and a decreased bone resorption (Weng <i>et al.</i> 2010) | |
| Itgav | integrin family of transmembrane proteins | heterodimer Itgav-Itgb3 is characteristic of osteoclasts, regulating its apoptosis and the process of bone resorption (Zhao <i>et al.</i> 2005) | various phenotypes, including cleft palate (Bader <i>et al.</i> 1998) | |
| Klf5 | transcription factor with Krüppel-like zinc finger domain | regulates the commitment of ES cells to mesoderm lineage (Aksoy <i>et al.</i> 2014) and the epithelial-mesenchymal transition (Zhang <i>et al.</i> 2013) | affects tooth development (Chen <i>et al.</i> 2009); when overexpressed calvaria bones are absent and mandible is underdeveloped (Sur <i>et al.</i> 2006) | |
| Lmx1b | transcription factor with homeobox domain | involved in a variety of developmental processes, including limbs, brain, kidney, eye, and calvarial bones (Dai <i>et al.</i> 2009) | multiple calvarial defects (Chen <i>et al.</i> 1998) | Nail-patella syndrome (NPS) including limb defects (Chen <i>et al.</i> 1998) |
| Mn1 | transcriptional activator | modifies Vitamin D (Sutton <i>et al.</i> 2005) and Vitamin A receptor mediated transcription (Meester-Smoor <i>et al.</i> 2005) in the context of bone formation and regulates osteoblast development (Sutton <i>et al.</i> 2005; Zhang <i>et al.</i> 2009) | craniofacial defects affecting exclusively membranous bones in the skull (Meester-Smoor <i>et al.</i> 2005) | involved in craniofacial deformations (Davidson <i>et al.</i> 2012) and palate cleft syndromes (Breckpot <i>et al.</i> 2015; Davidson <i>et al.</i> 2012) |
| Npr3 | natriuretic peptide receptor | among other functions involved in differentiation and proliferation of bone cells (Peake <i>et al.</i> 2014; Pejchalova <i>et al.</i> 2007) | skeletal-overgrowth syndrome with endochondral ossification defects (Jaubert <i>et al.</i> 1999; Peake <i>et al.</i> 2014). | |
| Rab3c | regulatory GTPase | regulates vesicular trafficking in the cell, is expressed in mouse calvaria osteoblast and is thought to play a role in bone mineralization (Pavlos <i>et al.</i> 2001) | in cell culture studies Rab3c regulates the formation of the ruffled membrane, the resorptive organelle of the osteoclast (Abu-Amer <i>et al.</i> 1999) | |
| Sh3pxd2b | substrate of Src tyrosine kinase | involved in EGF signaling pathway (Bögel <i>et al.</i> 2012) and the formation of podosomes, which are thought to contribute to tissue invasion and matrix remodeling | craniofacial and skeleton malformations in mice (Buschman <i>et al.</i> 2009; Mao <i>et al.</i> 2009; Yang <i>et al.</i> 2011a) | syndromes with craniofacial deformities, Frank-Ter Haar syndrome (Iqbal <i>et al.</i> 2010), and Borrone dermato-cardio-skeletal syndrome (Wilson <i>et al.</i> 2014) |
| Tbx15 | transcription factor with T-box domain | involved in early endochondral bone development in prehypertrophic chondrocytes of cartilaginous templates (Singh <i>et al.</i> 2005) | general reduction of bone size and changes of bone shape (Singh <i>et al.</i> 2005); droopy-eared mutation in mice (Candille <i>et al.</i> 2004; Curry 1959) | Cousin syndrome including craniofacial dysmorphism (Lausch <i>et al.</i> 2008) |

The genetic architecture of craniofacial traits

Craniofacial shape: Our results support the notion of a highly polygenic architecture for craniofacial shape in mice. This means that hundreds if not thousands of loci of small effect are involved in the tuning of these phenotypes. Data derived from other approaches also support this conclusion (Attanasio *et al.* 2013; Pallares *et al.* 2014). Such a highly polygenic architecture is expected to facilitate evolutionary modulations and transitions.

19 genomic regions were significantly associated with skull shape and 11 with mandible shape; together they explain only 3.9% and 2.2% of the total skull and mandible shape variation, respectively. The SNP heritability was estimated to be 43.6% for skull shape and 42.4% for mandible shape, indicating that there is much more additive genetic variation hidden in SNPs that did not cross the significance threshold.

We found little overlap of regions associated with both, skull and mandible traits (Table 2.1), although given the shared developmental origin of the mandible and some parts of the skull, one could have expected more overlap. Similarly, we found very little overlap with the genes we identified in our previous study in a wild mouse hybrid zone (Pallares *et al.* 2014). However, since it appears that the significant loci identified by GWAS constitute only a small proportion of the real number of functionally relevant loci, one should probably not expect a large overlap between studies, as long as one scratches only the surface of significant effect sizes. Accordingly, we would expect that an increase in sample size, and therefore an increase in power of detection will reveal more overlap between the studies.

Both principal components representing small (e.g. PC20) as well as large (e.g. PC1) proportions of the total phenotypic variation were significantly associated with genomic regions (Table 2.1). This pattern was also found previously (Boell 2013; Pallares *et al.* 2014). SNP heritability estimates showed that all PCs included in this study have moderate to high additive genetic variation (suppl. Tables 2.2 and 2.3) and therefore associations with genomic regions are expected regardless of the amount of phenotypic variation represented by individual PCs. Mapping approaches that do not rely on PCA analysis show that vectors different from PCs are associated with QTLs (see Maga *et al.* (2015)). The fact that many different vectors of shape variation associate with genetic variation would be an expected consequence of the highly polygenic architecture of craniofacial shape traits.

Craniofacial size: Only one genomic region was significantly associated with mandible size, while no significant associations were found for skull size. However, the SNP heritability estimates show that

35.4% and 36.4% of skull and mandible size variation, respectively, can be explained by all the SNPs used in the mapping.

Previous studies found up to 23 QTLs associated with mandible size variation (Klingenberg *et al.* 2001; Leamy *et al.* 2008; Leamy *et al.* 2000), and seven QTLs for skull size variation (Maga *et al.* 2015). Most of these studies are based on mouse lines with a specific contrast in size, i.e. they had been selected for their large and small size respectively. In a previous study using a wild-derived population of mice we did not find significant associations with craniofacial size either (Pallares *et al.* 2014). Given the large additive genetic variance of craniofacial size in the CFW mice used here, as well as in wild mice (Pallares *et al.* 2014), the absence of specific associations suggests that the effect size of loci involved in size variation is very small, even smaller than the effect of loci controlling shape, and therefore the power of these two studies was not enough to detect them.

Heritability of morphological traits

The heritability estimated in this study, ~43% for craniofacial shape and ~36% for craniofacial size, correspond to SNP heritability estimates. In humans, SNP heritability is considered an underestimate of the narrow sense heritability because it does not take into consideration rare alleles (Yang *et al.* 2010). However, in the CFW population used here, rare alleles are uncommon (Yalcin *et al.* 2010) and thus SNP heritability estimates may be closer to narrow sense heritability. Using a population of wild derived mice and a 3D approach, craniofacial (SNP) heritability was estimated in 65% for shape and 72% for size (Pallares *et al.* 2014). Given that the complex family structure of the population used in that study could have resulted in an overestimation of the true heritability, we considered such estimates an upper boundary for craniofacial shape heritability in mice.

Using a 2D approach and a pedigree design, the heritability of mouse mandible shape was found to be 0.29 for inbred mice (Klingenberg & Leamy 2001) and 0.61 for wild caught mice (Siahasarvie and Claude, personal communication). The estimates for mandible size heritability are 0.42 and 0.49, respectively.

Regardless of the method or the experimental design, the heritability estimates for mandible size and shape in mice are high. It remains to be seen if the same pattern is true for the skull; pedigree-derived data need to be collected.

In a recent study of wild soay sheep, the SNP heritability of mandible length was estimated to be 53%. Human studies estimate a narrow sense heritability of ~ 0.8 for facial morphology (Liu *et al.* (2012) and references in it). Although more data are needed, a pattern emerges from these studies that the form, shape and size, of craniofacial structures is a highly heritable trait.

Candidate genes

The resolution achieved here allowed us to explore all genes within the significant regions and most of the time we identified a single candidate gene for which previous relevant phenotypic information existed. Moreover, 71% of the regions overlap with previous studies (see Table 2.1 and Table 2.2); 7 of them with QTL regions derived from a F₂ cross (Maga *et al.* 2015), 21 of them overlap with some of the ~ 4000 enhancers active during craniofacial development in the mouse (Attanasio *et al.* 2013), and 1 region overlaps with a GWAS using a wild-derived population of mice (Pallares *et al.* 2014). Such overlaps cannot be explained by chance only (suppl. Figure 2.3). The high overlap with the enhancer dataset could be an indicator that some of the SNPs identified in this study could be tagging a causal variant located in the regulatory region of the candidate genes.

Many of the candidate genes are known craniofacial genes with reported craniofacial phenotypes. However, most of them were previously not quantitatively assessed and therefore knowledge of their specific effects on craniofacial shape variation requires a geometric morphometrics analysis of mutant mice. Preferably, such analysis should be done in heterozygous mice. In this way the genetic alterations and their phenotypic effects are closer to a natural within-population situation (Boell *et al.* 2013). Several other genes are new candidate genes for craniofacial shape formation; they are involved in diverse processes of bone formation but have not been directly involved in craniofacial development.

We found two pairs of genes involved in the same signaling pathway; *Sh3pxd2b* and *Gab1* are part of the epidermal growth factor signaling pathway – EGF; *Sh3pxd2b* regulates EGF-mediated cell migration (Bögel *et al.* 2012), and *Gab1* is involved in EGF-mediated cell growth (Itoh *et al.* 2000). *Mn1* and *Cldn18* are involved in the RANKL signaling pathway; *Mn1* regulates RANKL expression by stimulating RANKL's promoter (Zhang *et al.* 2009), and *Cldn18* regulates RANKL-mediated differentiation of osteoclasts (Linares *et al.* 2012).

Among the candidate genes, *Mn1* is a particularly interesting one, it was originally discovered for being involved in a myeloid leukemia phenotype and it was therefore named *meningioma 1*

(Lekanne Deprez *et al.* 1995). This gene has the largest effect size in our screen (Tables 2.1 and 2.2) and is associated to many PCs in the skull and in the mandible (regions 4, 8, 12 in Table 2.1, regions 2 and 3 in Table 2.2, Figure 2.4), thus being also the most pleiotropic gene in our study. Knockout studies of *Mn1* revealed that the leukemia phenotype of the gene is only a by-product of a particular fusion with another gene, while the core function of *Mn1* lies in regulating the development of membranous bones of the cranial skeleton (Meester-Smoor *et al.* 2005). Intriguingly, *Mn1* is an orphan gene specific to bony vertebrates (Euteleostomi), a taxon characterized by the formation of bones and a suture-structured head skeleton. The origin of such orphan genes is connected to the emergence of evolutionary novelties (Tautz & Domazet-Loaso 2011) and the *Mn1* knockout phenotype in mouse suggests that it plays a crucial function in the emergence of a vertebrate novelty. Hence, *Mn1* has the hallmarks of a very specific key gene in the genetic architecture of craniofacial development. The fact that it also emerges out of our genome wide analysis lends credence to the notion that the approach is suitable to detect relevant genes even for highly polygenic phenotypes.

Conclusion

There are long standing discussions about how to deal experimentally with polygenic traits and their implications for understanding the evolution of such traits (Donnelly 2008; Rockman 2012). Genome wide association studies have certainly moved us forward in this respect. Even relatively simple quantitative phenotypes like human height have a highly polygenic nature. Still, when a sufficiently powerful experimental design is used, key regulatory pathways influencing this phenotype can be identified (Lango Allen *et al.* 2010; Wood *et al.* 2014). The natural variants of these pathways have individually small effects, but the underlying genes can be major effect loci when knocked out.

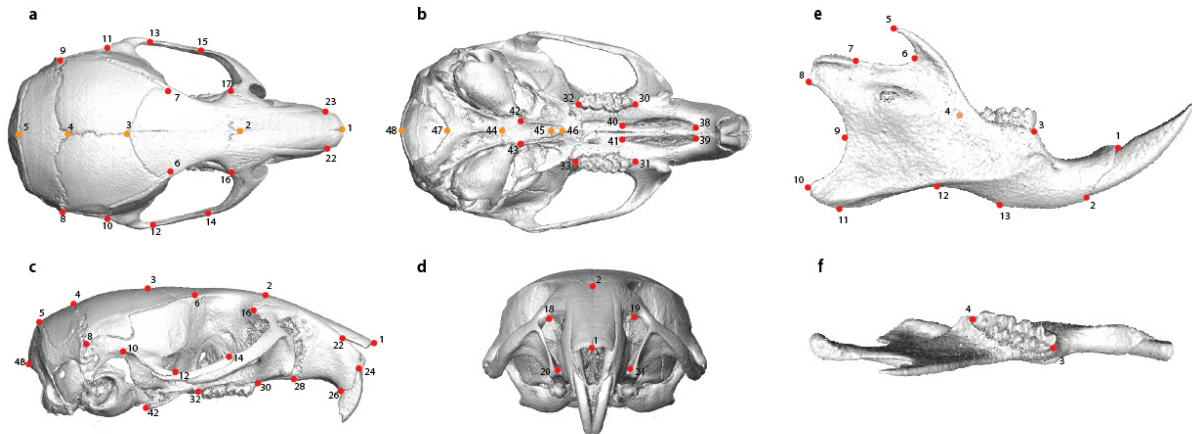
Here we have shown that we have a similar scenario regarding craniofacial shape, which is an enormously complex phenotype with a highly polygenic genetic architecture. But it is encouraging to see that even under such seemingly adverse genetic conditions, we can still identify good candidate genes previously studied in loss of functions experiments. This implies that genes occupying central positions in developmental pathways may also be the ones that carry enough natural variation to allow mapping through GWAS.

Human studies required ~25,000 individuals to explain 3-5% of height variation with genome-wide-significant SNPs (Visscher 2008), and ~250,000 to explain 16% (Wood *et al.* 2014). Using ~5400

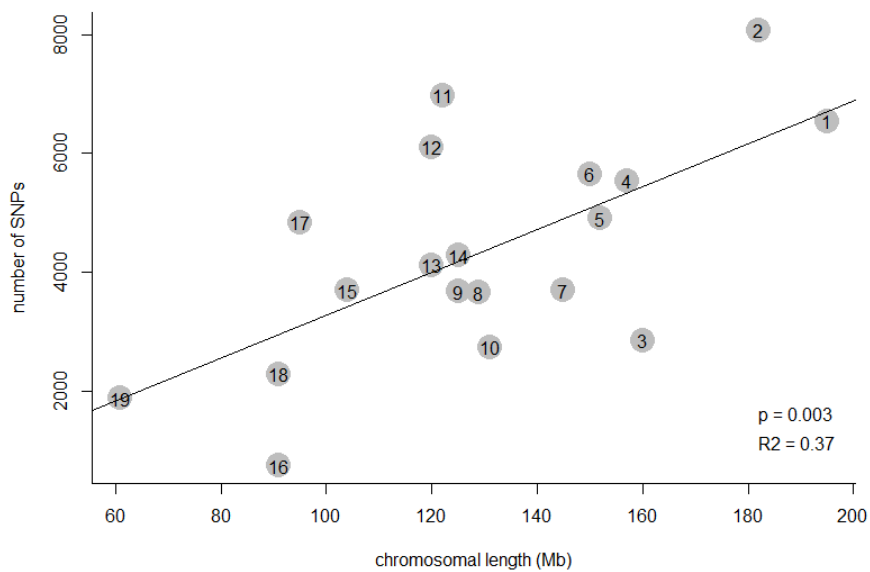
individuals, only 5 loci were significantly associated with facial morphology in humans (Liu *et al.* 2012). We have explained 2-4% of craniofacial variation using only ~700 mice. Given the development of semi-automatic tools to speed up the phenotyping of shape traits (e.g. Bromiley *et al.* (2014)), it seems feasible to extend both the number of animals involved, as well as to apply this to different mapping contexts. Hence, we are getting now more confident that an understanding of the biology behind craniofacial development will become possible.

Supplementary Figures

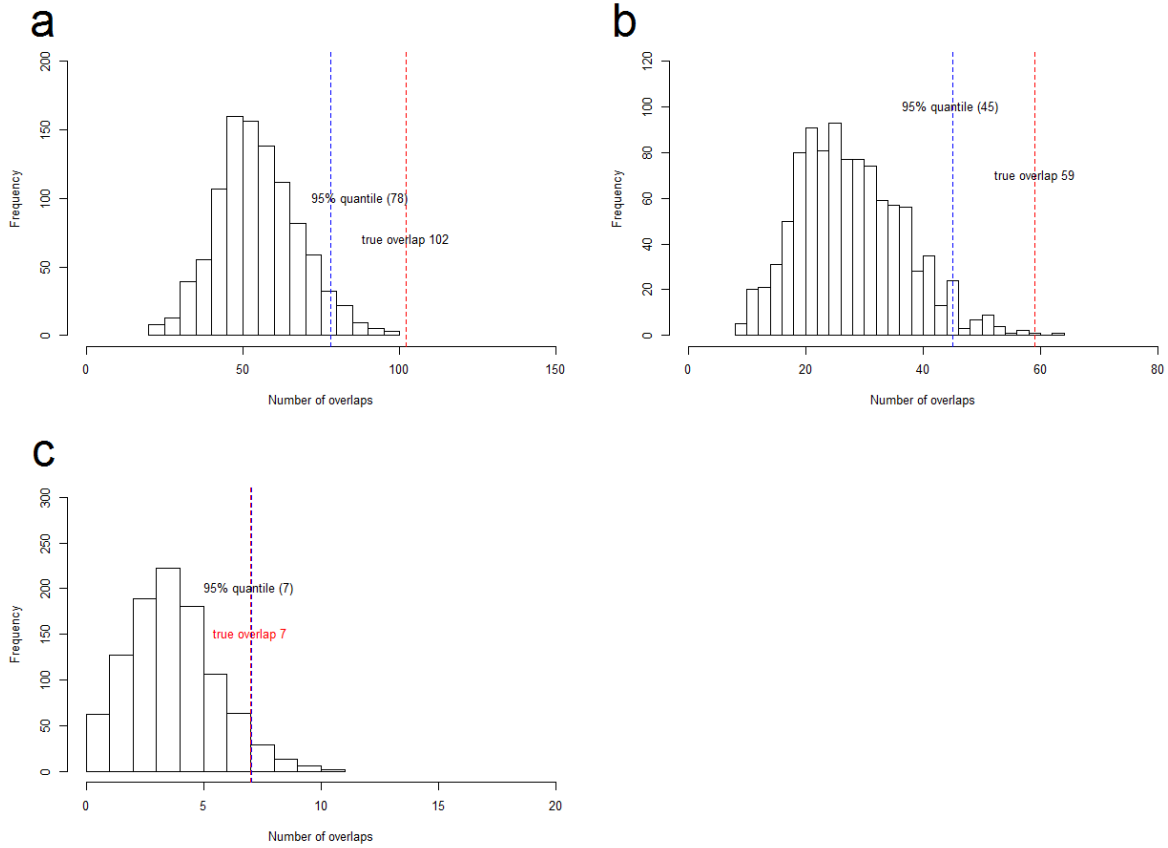
Supplementary Figure 2.1. Landmark points used to measure skull and mandible shape. See description of the points in suppl. Table 2.1.



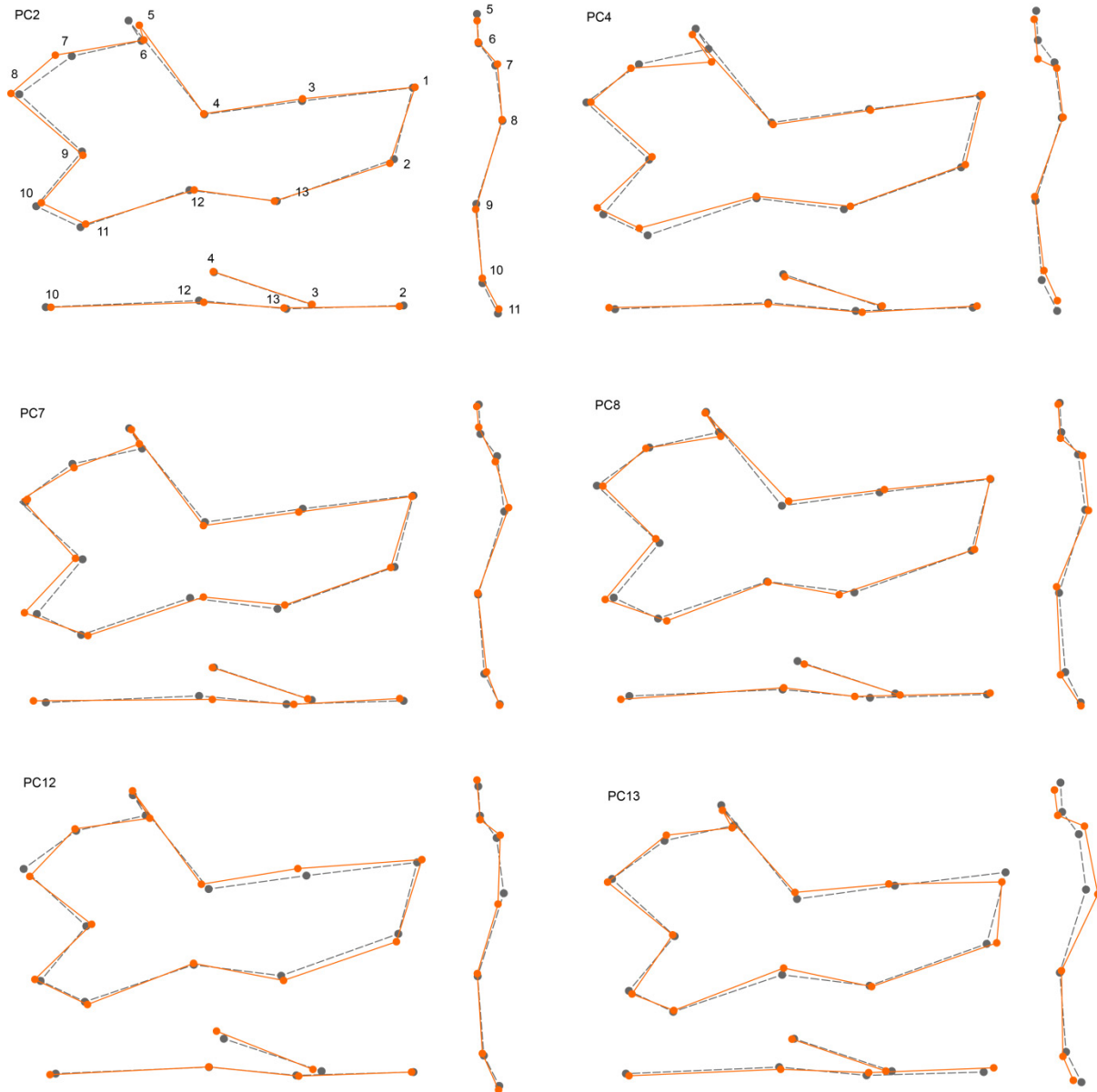
Supplementary Figure 2.2. Marker coverage of the genome. The number of SNPs per chromosome are shown.



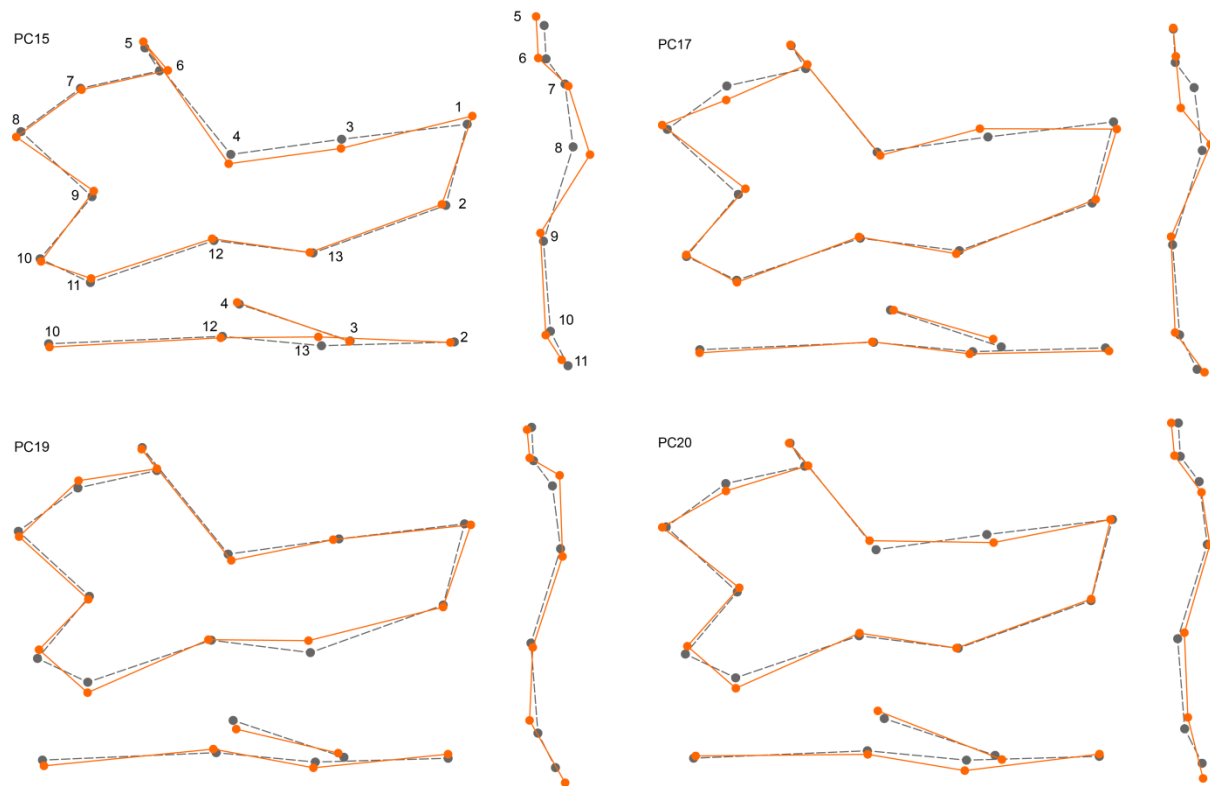
Supplementary Figure 2.3. Overlap with previous studies. 31 genomic regions were chosen randomly and their overlap with previous studies was calculated, this was repeated 1000 times. (a) overlap between 1Mb regions and the results from Attanasio *et al* 2014. (b) overlap between 500Kb regions and Attanasio *et al* 2014. (c) overlap of 1Mb regions and Maga *et al* 2015. The overlap with the results from Maga *et al* 2015 is constant even when the region size is reduced to 1Kb (data not shown).



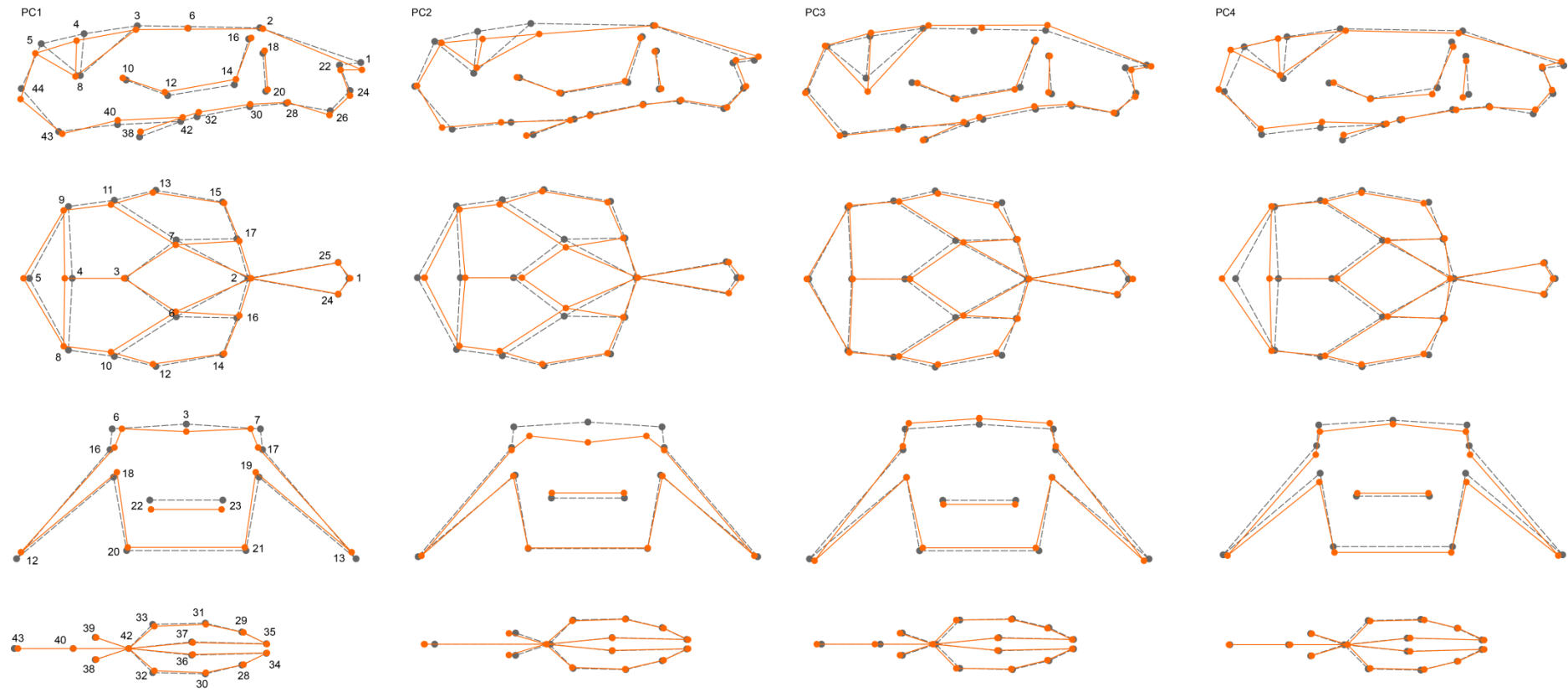
Supplementary Figure 2.4. 2D representation of the 3D mandible shape represented by the significant PC axes. PC2, PC4, PC7, PC8, PC12, and PC13 are shown. In grey (dotted lines) is the mean mandible shape of the population. In orange (continuous line) is the shape change associated with positive scores in the PC. Scale, 0.05 units of Procrustes distance. Lateral, dorsal and frontal views are shown, as well as the relevant landmarks for each view.



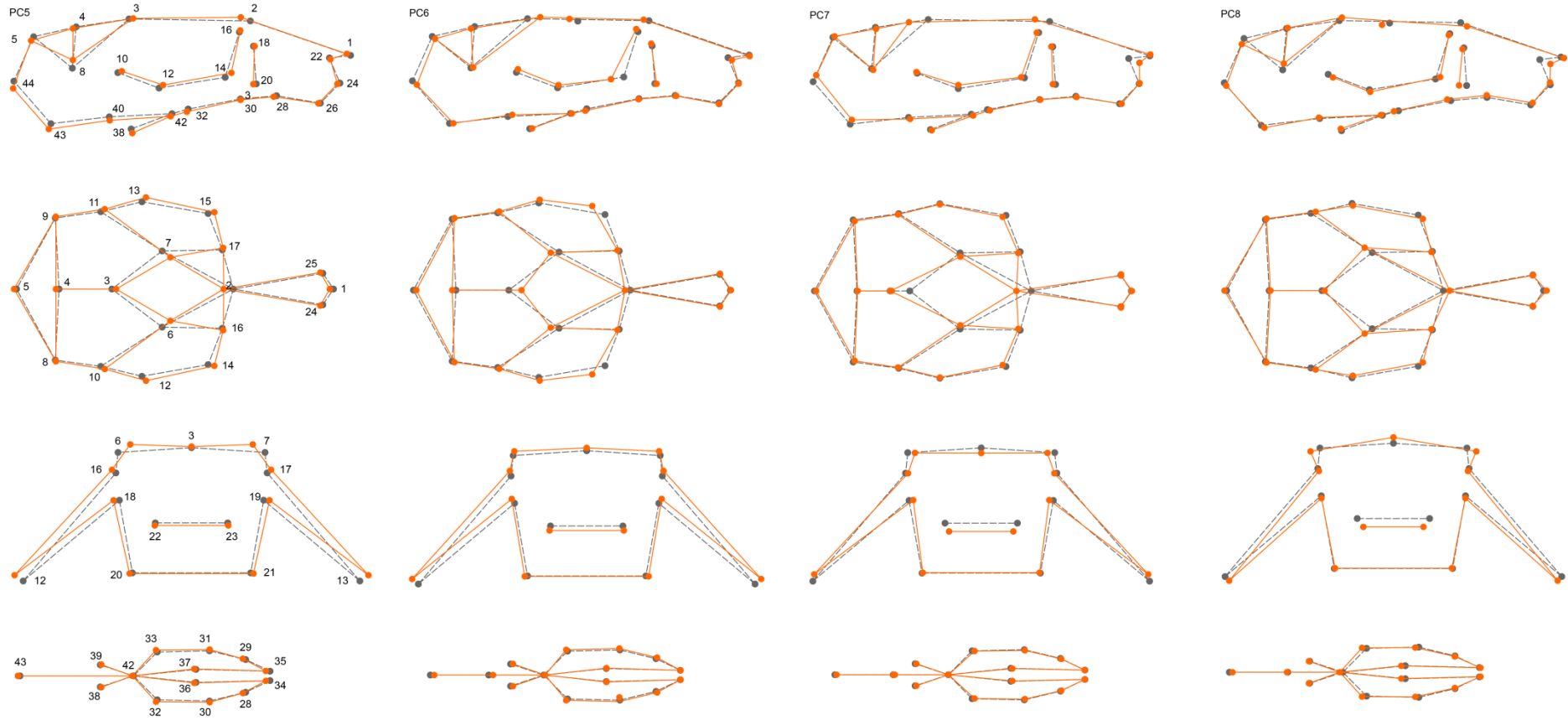
Supplementary Figure 2.5. 2D representation of the 3D mandible shape represented by the significant PC axes. PC15, PC17, PC19, and PC20 are shown. In grey (dotted lines) is the mean mandible shape of the population. In orange (continuous line) is the shape change associated with positive scores in the PC. Scale, 0.05 units of Procrustes distance. Lateral, dorsal and frontal views are shown, as well as the relevant landmarks for each view.



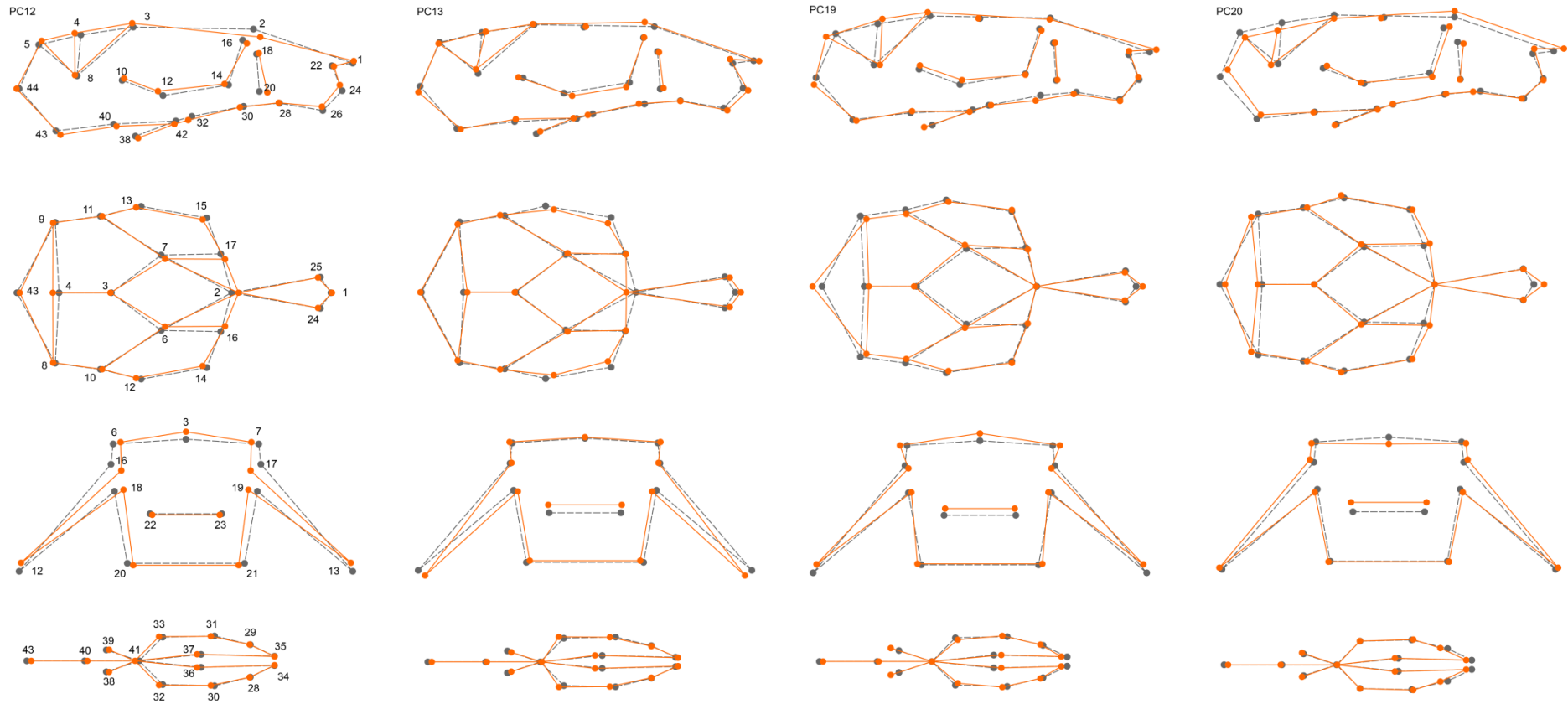
Supplementary Figure 2.6. 2D representation of the 3D skull shape represented by the significant PC axes. PC1 to PC4 are shown. In grey (dotted lines) is the mean mandible shape of the population. In orange (continuous line) is the shape change associated with positive scores in the PC. Scale, 0.05 units of Procrustes distance. Lateral, dorsal and frontal views are shown, as well as the relevant landmarks for each view.



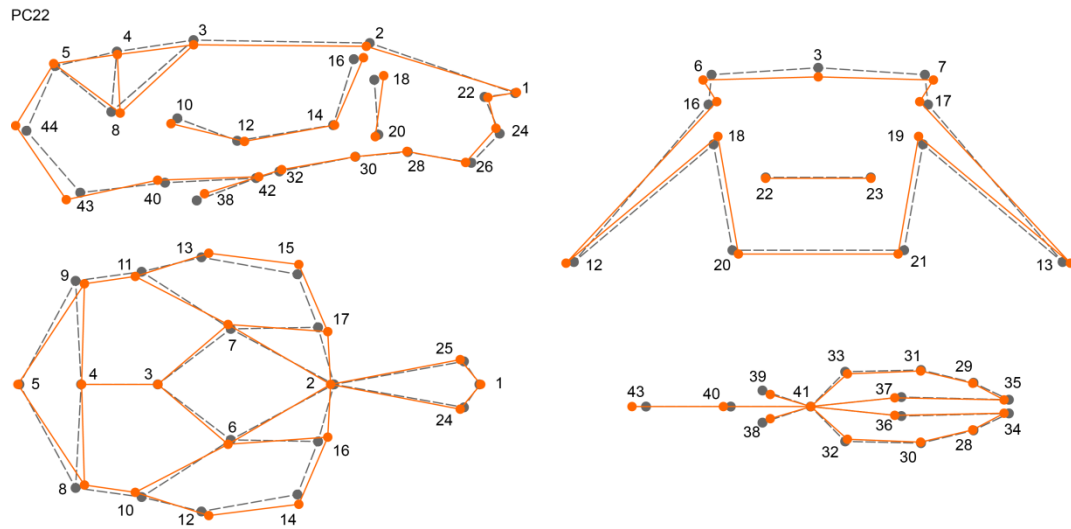
Supplementary Figure 2.7. 2D representation of the 3D skull shape represented by the significant PC axes. PC5 to PC8 are shown. In grey (dotted lines) is the mean mandible shape of the population. In orange (continuous line) is the shape change associated with positive scores in the PC. Scale, 0.05 units of Procrustes distance. Lateral, dorsal and frontal views are shown, as well as the relevant landmarks for each view.\



Supplementary Figure 2.8. 2D representation of the 3D skull shape represented by the significant PC axes. PC12, PC13, PC19 and PC20 are shown. In grey (dotted lines) is the mean mandible shape of the population. In orange (continuous line) is the shape change associated with positive scores in the PC. Scale, 0.05 units of Procrustes distance. Lateral, dorsal and frontal views are shown, as well as the relevant landmarks for each view.



Supplementary Figure 2.9. 2D representation of the 3D skull shape represented by the significant PC axes. PC22 is shown. In grey (dotted lines) is the mean mandible shape of the population. In orange (continuous line) is the shape change associated with positive scores in the PC. Scale, 0.05 units of Procrustes distance. Lateral, dorsal and frontal views are shown, as well as the relevant landmarks for each view.



Supplementary Tables

Supplementary Table 2.1 (part I). Description of the position of the landmarks used for the geometric morphometrics analysis.

| Landmark | Description |
|--------------|---|
| Skull | |
| 1 | Nasal bones most anterior suture |
| 2 | Nasal bones most posterior suture |
| 3 | Frontal bones most posterior suture |
| 4 | Parietal bones most posterior suture |
| 5 | Interparietal bone most posterior point on the median line |
| 6 | Right side, most anterior point of the suture between frontal and parietal bones |
| 7 | Left side, most anterior point of the suture between frontal and parietal bones |
| 8 | Right side, intersection between parietal, occipital and squamosal bones |
| 9 | Left side, intersection between parietal, occipital and squamosal bones |
| 10 | Right, most posterior junction of squamosal bone and the zygomatic process of the squamosal bone |
| 11 | Left, most posterior junction of squamosal bone and the zygomatic process of the squamosal bone |
| 12 | Right side, most anterior suture of the zygomatic process of the squamosal bone and jugal bone |
| 13 | Left side, most anterior suture of the zygomatic process of the squamosal bone and jugal bone |
| 14 | Right side, most anterior suture of jugal bone and the zygomatic process of the maxillary bone |
| 15 | Left side, most anterior suture of jugal bone and the zygomatic process of the maxillary bone |
| 16 | Right side, intersection of the frontal, lacrimal and the zygomatic process of the maxillary bone |
| 17 | Left side, intersection of the frontal, lacrimal and the zygomatic process of the maxillary bone |
| 18 | Right infraorbital foramen most superior point |
| 19 | Left infraorbital foramen most superior point |
| 20 | Right infraorbital foramen most inferior point |
| 21 | Left infraorbital foramen most inferior point |
| 22 | Right premaxilla-right nasal bone most anterior point of suture |
| 23 | Left premaxilla-left nasal bone most anterior point of suture |
| 24 | Most superior point of the right incisor alveolus |
| 25 | Most superior edge of the left incisor alveolus |
| 26 | Most inferior point of the right incisor alveolus |
| 27 | Most inferior point of the left incisor alveolus |
| 28 | Right premaxilla-maxilla most ventral junction |
| 29 | Left premaxilla-maxilla most ventral junction |
| 30 | Most anterior point of the right first molar alveolus |
| 31 | Most anterior point of the left first molar alveolus |
| 32 | Most posterior point of the right third molar alveolus |
| 33 | Most posterior point of the left third molar alveolus |
| 34 | Most anterior point of the right anterior palatine foramen |
| 35 | Most anterior point of the left anterior palatine foramen |
| 36 | Most posterior point of the right anterior palatine foramen |
| 37 | Most posterior point of the left anterior palatine foramen |
| 38 | Right pterygoid process, most posterior point |
| 39 | Left pterygoid process, most posterior point |
| 40 | Median-line point of the suture between occipital and basisphenoid bones |
| 41 | Median-line point of the suture between basisphenoid and presphenoid bones |
| 42 | Most posterior point of the suture between palatine bones |
| 43 | Foramen magnum most anterior point, Basion |
| 44 | Foramen magnum most posterior point, Bregma |

Supplementary Table 2.1 (part II). Description of the position of the landmarks used for the geometric morphometrics analysis.

| Landmark | Description |
|-----------------|---|
| Mandible | |
| 1 | Most superior point of the incisor alveolus |
| 2 | Most inferior point of the incisor alveolus |
| 3 | Most anterior point of the first molar alveolus |
| 4 | Most posterior point of the third molar alveolus |
| 5 | Most posterior tip of the coronoid process |
| 6 | Most anterior concave point of coronoid process |
| 7 | Most anterior point of the articular surface of the condyle |
| 8 | Most posterior tip of the condyle |
| 9 | Most anterior concave point between condyle and angular process |
| 10 | Most posterior tip of angular process |
| 11 | Most inferior point of angular process |
| 12 | Ascending ramus dorsal-most ventral point |
| 13 | Alveolar region most inferior point |

Supplementary Table 2.2. Principal component axes used in the mapping of mandible shape. %var, portion of the total skull variation accounted for by each PC axis. %cum, cumulative variance accounted for by the PC axes. PVE, portion of the PC variance accounted for by the SNPs used in the mapping. se(PVE), standard error of PVE estimate. PCA was run in MorphoJ. PVE estimates were obtained from the LMM implemented in GEMMA. The SNP heritability for mandible shape was calculated by multiplying PVE per PC with the %var per PC.

| PC | %var | %cum | PVE | se(PVE) |
|---|------|------|-------|---------|
| 1 | 14.9 | 14.9 | 72.09 | 10.9 |
| 2 | 13.8 | 28.7 | 42.29 | 11.1 |
| 3 | 9.0 | 37.7 | 35.37 | 10.1 |
| 4 | 8.5 | 46.2 | 78.19 | 10.0 |
| 5 | 6.4 | 52.6 | 32.22 | 11.0 |
| 6 | 5.8 | 58.4 | 32.73 | 11.5 |
| 7 | 5.2 | 63.5 | 49.17 | 10.9 |
| 8 | 4.3 | 67.8 | 16.50 | 10.8 |
| 9 | 3.7 | 71.6 | 34.60 | 11.9 |
| 10 | 3.2 | 74.7 | 35.01 | 9.5 |
| 11 | 2.9 | 77.6 | 35.89 | 11.9 |
| 12 | 2.6 | 80.2 | 48.10 | 11.1 |
| 13 | 2.2 | 82.4 | 47.51 | 10.6 |
| 14 | 2.1 | 84.5 | 23.58 | 9.9 |
| 15 | 1.9 | 86.4 | 49.35 | 11.4 |
| 16 | 1.7 | 88.0 | 41.04 | 10.2 |
| 17 | 1.5 | 89.6 | 23.19 | 12.8 |
| 18 | 1.3 | 90.9 | 26.29 | 10.4 |
| 19 | 1.2 | 92.1 | 52.87 | 10.1 |
| 20 | 1.1 | 93.2 | 47.94 | 12.2 |
| 21 | 1.0 | 94.1 | 31.86 | 11.7 |
| SNP heritability of mandible shape | | | 43.58 | |
| SNP heritability of mandible size | | | 36.40 | 10.20 |

Supplementary Table 2.3. Principal component axes used in the mapping of skull shape. %var, portion of the total skull variation accounted for by each PC axis. %cum, cumulative variance accounted for by the PC axes. PVE, portion of the PC variance accounted for by the SNPs used in the mapping. se(PVE), standard error of PVE estimate. PCA was run in MorphoJ. PVE estimates were obtained from the LMM implemented in GEMMA. PVE estimates were obtained from the LMM implemented in GEMMA. SNP heritability for mandible shape was calculated by multiplying PVE per PC with the %var per PC.

| PC | %var | %cum | PVE | se(PVE) |
|--|-------------|-------------|------------|----------------|
| 1 | 15.7 | 15.7 | 66.2 | 9.8 |
| 2 | 9.5 | 25.2 | 52.8 | 10.7 |
| 3 | 8.4 | 33.6 | 66.9 | 8.1 |
| 4 | 5.1 | 38.7 | 36.3 | 9.3 |
| 5 | 4.7 | 43.4 | 51.8 | 9.4 |
| 6 | 4.5 | 47.9 | 58.9 | 8.8 |
| 7 | 4.1 | 52.0 | 46.9 | 9.6 |
| 8 | 4.0 | 56.0 | 42.0 | 10.6 |
| 9 | 3.5 | 59.5 | 40.7 | 9.3 |
| 10 | 3.0 | 62.5 | 26.9 | 10.2 |
| 11 | 2.9 | 65.3 | 36.3 | 9.4 |
| 12 | 2.5 | 67.8 | 45.0 | 10.6 |
| 13 | 2.3 | 70.1 | 61.5 | 10.6 |
| 14 | 2.2 | 72.3 | 29.7 | 9.9 |
| 15 | 2.0 | 74.3 | 14.0 | 8.6 |
| 16 | 1.8 | 76.0 | 43.0 | 9.9 |
| 17 | 1.6 | 77.7 | 47.3 | 9.1 |
| 18 | 1.4 | 79.1 | 42.1 | 9.9 |
| 19 | 1.3 | 80.3 | 55.2 | 9.1 |
| 20 | 1.2 | 81.6 | 58.2 | 9.0 |
| 21 | 1.2 | 82.8 | 51.2 | 9.3 |
| 22 | 1.1 | 83.8 | 38.5 | 9.4 |
| SNP heritability of skull shape | | | 42.44 | |
| SNP heritability of skull size | | | 35.4 | 10.4 |

Supplementary Table 2.4. Regions associated with skull shape variation. The regions were defined by LD blocks around the focal SNP using a threshold of $r^2 \geq 0.8$ with the focal SNP. The genes contained in the regions are shown. When it was not possible to define regions due to lack of strong LD between the focal SNP and the neighboring SNPs, the focal gene is shown (*), or genes close to the focal SNP that could be considered candidate genes. Where no gene is shown no focal gene or interesting neighboring gene was found. The gene (genebody in Attanasio *et al* 2014) associated with the closer enhancer to the focal SNP is shown (**).

| Region | Skull | Region | Genes |
|--------|-------|--------------------------|--|
| 1 | PC1 | - | Sh3pxd2b* |
| 2 | PC1 | - | Rab3c*, Plk2, Pde4d** |
| 3 | PC2 | chr8:80366708-82427186 | Gypa, Frem3, Smarca5, Il15, Gab1, Usp38, Inpp4b |
| 4 | PC3 | chr5:111215141-111426493 | Pitpnb, Mn1, Ttc28** |
| 5 | PC4 | chr9:99662257-99713529 | Cldn18, Dzip1l, 4930519F24Rik** |
| 6 | PC5 | chr2:33284278-34883623 | Hspa5, Zbtb43, Lmx1b**, Rabepk, Fbxw2, Cutal, Ralgps1, Zbtb34, Mvb12b, Pbx3, Psm5, Gapvd1, Mapkap1 |
| 7 | PC5 | - | Copb2*, Foxl2** |
| 8 | PC6 | chr5:111626960-112398133 | Srrd, Asphd2, Crybb1, Tpst2, Cryba4, Hps4, Tfip11, C130026L21Rik** |
| 9 | PC6 | chr19:4001698-4180585 | Nudt8, Doc2g, Ndufv1, Gstp2, Gstp1, BC021614, Cabp2, Cdk2ap2, Aip, Cabp4, Ptprcap, Coro1b, Carns1, Rps6kb2, Pitpnm1, Gpr152, Tmem134, Kdm2a** |
| 10 | PC7 | - | Foxf2**, Foxc1 |
| 11 | PC8 | chr3:98278704-99786152 | Hsd3b5, Hsd3b1, Phgdh, Zfp697, Hsd3b4, Gm4450, Hsd3b6, Hsd3b2, Hsd3b3, Hao2**, Hmgcs2, Wars2, Tbx15 |
| 12 | PC8 | - | Ttc28* **, Mn1 |
| 13 | PC8 | - | - |
| 14 | PC12 | - | Sh3pxd2b* |
| 15 | PC13 | - | Frmd6* ** |
| 16 | PC19 | - | Phb** |
| 17 | PC20 | chr2:82522884-84982758 | Btbd18, 2700094K13Rik, Med19, Clp1, Timm10, Prg2, Zc3h15, Fam171b, Zswim2, Tfpi, Ctnnd1, Serping1, Ypel4, Zdhhc5, Slc43a1, Smtnl1, Rtn4rl2, Slc43a3, Itgav, Fsip2, Calcl, Ube2l6, Tmx2 |
| 18 | PC20 | chr11:94826955-95144609 | Hils1, Sgca, Dlx3, Col1a1, Samd14, Ppp1r9b, Dlx4, Itga3, Pdk2, Gm11544** |
| 19 | PC22 | chr15:11384042-12107575 | Tars, Npr3, Sub1, Adamts12** |

Supplementary Table 2.5. Regions associated with mandible shape variation. The regions were defined by LD blocks around the focal SNP using a threshold of $r^2 \geq 0.8$ with the focal SNP. The genes contained in the regions are shown. When it was not possible to define regions due to lack of strong LD between the focal SNP and the neighboring SNPs, the focal gene is shown (*), or genes close to the focal SNP that could be considered candidate genes. Where no gene is shown no focal gene or interesting neighboring gene was found. The gene (genebody in Attanasio *et al* 2014) associated with the closer enhancer to the focal SNP is shown (**).

| Region | Mandible | Region | Genes |
|--------|---------------|--------------------------|-------------------------------|
| 1 | PC2 | - | - |
| 2 | PC4 | - | Ttc28*, Mn1 |
| 3 | PC7 | chr5:111215141-111426493 | Pitpnb, Mn1**, Ttc28 |
| 4 | PC7 | - | Slit3* ** |
| 5 | PC8 | - | Cldn18, 4930519F24Rik** |
| 6 | PC12 | - | - |
| 7 | PC13 | - | Suclg2* |
| 8 | PC15 | chr14:98366257-99303998 | Bora, Mzt1, Klf5, Pibf1, Dis3 |
| 9 | PC17 | - | Apbb2** |
| 10 | PC19 | chr11:96201066-96737262 | Hoxb1-8, Skap1, Igf2bp1** |
| 11 | PC20 | - | - |
| 12 | Centroid size | - | Dhx9*, Rgs8** |

Morphological transitions along a hybridization gradient: implications for the genetic architecture of shape variation

Introduction

The European hybrid zone between *Mus musculus musculus* and *Mus musculus domesticus*, two subspecies of the house mouse group, was extensively studied in the past decades. The main focus of such studies was related to speciation and the relative fitness of hybrids compared to pure subspecies. Some examples of the phenotypes that were explored are: parasites load (Baird *et al.* 2012), microbiota composition (Wang *et al.* 2015), sterility phenotypes (Payseur *et al.* 2004; Teeter *et al.* 2008; Turner & Harr 2014; Turner *et al.* 2012), and behavior (Bimova *et al.* 2011; Latour *et al.* 2013).

Some studies have also addressed morphological traits in the hybrid zone; most of them have used characters like skull (Alibert *et al.* 1994; Mikula *et al.* 2010b; Mikula & Macholán 2008), mandible (Alibert *et al.* 1994; Mikula *et al.* 2010b; Mikula & Macholán 2008) and molar teeth (Alibert *et al.* 1994; Mikula *et al.* 2010b; Mikula & Macholán 2008) to explore the degree of developmental stability of hybrid mice relative to the pure subspecies. Patterns of shape asymmetry, specifically fluctuating asymmetry –random deviations from symmetry–, can be used to estimate how robust the developmental program of an organism is (Klingenberg 2015; Moller 1997). An increase in asymmetry indicates reduced developmental stability, and this is commonly associated with the disruption of co-adapted genomes (e.g. hybridization), an increase in homozygosity (e.g. inbred strains), or exposure to environmental stress.

On the other hand, normal variation in shape can be studied by using the symmetric component of shape (Klingenberg 2015; Klingenberg *et al.* 2002). Up to this day, only one study has explored how symmetric shape variation varies along the house mouse hybrid zone (Auffray *et al.* 1996a). Auffray and colleagues used 2D-geometric morphometrics to measure the ventral side of the skull in a transect of the Danish hybrid zone. They showed that the shape changes are correlated with the

percentage of hybridization, and such correlation follows a continuous gradient. However, the cline of skull shape was steeper than the cline of hybridization index, suggesting that skull development might be disturbed in some hybrid classes.

To determine whether the continuous transition found for the ventral side of the skull is a general property of morphological shape in mouse, in this chapter I formally test the transition patterns of 3D skull and mandible shape related to the percentage of hybridization between *M. m. musculus* and *M. m. domesticus*. I also expand the analysis to include variation in size. In chapter one and two I had defined the genetic architecture of craniofacial shape and size, here I explore whether inferences from morphological patterns are coherent with the genetic results.

This chapter should not be understood as an analysis of phenotypic clines since geographical information is not considered and the mice used for this study were raised under controlled conditions in the laboratory.

Methods

Mouse samples

249 mice (198 male and 51 female) were used for the analyses. 178 correspond to the mice used in chapter 1, and 71 are new additions. All individuals are first generation mice bred in the laboratory from wild-caught hybrid mice captured in the Bavarian hybrid zone in Germany (see methods of Chapter 1 for details). Mice were sacrificed by CO₂ asphyxiation in a window of 9-13 weeks. A portion of the mice had been genotyped for 200 SNP markers and others for 37 SNPs fixed in the pure populations – *M. m. musculus* or *M. m. domesticus*. The number of *M. m. domesticus* markers was used to classify the mice in 10 hybrid groups (Table 3.1).

Phenotype

Mice heads were scanned and phenotyped in the same way described in chapter 2. In short, 44 3D-landmarks were located in the skull and 13 in each hemimandible. For details on the landmark positions see Supp. Figure 2.1 and Supp. Table 2.1 in chapter two. A generalized Procrustes analysis (GPA) was performed on the landmark coordinates in MorphoJ (Klingenberg 2011) and the

symmetric component of mandible and skull shape was used for the following analyses (for details see Chapter2). The result of the GPA is a shape vector and a value of centroid size (CS) per individual.

The shape vector is composed of the x , y , and z coordinates of each landmark, this result in a 132-dimensions vector for skull shape, and 39-dimensions vector for mandible shape. Centroid size is the squared root of the sum of the squared distances of all landmarks from their centroid.

All analyses of skull and mandible shape were performed in MorphoJ (Klingenberg 2011). All analyses dealing with size were done in R (R-Core-Team 2013).

Hybrid groups

To estimate the mean size and shape of musculus and domesticus, the 28 mice from hybrid groups 0 and 1 (less than 20% of *M. m. domesticus* alleles) and the 29 mice from hybrid groups 8 and 9 (more than 80% of *M. m. domesticus* alleles) were used. These groups of mice will be called musculus (mus) and domesticus (dom), respectively.

Group 7 has very small sample size (four mice) and was not included in the analyses as an independent group; instead, the four mice were distributed to their closest group, either 6 or 8.

For regression and PCA analyses the 9 groups described in Table1 were used –except for group 7 (see above). Between-groups analyses like discriminant analysis are very sensitive to small sample size; therefore only seven groups were used: mus, 2, 3, 4, 5, 6, and dom.

Size differences

The non-parametric Mann-Whitney test was used to compare the mean size between the mus and dom groups.

A linear regression of centroid size on hybrid groups was performed. Pairwise Mann-Whitney tests were done for all group pairs and the results were adjusted for multiple testing using Bonferroni correction.

Shape differences between *M. m. musculus* and *M. m. domesticus*

The mean shape of each group (*musculus* and *domesticus*) and the Procrustes distance between them were calculated. The Procrustes distance is the squared root of the sum of squared distances between corresponding landmarks from two configurations after GPA.

A permutation procedure was used to estimate the significance of such distance: two groups of 28 and 29 mice were chosen randomly from the total of 57 mice available, and the Procrustes distance between them was calculated. This was repeated 1,000 times to estimate the probability that the true Procrustes distance was due to chance.

The separation between the groups was evaluated by a discriminant analysis and the leaving-one-out cross-validation procedure. This analysis indicates the number of individuals that were assigned by the discriminant function to a group different to the one they are originally part of. For example, an individual is part of group 9 because it has more than 90% *domesticus* alleles; however the discriminant function places it in group 7 because its shape is more similar to individuals from group 7.

Shape transition along the hybrid gradient

A multivariate regression of skull and mandible shape vectors on the hybrid groups was used to evaluate whether craniofacial shape is correlated with the level of hybridization. The individuals assigned to each group were permuted 10,000 times to calculate the significance of the correlation between shape and level of hybridization. To have a graphic representation of the regression, a univariate score was calculated for each individual by projecting each individual's shape vector onto the regression vector. The shape changes associated with the transition from the *musculus* end towards the *domesticus* end were obtained.

To explore the similarity between the shape vector derived from the regression and from the *musculus*-*domesticus* differences (see section above), the angle between them was calculated. Then, the probability that two random vectors form the same angle or smaller was estimated to determine the significance of the similarity between the original vectors.

A principal component analysis (PCA) on the covariance matrix of skull and mandible shape was performed as a second way to explore the distribution of the mice according to the hybrid group. A

regression of the individual PC axes over hybrid group was done to determine their correlation, and the shape changes associated to the significant PCs were generated.

Shape differences between hybrid groups

With the aim of determining if each hybrid group is characterized by a unique craniofacial shape, skull and mandible mean shapes were compared between groups following the same procedure described above for *M. m. musculus* and *M. m. domesticus*.

To determine if shape transition between groups has the same direction as the transition between musculus and domesticus shape, first, the vector of shape transition between group's means was calculated, and second, this vector was compared to the vector derived from the multivariate regression of shape on hybrid group. For example, the mean skull shape of group 8 is represented by a multivariate vector of 132 dimensions; the same is true for the mean skull shape of group 9. The difference between these two vectors represents the shape transition from group 8 to 9. The similarity between this 8-to-9 transition vector and the vector derived from the multivariate regression of skull shape on hybrid group is tested as described in the previous section.

Results

The hybrid groups were defined based on the percentage of *M. m. domesticus* (from now on domesticus) alleles (Table 3.1). Such groups represent a hybridization continuum, with the lower groups, 0 and 1, representing almost pure *M. m. musculus* (from now on musculus) individuals, and the higher groups, 8 and 9, almost pure domesticus individuals.

Size differences

The centroid size (CS) was used as a measure of skull and mandible size. There was no significant difference in mandible CS between musculus (group 0 and 1) and domesticus (group 8 and 9) ($p = 0.52$). Skull CS was marginally significant ($p = 0.03$), with musculus having a smaller skull (CS = 4.43) than domesticus (CS = 4.50).

Table 3.1. Mice used for the analyses. Groups are defined based on the percentage of *M. m. domesticus* alleles (%DomMarkers). The number of mice, average age, and average percentage of *M. m. domesticus* alleles per group are shown. If sample size for skull is different from mandible, this is indicated in parenthesis.

| Hybrid Group | %Dom markers | %Dom Markers (average) | Average Age (weeks) | Sample Size |
|--------------------------|--------------|------------------------|---------------------|------------------|
| 0 | 0-9 | 8.4 | 11.5 | 9 |
| 1 | 10-19 | 14.7 | 10.8 | 19 |
| 2 | 20-29 | 27.3 | 11.5 | 47 (45) |
| 3 | 30-39 | 31.7 | 11.3 | 49 (48) |
| 4 | 40-49 | 43.3 | 11.4 | 37 |
| 5 | 50-59 | 55.9 | 11.2 | 42 |
| 6 | 60-69 | 60.6 | 11.2 | 13 |
| 7 | 70-79 | 76.9 | 11.0 | 4 |
| 8 | 80-89 | 86.7 | 12.6 | 9 |
| 9 | 90-100 | 93.7 | 11.9 | 20 |
| Total sample size | | | | 249 (246) |

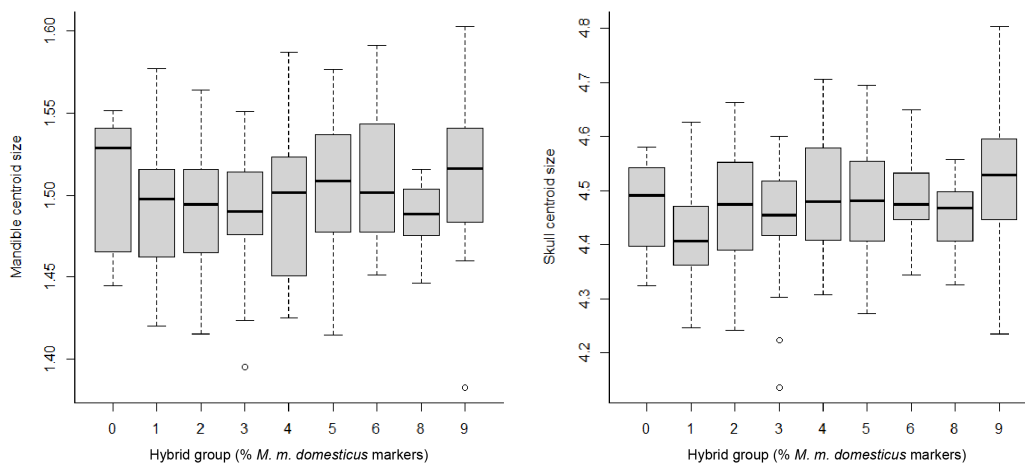


Figure 3.1. Variation of mandible and skull size (centroid size) according to hybrid groups. The mean size and the quartiles of the distribution are shown. Linear regression of CS on hybrid group, $p(\text{skull}) = 0.008$, $r^2(\text{skull}) = 2.5\%$, $p(\text{mandible}) = 0.055$.

Skull CS was significantly correlated with hybrid group ($p = 0.008$, $r^2=2.5\%$), while mandible CS shows a marginal significance ($p = 0.055$) (Figure 3.1). However, Mann-Whitney tests showed no significant differences between the CS of the groups, neither for the skull nor for the mandible. Due to this lack of differentiation in size no further analyses were pursued.

Shape differences between musculus and domesticus

The differences between the mean craniofacial shape of musculus and domesticus are shown for skull in Figure 3.2 (panel a-d) and for mandible in Figure 3.3 (panel a-c). Musculus mice are characterized by a wider and higher rostrum relative to the back of the skull; longer frontal bone relative to the nasal and parietal bones; and a straight upper molar row, while in domesticus, the last upper molar is shifted towards the interior. The mandible of domesticus mice is more straight compared to the musculus mandible; this is visible by the relative arrangement of the condyle, coronoid and angular processes. The lower molar row of musculus is shorter and more distant from the body of the mandible. Musculus mice have a shorter alveolar ramus, but a higher ascending ramus; a more pronounced angular process relative to the condyle.

The discriminant analysis showed that the skull and mandible shapes of musculus and domesticus are significantly different ($p(1,000$ permutations) <0.0001). The Procrustes distance between mean skull shapes is 0.028 and 0.039 between mean mandible shapes. The percentage of misclassification for skull is 7% and for mandible 1.7%, indicating a good separation between the musculus and domesticus individuals.

Shape transition along the hybrid gradient

The correlation between craniofacial shape and hybrid groups is significant ($p(10,000$ permutations) < 0.0001 , skull- $r^2 = 8.1\%$, mandible- $r^2 = 9.5\%$) indicating that shape changes are associated to the percentage of hybridization of the mice. The transition of shape between the musculus end of the population towards the domesticus end is continuous (Figure 3.4). The shape changes associated with such transition are shown for skull in Figure 3.2 (panel e-h), and for mandible in Figure 3.3 (panel d-f).

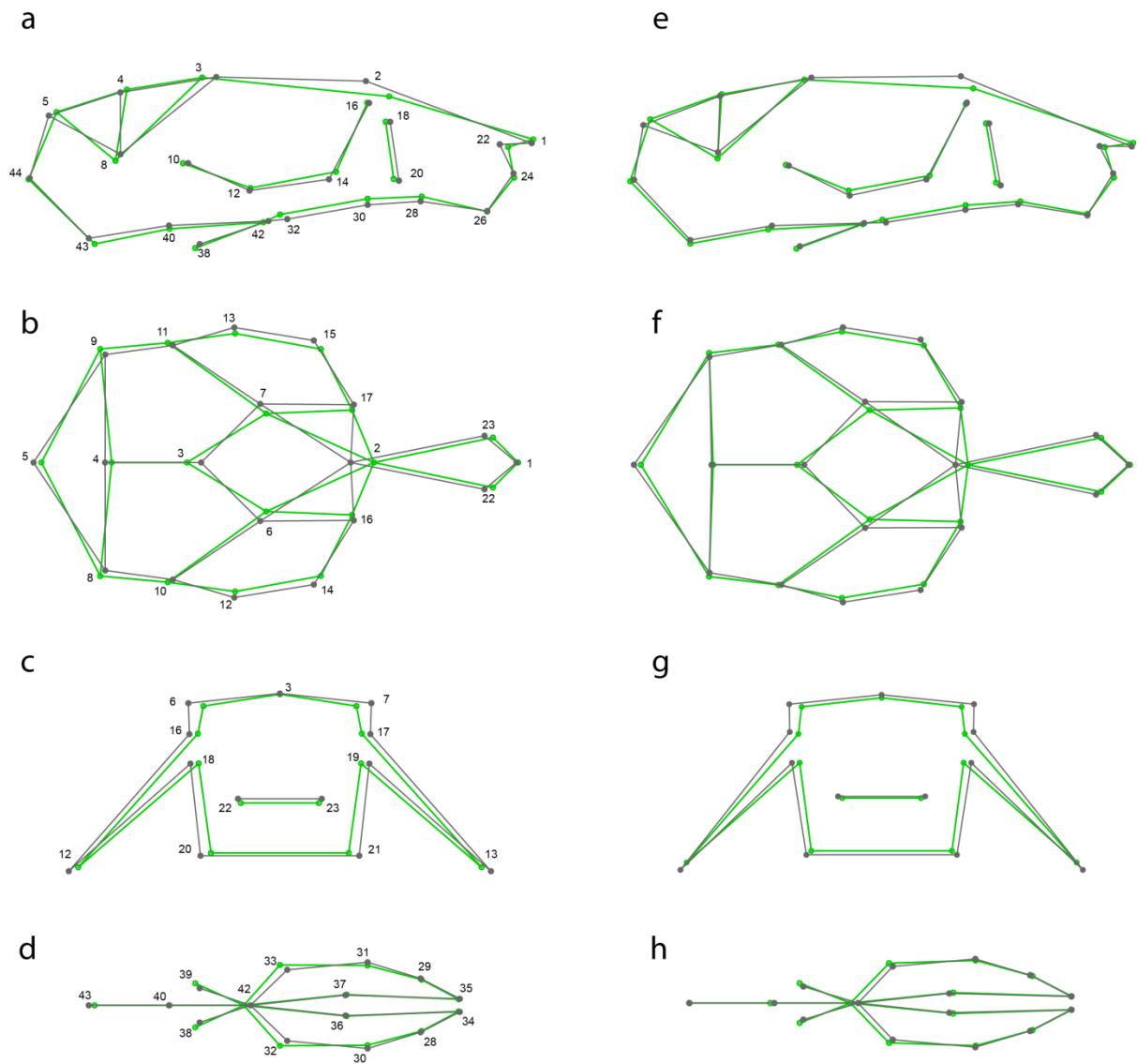


Figure 3.2. 2D visualization of the 3D-differences between the skull shape of *M. m. domesticus* (green) and *M. m. musculus* (grey). a-d, mean shape differences, scale 2x. e-h, shape changes correlated with hybrid group, scale 10x. Lateral (a,e), dorsal (b,f), frontal (c,g) and ventral (d,h) views are depicted. The relevant landmarks for each view are shown. Scale 2x.

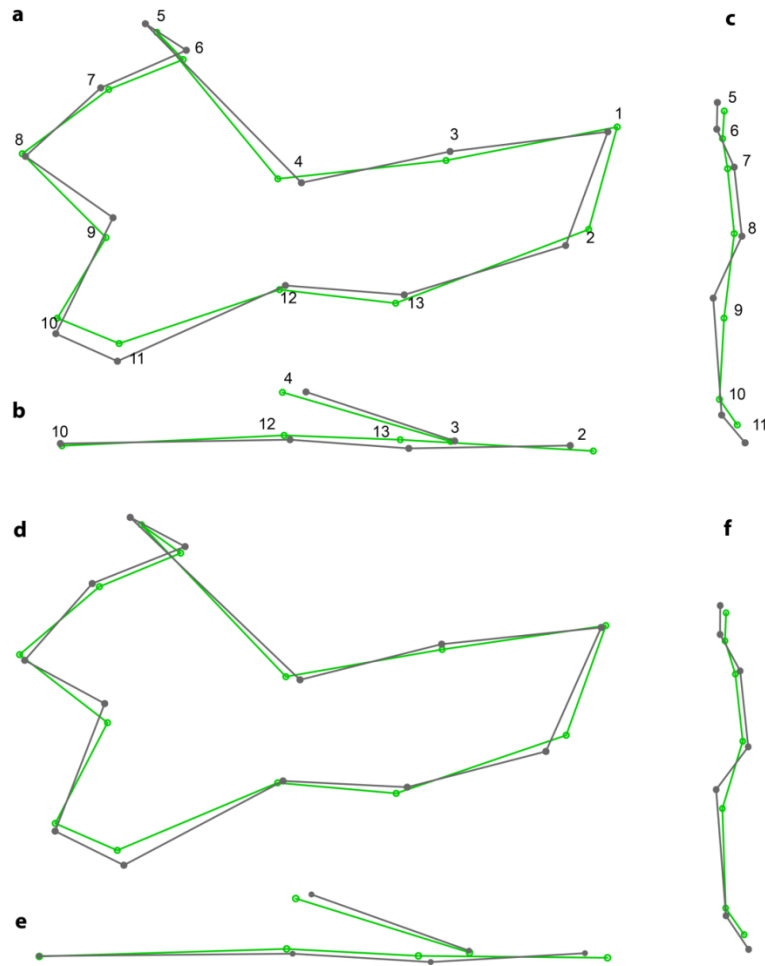


Figure 3.3. 2D visualization of the 3D-differences between mandible shape of *M. m. domesticus* (green) and *M. m. musculus* (grey). (a-c) mean shape differences, scale 2x. (d-f) shape changes correlated with hybrid group, scale 15x. Lateral (a,d), dorsal (b,e), and frontal (c,f) views are depicted. The relevant landmarks for each view are shown.

The shape vector derived from the multivariate regression of shape on hybrid group, and the vector derived from the discriminant function between musculus and domesticus are more similar than expected by chance (angle between vectors 23.8° , $p < 0.00001$). This indicates that the shape changes associated with shape transition in the hybrid zone resemble true musculus and domesticus differences. Figure 2 and Figure 3 illustrate both types of changes in skull and mandible shape, respectively.

The same pattern of continuity can be seen with the Procrustes distances among the mean shape of the groups. Such distance increases as the percentage of hybridization increases (Table 3.2).

The distribution of the shapes on individual mice in a principal component analysis indicates that some axes may be correlated with shape transitions between hybrid groups (Figure 3.5). A regression of PC scores of the skull on hybrid group shows a significant correlation for PC1, PC2, PC4, and PC5 ($p(10,000 \text{ permutations}) < 0.0001$, $PC1-r^2 = 26\%$, $PC2-r^2 = 13\%$, $PC4-r^2 = 15\%$, $PC5-r^2 = 7\%$). Regarding mandible, a significant correlation is found between PC1 and PC2, and hybrid group ($p(10,000 \text{ permutations}) < 0.0001$, $PC1-r^2 = 18.4\%$, $PC2-r^2 = 36\%$). The shape changes associated to these PCs are depicted in Figure 3.6 for skull and Figure 3.7 for mandible.

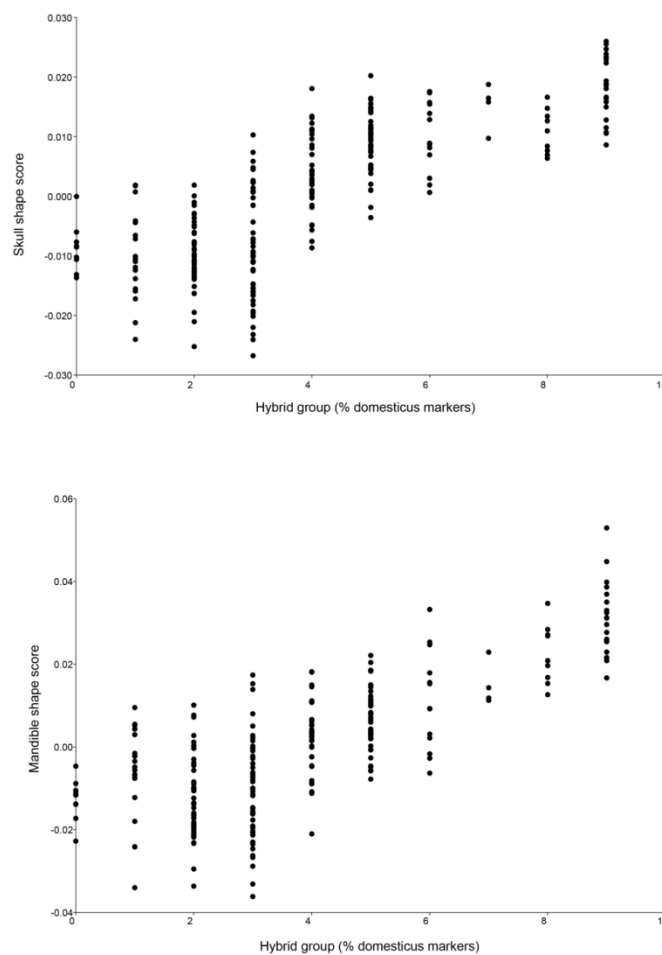


Figure 3.4. Multivariate regression of skull and mandible shape (shape vector of 132 dimensions for skull and 39 for mandible) on hybrid group. For purposes of visualization a univariate score is defined for each mice (Drake & Klingenberg 2008), but the significance is calculated using the multivariate vector. $p(10,000 \text{ permutations}) < 0.0001$, $skull-r^2 = 8.1\%$, $mandible-r^2 = 9.5\%$.

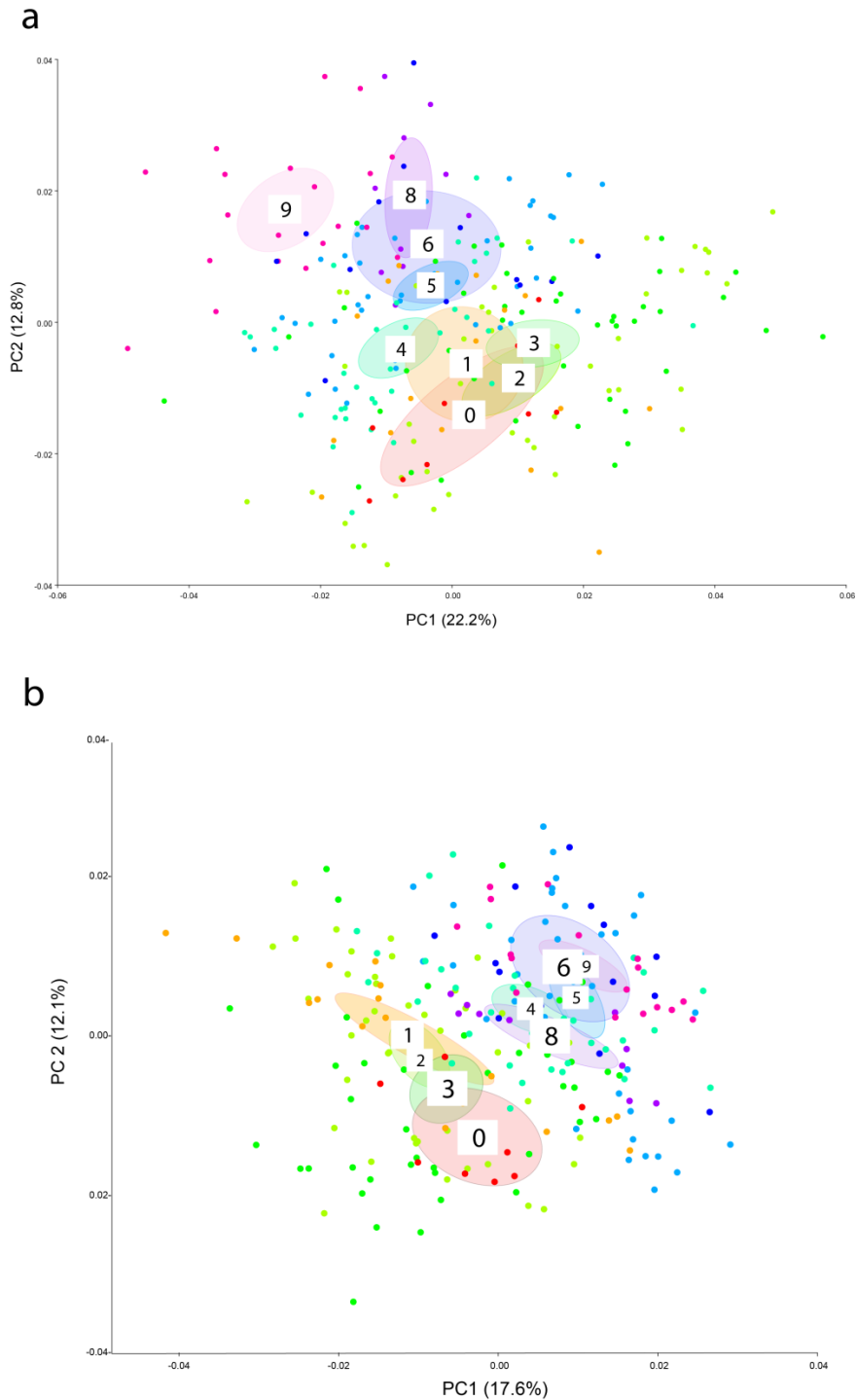


Figure 3.5. Principal component analysis of skull (b) and mandible (a) shape variation. The first two principal component axes (PC) are shown. The numbers represent the hybrid groups. According to the percentage of domesticus alleles the groups are: 0 (0-10% dom alleles), 1 (10-20%), 2 (20-30%), 3 (30-40%), 4 (40-50%), 5 (50-60%), 6 (60-70%), 8 (80-90%), 9 (90-100%). The ellipses represent 95% confidence intervals for the mean.

Shape differences between groups

Each pair of hybrid groups was tested for differences in skull and mandible mean shape. All means differ significantly from each other; with the exception of group 5 and 6 where the mean shapes seem to be similar (Table 3.2). This is also evident in the small Procrustes distance between these two groups relative to the others (0.0087 for skull shape, 0.0102 for mandible shape) (Table 3.2).

The shape transition between each pair of hybrid groups was compared to the shape transition in the musculus-domesticus continuum (derived from the regression of shape on hybrid group). The transition between all pairs of groups resembles significantly the shape changes from musculus to domesticus, with the exception of five pairs (see Table 3.3).

Table 3.2. Differences between the mean skull and mandible shape of the hybrid groups. Mus and Dom correspond to groups 0 and 1, and 8 and 9, respectively. The groups from 2 to 6 correspond to the original groups described in Table 1. The lower diagonal (blue) shows the Procrustes distances between mean shapes. The upper diagonal (red) shows the discriminant analysis results. In parenthesis is the percentage of individuals that were classified in the wrong group.

| SKULL | Mus | 2 | 3 | 4 | 5 | 6 | Dom |
|-------|--------|-----------|-----------|-----------|-----------|-----------|-----------|
| Mus | | *** (38%) | *** (21%) | *** (5%) | *** (43%) | *** (0%) | *** (8%) |
| 2 | 0.0160 | | *** (29%) | *** (16%) | *** (8%) | *** (8%) | *** (6%) |
| 3 | 0.0177 | 0.0106 | | *** (25%) | *** (2%) | *** (18%) | *** (3%) |
| 4 | 0.0225 | 0.0185 | 0.0167 | | *** (42%) | ** (20%) | *** (39%) |
| 5 | 0.0252 | 0.0241 | 0.0230 | 0.0103 | | ns (50%) | *** (24%) |
| 6 | 0.0258 | 0.0257 | 0.0254 | 0.0135 | 0.0087 | | *** (15%) |
| Dom | 0.0275 | 0.0273 | 0.0277 | 0.0212 | 0.0200 | 0.0196 | |

| MANDIBLE | Mus | 2 | 3 | 4 | 5 | 6 | Dom |
|----------|--------|-----------|-----------|-----------|-----------|-----------|-----------|
| Mus | | *** (17%) | *** (14%) | *** (8%) | *** (11%) | *** (33%) | *** (2%) |
| 2 | 0.0179 | | ** (30%) | *** (10%) | *** (12%) | *** (15%) | *** (1%) |
| 3 | 0.0197 | 0.0125 | | *** (12%) | *** (12%) | *** (17%) | *** (0%) |
| 4 | 0.0185 | 0.0242 | 0.0255 | | *** (23%) | *** (35%) | *** (1%) |
| 5 | 0.022 | 0.0259 | 0.0263 | 0.0157 | | ns (48%) | *** (11%) |
| 6 | 0.0258 | 0.0295 | 0.0292 | 0.0207 | 0.0102 | | *** (39%) |
| Dom | 0.0381 | 0.0408 | 0.0397 | 0.0318 | 0.0296 | 0.0263 | |

p(1,000 permutations) *** <0.009 ** <0.02 ^{ns} the mean shapes are not significantly different.

Table 3.3. Comparison between shape vectors. The shape change (shape vector) between each hybrid group is compared to the shape change between *musculus* and *domesticus*. The angle between the two vectors is shown for skull and mandible. The shape changes that do not resemble mus-dom transition are in red.

| Group pair | Angle(degrees) | |
|------------|---------------------|---------------------|
| | Skull | Mandible |
| Mus-2 | 90.9 | 103 |
| mus-3 | 88.3 | 96.8 |
| mus-4 | 54.5 ^{***} | 54.7 ^{***} |
| mus-5 | 42.3 ^{***} | 47.2 ^{***} |
| mus-6 | 37.8 ^{***} | 39.9 ^{***} |
| mus-dom | 23.1 ^{***} | 20.9 ^{***} |
| 2-3 | 85.7 | 82.3 |
| 2-4 | 43.8 ^{***} | 52.4 ^{***} |
| 2-5 | 38.3 ^{***} | 43.0 ^{***} |
| 2-6 | 36.5 ^{***} | 36.2 ^{***} |
| 2-dom | 20.4 ^{***} | 13.5 ^{***} |
| 3-4 | 41.3 ^{***} | 59.2 ^{**} |
| 3-5 | 38.1 ^{***} | 49.0 ^{***} |
| 3-6 | 38.5 ^{***} | 40.8 ^{***} |
| 3-dom | 26.4 ^{***} | 17.2 ^{***} |
| 4-5 | 57.4 ^{***} | 74.4 |
| 4-6 | 57.4 ^{***} | 63.9 ^{**} |
| 4-dom | 54.6 ^{***} | 38.4 ^{***} |
| 5-6 | 78.4 [*] | 61.6 ^{**} |
| 5-dom | 70.3 ^{**} | 45.6 ^{***} |
| 6-dom | 75.2 ^{**} | 52.9 ^{***} |

pvalue *** <0.00001, ** <0.01, *0.05

Discussion

I have quantified and described the changes in craniofacial shape associated to a hybridization gradient between *M. m. musculus* and *M. m. domesticus* subspecies.

The mice used in this study are representative of a natural hybridization context since they are first generation offspring of wild-caught hybrid mice, and at the same time have a maximal correlation between phenotype and genotype due to the controlled laboratory conditions they were raised in.

These characteristics allowed the measurement of the subtle phenotypic changes associated to small differences in the genetic composition that will be expected under a highly polygenic architecture.

Size

The size of the mandible and skull does not change across the hybrid groups, and the difference between the most extreme groups (musculus-like and domesticus-like) is only marginally significant for skull size. This contrasts with previous reports of hybrid heterosis in crosses of wild-derived strains of *M. m. musculus* and *M. m. domesticus*. Size heterosis has been reported for molars in F₁, F₂, and backcrosses (Alibert *et al.* 1997), and for mandible in F₁ (Renaud *et al.* 2009). However, the heterosis in mandible is lost in the F₂ (Renaud *et al.* 2012). Heterosis in size traits may be, after all, not as pervasive as previously thought.

Shape

The skull and mandible shape differences between musculus-like and domesticus-like mice was confirmed. The separation between groups was very accurate considering that mice with up to 20% admixture were used for these estimates.

There is a continuous transition from the craniofacial shape of musculus to that of domesticus. The first evidence of this continuous pattern was obtained for the ventral side of the skull using mice from the Danish hybrid zone and 2D geometric morphometrics (Auffray *et al.* 1996a). Here we have explored mandible and skull shape using 3D geometric morphometrics and the symmetric component of shape. The continuous pattern across the hybrid groups indicates that the development of the structures (skull and mandible) is not significantly affected by the degree of admixture, and therefore it is tempting to speculate that there is not selection against the range of shapes described here. However, the mice used here were raised in the laboratory and therefore we cannot exclude the possibility that in a natural context some environmental constraints are acting on certain craniofacial shapes. The results of Auffray *et al.* (1996a) suggest that the morphological cline for ventral skull may be steeper than the change in hybrid index, and therefore that some impairment in skull development could be associated to certain hybrid groups. Neither Auffray and colleagues nor I made a formal analysis of the morphological clines; such analyses will be necessary to establish if indeed there is or not some selection for craniofacial shape in the hybrid zone (Barton & Hewitt 1985; Gay *et al.* 2008).

Skull and mandible shape show very similar transition patterns across the hybrid groups and therefore in the following they will be discussed together as craniofacial shape.

Craniofacial shape transition is correlated with the percentage of admixture of the genomes, however the correlation is weak ($r^2 < 10\%$). This is expected given the relatively high within population shape variability present in wild mice (Boell & Tautz 2011; Siahsarvie *et al.* 2012). Some PC axes are better correlated with the mus-dom transition; for example, there is a correlation of 26% between skull-PC1 and hybrid groups, and of 36% for mandible-PC2. However, we have shown that the shape changes of these PCs, although correlated with shape changes from mus to dom, represent a specific type of shape variation and do not represent the overall transition in craniofacial shape (See Figures 3.2, 3.3, 3.6, 3.7). Such general shape transition is recovered when the complete shape vectors are analyzed (as in a multivariate regression), in contrast with the decomposition that a PCA implies.

The shape differences between hybrid groups always go in the same direction as the shape differences from mus to dom, adding to the argument that a true continuous transition is generated when the amount of admixture in the genomes increases (or decreases). Interestingly, the mean craniofacial shape differs between all groups, with exception of the comparison between groups 5 and 6, showing that different craniofacial shapes can be attained by slight quantitative changes in genetic composition while the direction of change is conserved.

The fact that the mice used here were generated by crossing wild hybrid mice implies that their genetic composition is very diverse, and many combinations of the loci relevant for craniofacial shape are likely to be present within the same hybrid group. Based on this, it may be reasonable to argue that it is not the specific locus what matters for craniofacial shape, but the relative frequency of each locus in the population. An increase (or decrease) in admixture will result in a new distribution of allele frequencies and that will be enough for a quantifiable change in mean shape. The closer a hybrid group gets to one of the “pure” extremes, the closer it gets to the allele frequency distribution that results in the mean shape characteristic of *musculus* or *domesticus*.

This is supported by the results found in chapter one; there, we used a similar population to the one used here. The mapping results showed that almost none of the loci associated with craniofacial shape were fixed between subspecies, but were segregating within them.

Phenotypic transition as a scenario for complex traits' evolution

In the previous chapters I identified a highly polygenic architecture for skull and mandible shape. Here I show that the way in which craniofacial shape transitions between two phenotypically distinct

subspecies corresponds to what would be expected for traits with such complex but still mainly additive genetic make-up.

The results of this chapter showed that quantitative changes in the composition of the genome result in quantitative changes in the phenotype, however such changes are reflected in the mean shape between groups while the variation within-groups keeps being high. This could be the way in which highly complex phenotypes –underlied by hundreds of loci with small phenotypic effect- evolve from standing variation.

We can imagine a scenario where the ancestral population of the house mouse complex, for whatever reasons –drift or selection- shifts its mean shape as the result of slight changes in allele frequencies. With enough time and enough population size –a plausible scenario for mice-, it will end up, with no big disturbances to the functionality of craniofacial shape, in a different position in the morphospace (theoretical multivariate space where all the possible shapes are located). Given the high shape variability within mice populations, a minor change in the evolutionary conditions of such ancestral population could result in a different position in the morphospace. Such new positions in the universe of possible shapes, we can imagine, is what we call today *M. m. musculus* and *M. m. domesticus*.

Conclusion

The results of this chapter indicate that the morphospace between the mean shape of *M. m. musculus* and *M. m. domesticus* is continuous. All intermediate shapes are realized in nature and no developmental constrain seems to arise from the degree of hybridization.

The continuous transition along hybrid groups correlates with the percentage of hybridization. This is expected for traits with a highly polygenic architecture where a quantitative change in genomic composition should result in a quantitative change in the phenotype. The results from morphological transitions are therefore consistent with the genetic results obtained in chapter one and two.

I propose that the patterns observed in this study, like the consistent direction of shape changes and the continuous transition along hybrid groups as well as between pair of groups, illustrate the way in which a complex trait can evolve in nature.

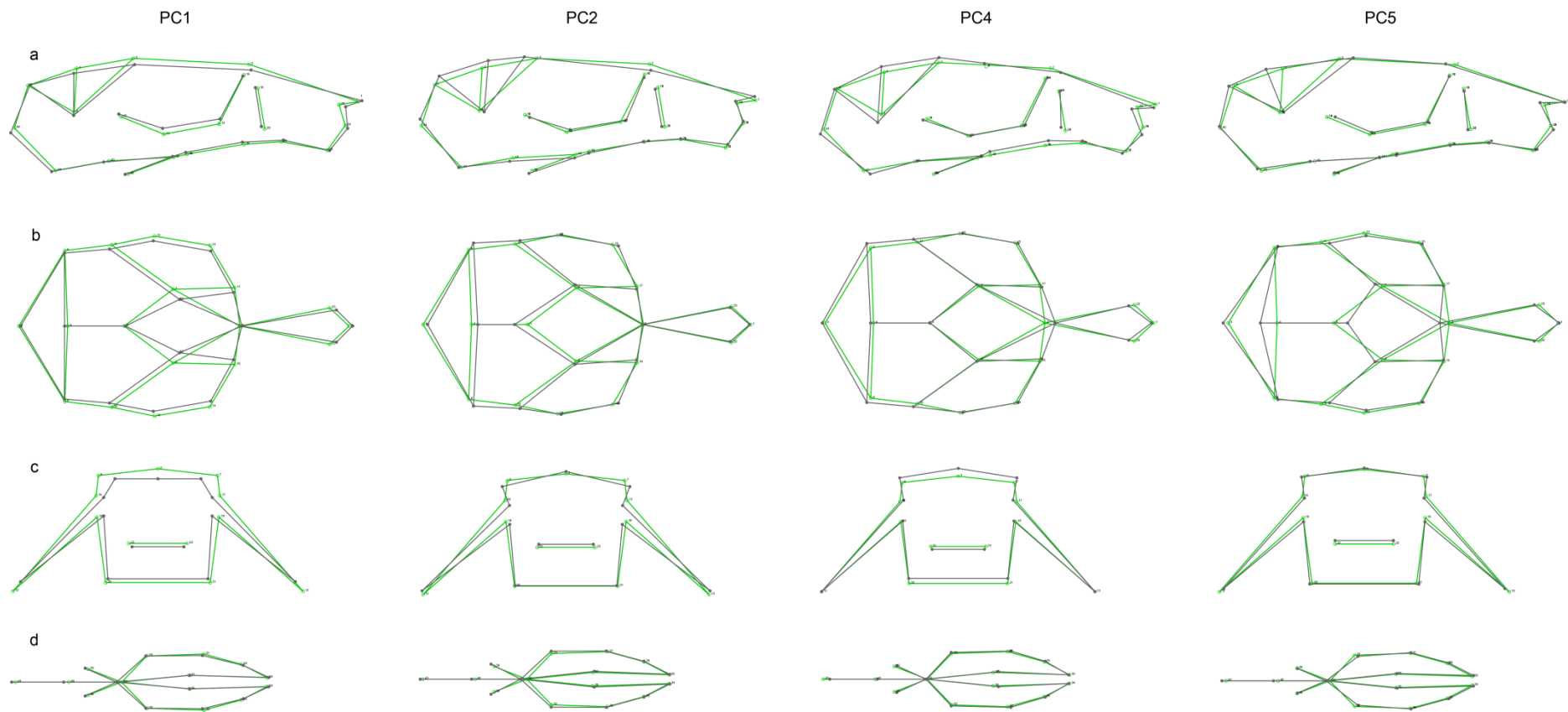


Figure 3.6. 2D representation of the 3D shape of the skull represented by principal component one, two, four, and five. These PC axes are correlated with the transition from musculus to domesticus. Lateral (a), dorsal (b), frontal (c), and ventral (d) views are shown. Green represents the mean skull shape. Grey represents skull shape at 0.05 units of Procrustes distance from the mean. For reference, the Procrustes distance between musculus and domesticus is 0.028.

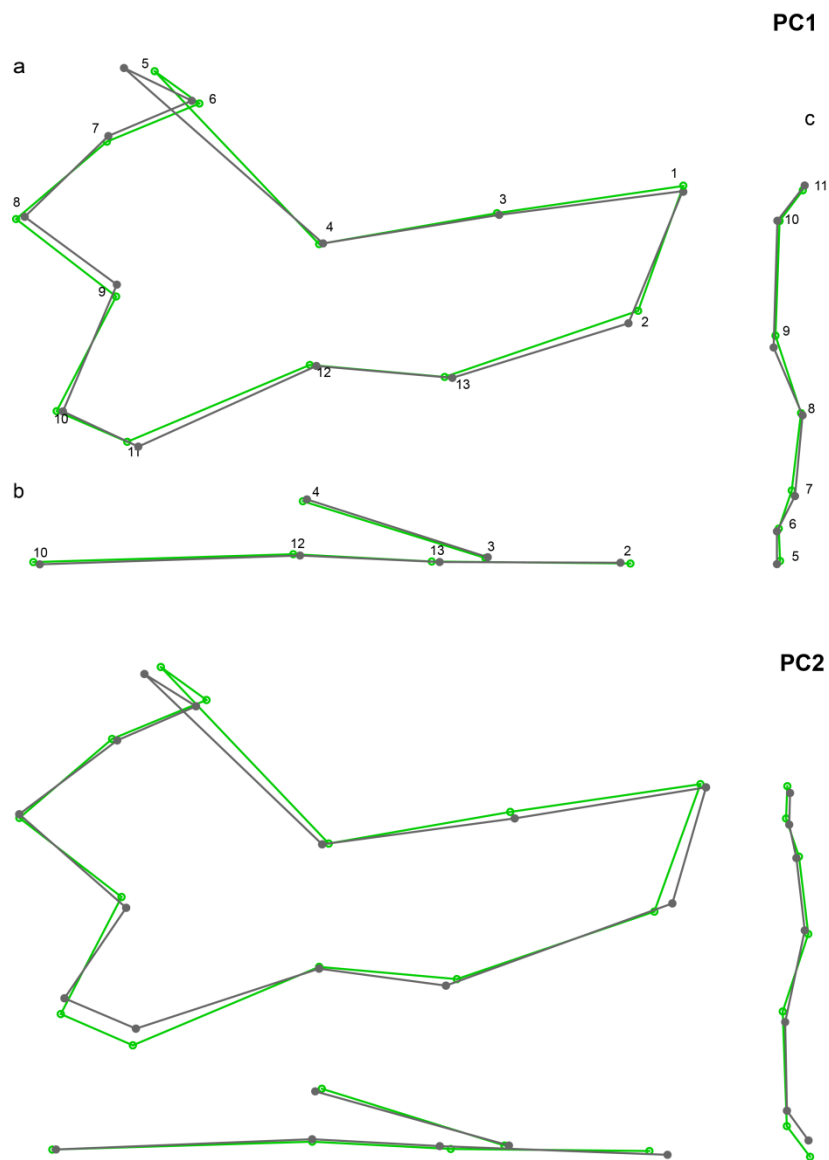


Figure 3.7. 2D representation of the 3D shape of the mandible. Shape changes associated with PC1 and PC2 are shown. These PC axes are correlated with the transition from musculus to domesticus. Lateral (a), dorsal (b), and frontal (c). Green represents the mean skull shape. Grey represents skull shape at 0.05 units of Procrustes distance from the mean. For reference, the Procrustes distance between musculus and domesticus is 0.039.

Contributions to the thesis

Chapter one

This chapter was published in the journal *Molecular Ecology* in October 2014 (doi: 10.1111/mec.12968)

Citation: Pallares LF, Harr B, Turner LM, Tautz D (2014). Use of a natural hybrid zone for genome wide association mapping of craniofacial traits in the house mouse. *Molecular Ecology* 23, 5756-5770.

I designed the study, collected the phenotypic data, performed the analyses, and wrote the first version of the manuscript. Bettina Harr and Leslie M. Turner provided the samples (mouse heads) and the genotypes. B. Harr assisted with the analyses. Jung Wang and John Baines provided the pure mice from the hybrid zone.

Chapter two

This chapter will be submitted in the following weeks to the journal *PLoS Genetics*.

Citation: Pallares LF, Carbonetto P, Gopalakrishnan S, Parker CC, Palmer AA, Tautz D (2015). Mapping of craniofacial traits in outbred mice identifies major developmental genes involved in skull formation.

I designed the study, collected the phenotypic data, performed the analyses, and wrote the first version of the manuscript. The coauthors provided the samples (mouse heads) and the genotypes. Carbonetto P and Gopalakrishnan S assisted with the analyses. Elke Blohm-Sievers helped scanning the mice.

Chapter three

This chapter will be submitted as contribution to the special issue of the symposium "Size and Shape" (Gottingen 2014) to the journal *Development Genes and Evolution*.

I designed the study, collected the phenotypic data and performed the analyses. Bettina Harr and Leslie M. Turner provided the samples (mouse heads) and the genotypes. Elke Blohm-Sievers helped scanning the mice.

Perspectives

Geometric morphometrics methods allow the precise quantification of subtle differences in morphological shape between individuals. Genome-wide associating studies (GWAS) make it possible to map the genetic loci involved in phenotypic variation within populations. These two fields, combined, opened up the possibility to study morphological diversity from a micro-evolutionary perspective within a natural context.

Today, we have the capability of understand the genetic basis of shape variation within populations; the results of this thesis show that the fine-tuning of morphological shape is controlled by a large number of loci in a within-population context (i.e. results from outbred lab mice), but also in a between-subspecies scenario (i.e. results from wild hybrid mice). These empirical data indicates that, at least for craniofacial shape in mouse, the evolution of new phenotypes occurs by subtle genetic changes and not due to few loci of large effect.

Accordingly, the evolution of this type of traits cannot be understood from the traditional theoretical framework of adaptation (see Orr (2005a)), and urges the development of new models addressing how highly polygenic traits can evolve.

Acknowledgements

Foremost I want to thank Prof. Dr. Diethard Tautz for undertaking together with me the task of solving all problems in complex traits genetics. We didn't solve everything, but there is still time. I am grateful for his advice and support, and for the freedom he gave me to develop my own ideas. I am thankful for the independence he granted me during these years, and for the pressure of the last few weeks. It was always, exactly what I needed.

I thank the members of my thesis committee, Prof. Dr. Thomas Bosch and Dr. Arne Nolte, for making sure everything was going on track and for very productive discussions.

I am deeply indebted to Bettina Harr, Leslie Turner, and Abraham Palmer for providing the mice samples used in this thesis. The work presented here would not have been possible to achieve in the time frame of a PhD thesis if the mouse samples would not have been available. I am also grateful for their input along this process. I thank Jun Wang and John Baines for the mice they provided for chapter one.

I thank Bettina Harr, Peter Carbonetto, Shyam Gopalakrishnan, and Rafik Neme for their readiness to answer my innumerable questions and emails.

I thank Elke Blohm-Sievers for her help scanning thousands of mice used in this thesis and in other projects.

I am grateful to Christine Pfeifle who helped me with the organizational part of my projects. I thank the Mouse Team in Plön, in particular Maik Görtz-Sonnwald and Till Sckerl for taking care of my mice.

When I first came to the MPI and started working on my to-be PhD thesis, Anja Schunke and Louis Boell happened to share part of my scientific interests, and fortunately happened to be my office mates. They introduced me to many of the software, methods, and literature that I used for this thesis. I'm grateful for the many discussions, and for the many *Physalis* shared in our office.

I am grateful to the International Max Planck Research School for funding my PhD, and to the IMPRS coordinators, Kerstin Mehnert and Natascha Hasenkamp, for always giving me a hand when required.

This thesis is much better thanks to the people who commented on previous drafts and to my coauthors that made a good job dealing with my non-native English and my long sentences. I thank Anja Schunke, Miriam Linnenbrink, Rafik Neme, Abraham Palmer, Peter Carbonetto, Bettina Harr, and Leslie Turner.

I'm thankful to all the people with whom I shared time, beers, currywursts and innumerable cups of coffee, you made my time in Plön always enjoyable.

I had great scientific and non-scientific discussions with Ozan Bozdog and Jorge Peña. I thank them for that and for all the good times together.

My work trips and holidays would not have been possible without all the people that took care of Lola while I was away. Thank you so much Christine, Miri, Jorge, Leslie, Anja y Reiner, Till, Noemie, Neva, Joshka, Cristina, Freddy and Megan, Sebastian, and Chen.

I thank Rafik Neme for being the best company I could have wished for during this process, for being so patient during the bad moments, and for sharing my happiness during the good ones.

Finally, I want to specially thank my father Oscar and my mother Duby for always being there with me and for me, for their unconditional support and love. I thank my sister Maria Alejandra for being present in each one of my days here, filling them with joy and love.

I am grateful because in spite of the distance they made sure I always felt their company.

References

- Abu-Amer Y, Teitelbaum SL, Chappel JC, Schlesinger P, Ross FP (1999) Expression and Regulation of RAB3 Proteins in Osteoclasts and Their Precursors. *Journal of Bone and Mineral Research* **14**, 1855-1860.
- Abzhanov A, Kuo WP, Hartmann C, *et al.* (2006) The calmodulin pathway and evolution of elongated beak morphology in Darwin's finches. *Nature* **442**, 563-567.
- Abzhanov A, Protas M, Grant BR, Grant PR, Tabin CJ (2004) Bmp4 and morphological variation of beaks in Darwin's finches. *Science* **305**, 1462-1465.
- Abzhanov A, Rodda SJ, McMahon AP, Tabin CJ (2007) Regulation of skeletogenic differentiation in cranial dermal bone. *Development* **134**, 3133-3144.
- Adams DC, Rohlf FJ, Slice DE (2004) Geometric morphometrics: ten years of progress following the 'revolution'. *Ital. J. Zool.* **71**, 5-16.
- Adams DC, Rohlf FJ, Slice DE (2013) A field comes of age: geometric morphometrics in the 21st century. *Hystrix* **24**, 7-14.
- Aksoy I, Giudice V, Delahaye E, *et al.* (2014) Klf4 and Klf5 differentially inhibit mesoderm and endoderm differentiation in embryonic stem cells. *Nat Commun* **5**, 3719.
- Albertson RC, Streelman JT, Kocher TD (2003) Directional selection has shaped the oral jaws of Lake Malawi cichlid fishes. *Proc Natl Acad Sci U S A* **100**, 5252-5257.
- Albertson RC, Streelman JT, Kocher TD, Yelick PC (2005) Integration and evolution of the cichlid mandible: The molecular basis of alternate feeding strategies. *Proc Natl Acad Sci U S A* **102**, 16287-16292.
- Alcaraz WA, Chen E Fau - Valdes P, Valdes P Fau - Kim E, *et al.* (2011) Modifier genes and non-genetic factors reshape anatomical deficits in Zfp423-deficient mice.
- Alibert P, Fel-Clair F, Manolakou K, Britton-Davidian J, Auffray JC (1997) Developmental Stability, Fitness, and Trait Size in Laboratory Hybrids Between European Subspecies of the House Mouse. *Evolution* **51**, 1284-1295.
- Alibert P, Renaud S, Dod B, Bonhomme F, Auffray JC (1994) Fluctuating Asymmetry in the Mus musculus Hybrid Zone: A Heterotic Effect in Disrupted Co-Adapted Genomes. *Proceedings: Biological Sciences* **258**, 53-59.
- Alonso CR, Wilkins AS (2005) The molecular elements that underlie developmental evolution. *Nat Rev Genet* **6**, 709-715.
- Alshbool FZ, Mohan S (2014) Emerging multifunctional roles of Claudin tight junction proteins in bone. *Endocrinology* **155**, 2363-2376.
- Atchley WR, Hall BK (1991) A model for development and evolution of complex morphological structures. *Biol Rev* **66**, 101-157.

- Atchley WR, Plummer AA, Riska B (1985) Genetics of mandible form in the mouse. *Genetics* **111**, 555-577.
- Attanasio C, Nord AS, Zhu Y, *et al.* (2013) Fine Tuning of Craniofacial Morphology by Distant-Acting Enhancers. *Science* **342**, 1241006.
- Auffray J-C, Britton-Davidian J (2012) The house mouse and its relatives. In: *Evolution of the House Mouse* (eds. Macholán M, Baird SJE, Munclinger P, Pialek J), pp. 1-34. Cambridge University Press.
- Auffray JC, Alibert P, Latieule C (1996a) Relative warp analysis of skull shape across the hybrid zone of the house mouse (*Mus musculus*) in Denmark. *Journal of Zoology* **240**, 441-455.
- Auffray JC, Alibert P, Latieule C, Dod B (1996b) Relative warp analysis of skull shape across the hybrid zone of the house mouse (*Mus musculus*) in Denmark. *Journal of Zoology* **240**, 441-455.
- Bader BL, Rayburn H, Crowley D, Hynes RO (1998) Extensive vasculogenesis, angiogenesis, and organogenesis precede lethality in mice lacking all alpha v integrins. *Cell* **95**, 507-519.
- Baird SJE, Macholán M (2012) What can the *Mus musculus musculus*/*M. m. domesticus* hybrid zone tell us about speciation? In: *Evolution of the House Mouse* (eds. Macholán M, Baird SJE, Munclinger P, Pialek J), pp. 334-372. Cambridge University Press, Cambridge.
- Baird SJE, Ribas A, Macholán M, *et al.* (2012) WHERE ARE THE WORMY MICE? A REEXAMINATION OF HYBRID PARASITISM IN THE EUROPEAN HOUSE MOUSE HYBRID ZONE. *Evolution* **66**, 2757-2772.
- Barrett RD, Hoekstra HE (2011) Molecular spandrels: tests of adaptation at the genetic level. *Nat Rev Genet* **12**, 767-780.
- Barton NH, Hewitt GM (1985) Analysis of Hybrid Zones. *Annual Review of Ecology and Systematics* **16**, 113-148.
- Basel D, Steiner RD (2009) Osteogenesis imperfecta: recent findings shed new light on this once well-understood condition. *Genet Med* **11**, 375-385.
- Beavis WD (1998) QTL analyses: power, precision, and accuracy. In: *Molecular Analysis of Complex Traits* (ed. Paterson A), pp. 145-161. CRC Press.
- Beraldi D, McRae AF, Gratten J, *et al.* (2007) Mapping quantitative trait loci underlying fitness-related traits in a free-living sheep population. *Evolution* **61**, 1403-1416.
- Béréños C, Ellis PA, Pilkington JG, *et al.* (2015) Heterogeneity of genetic architecture of body size traits in a free-living population. *Molecular Ecology*, n/a-n/a.
- Bimova BV, Macholan M, Baird SJE, *et al.* (2011) Reinforcement selection acting on the European house mouse hybrid zone. *Molecular Ecology* **20**, 2403-2424.
- Boehringer S, van der Lijn F, Liu F, *et al.* (2011) Genetic determination of human facial morphology: links between cleft-lips and normal variation. *Eur J Hum Genet* **19**, 1192-1197.
- Boell L (2013) Lines of least resistance and genetic architecture of house mouse (*Mus musculus*) mandible shape. *Evolution & Development* **15**, 197-204.

- Boell L, Gregorova S, Forejt J, Tautz D (2011) A comparative assessment of mandible shape in a consomic strain panel of the house mouse (*Mus musculus*)--implications for epistasis and evolvability of quantitative traits. *BMC Evol Biol* **11**, 309.
- Boell L, Pallares LF, Brodski C, *et al.* (2013) Exploring the effects of gene dosage on mandible shape in mice as a model for studying the genetic basis of natural variation. *Development Genes and Evolution* **223**, 279-287.
- Boell L, Tautz D (2011) Micro-evolutionary divergence patterns of mandible shapes in wild house mouse (*Mus musculus*) populations. *BMC Evol Biol* **11**.
- Bögel G, Gujdár A, Geiszt M, *et al.* (2012) Frank-ter Haar Syndrome Protein Tks4 Regulates Epidermal Growth Factor-dependent Cell Migration. *J Biol Chem* **287**, 31321-31329.
- Bonnard C, Strobl AC, Shboul M, *et al.* (2012) Mutations in IRX5 impair craniofacial development and germ cell migration via SDF1. *Nat Genet* **44**, 709-713.
- Bookstein F (1996) Biometrics, biomathematics and the morphometric synthesis. *Bulletin of Mathematical Biology* **58**, 313-365.
- Boyko AR, Quignon P, Li L, *et al.* (2010) A Simple Genetic Architecture Underlies Morphological Variation in Dogs. *PLoS Biol* **8**, e1000451.
- Breckpot J, Anderlid B-M, Alanay Y, *et al.* (2015) Chromosome 22q12.1 microdeletions: confirmation of the MN1 gene as a candidate gene for cleft palate. *Eur J Hum Genet.*
- Bromiley PA, Schunke AC, Ragheb H, Thacker NA, Tautz D (2014) Semi-automatic landmark point annotation for geometric morphometrics. *Frontiers in Zoology* **11**.
- Buerkle CA, Lexer C (2008) Admixture as the basis for genetic mapping. *Trends Ecol Evol* **23**, 686-694.
- Burgio G, Baylac M, Heyer E, Montagutelli X (2009) Genetic analysis of skull shape variation and morphological integration in the mouse using interspecific recombinant congenic strains between C57BL/6 and mice of the *Mus spretus* species. *Evolution* **63**, 2668-2686.
- Burgio G, Baylac M, Heyer E, Montagutelli X (2012a) Exploration of the Genetic Organization of Morphological Modularity on the Mouse Mandible Using a Set of Interspecific Recombinant Congenic Strains Between C57BL/6 and Mice of the *Mus spretus* Species. *G3* **2**, 1257-1268.
- Burgio G, Baylac M, Heyer E, Montagutelli X (2012b) Nasal Bone Shape Is under Complex Epistatic Genetic Control in Mouse Interspecific Recombinant Congenic Strains. *PLoS ONE* **7**, e37721.
- Burgio G, Szatanik M, Guenet JL, *et al.* (2007) Interspecific recombinant congenic strains between C57BL/6 and mice of the *Mus spretus* species: a powerful tool to dissect genetic control of complex traits. *Genetics* **177**, 2321-2333.
- Buschman MD, Bromann PA, Cejudo-Martin P, *et al.* (2009) The Novel Adaptor Protein Tks4 (SH3PXD2B) Is Required for Functional Podosome Formation. *Mol Biol Cell* **20**, 1302-1311.
- Candille SI, Raamsdonk CDV, Chen C, *et al.* (2004) Dorsoventral Patterning of the Mouse Coat by Tbx15. *PLoS Biol* **2**, e3.

- Carroll SB (2000) Endless Forms: The Evolution of Gene Regulation and Morphological Diversity. *Cell* **101**, 577-580.
- Carroll SB (2008) Evo-devo and an expanding evolutionary synthesis: a genetic theory of morphological evolution. *Cell* **134**, 25-36.
- Chen F, Guo R, Itoh S, *et al.* (2014) First mouse model for combined osteogenesis imperfecta and Ehlers-Danlos syndrome. *J Bone Miner Res* **29**, 1412-1423.
- Chen H, Ovchinnikov D, Pressman CL, *et al.* (1998) Multiple calvarial defects in *lmx1b* mutant mice. *Dev Genet* **22**, 314-320.
- Chen Z, Couble ML, Mouterfi N, Magloire H, Bleicher F (2009) Spatial and temporal expression of KLF4 and KLF5 during murine tooth development. *Arch Oral Biol* **54**, 403-411.
- Cheng LE, Reed RR (2007) *Zfp423/OAZ* participates in a developmental switch during olfactory neurogenesis. *Neuron* **54**, 547-557.
- Cheng R, Parker CC, Abney M, Palmer AA (2013) Practical Considerations Regarding the Use of Genotype and Pedigree Data to Model Relatedness in the Context of Genome-Wide Association Studies. *G3: Genes/Genomes/Genetics* **3**, 1861-1867.
- Cheung MS, Arponen H, Roughley P, *et al.* (2011) Cranial base abnormalities in osteogenesis imperfecta: phenotypic and genotypic determinants. *J Bone Miner Res* **26**, 405-413.
- Cheverud JM, Routman EJ, Irschick DJ (1997) Pleiotropic Effects of Individual Gene Loci on Mandibular Morphology. *Evolution* **51**, 2006-2016.
- Claes P, Liberton DK, Daniels K, *et al.* (2014) Modeling 3D Facial Shape from DNA. *PLoS Genet* **10**, e1004224.
- Cobrinik D, Lee M-H, Hannon G, *et al.* (1996) Shared role of the pRB-related p130 and p107 proteins in limb development. *Genes & Development* **10**, 1633-1644.
- Crisponi L, Deiana M, Loi A, *et al.* (2001) The putative forkhead transcription factor FOXL2 is mutated in blepharophimosis/ptosis/epicanthus inversus syndrome. *Nat Genet* **27**, 159-166.
- CTC (2004) The Collaborative Cross, a community resource for the genetic analysis of complex traits. *Nat Genet* **36**, 1133-1137.
- Curry GA (1959) Genetical and Developmental Studies on Droopy-eared Mice. *J Embryol exp Morph* **7**, 39-65.
- Dai JX, Johnson RL, Ding YQ (2009) Manifold functions of the Nail-Patella Syndrome gene *Lmx1b* in vertebrate development. *Dev Growth Differ* **51**, 241-250.
- Davidson TB, Sanchez-Lara PA, Randolph LM, *et al.* (2012) Microdeletion del(22)(q12.2) encompassing the facial development-associated gene, MN1 (meningioma 1) in a child with Pierre-Robin sequence (including cleft palate) and neurofibromatosis 2 (NF2): a case report and review of the literature. *BMC Med Genet* **13**, 19.
- Delous M, Baala L, Salomon R, *et al.* (2007) The ciliary gene *RPGRIP1L* is mutated in cerebello-oculorenal syndrome (Joubert syndrome type B) and Meckel syndrome. *Nat Genet* **39**, 875-881.

- Depew MJ, Simpson CA, Morasso M, Rubenstein JL (2005) Reassessing the Dlx code: the genetic regulation of branchial arch skeletal pattern and development. *J Anat* **207**, 501-561.
- Donnelly P (2008) Progress and challenges in genome-wide association studies in humans. *Nature* **456**, 728-731.
- Drake AG, Klingenberg CP (2008) The pace of morphological change: historical transformation of skull shape in St Bernard dogs. *Proceedings of the Royal Society B: Biological Sciences* **275**, 71-76.
- Duverger O, Isaac J, Zah A, *et al.* (2013) In vivo impact of Dlx3 conditional inactivation in neural crest-derived craniofacial bones. *J Cell Physiol* **228**, 654-664.
- Eppig JT, Blake JA, Bult CJ, Kadin JA, Richardson JE (2012) The Mouse Genome Database (MGD): comprehensive resource for genetics and genomics of the laboratory mouse. *Nucleic Acids Res* **40**, D881-886.
- Eppig JT, Blake JA, Bult CJ, Kadin JA, Richardson JE (2015) The Mouse Genome Database (MGD): facilitating mouse as a model for human biology and disease. *Nucleic Acids Res* **43**, D726-736.
- Fisher R (1930) *The Genetical Theory of Natural Selection* Oxford University Press, Oxford.
- Flint J, Eskin E (2012) Genome-wide association studies in mice. *Nat Rev Genet* **13**, 807-817.
- Fondon JW, 3rd, Garner HR (2004) Molecular origins of rapid and continuous morphological evolution. *Proc Natl Acad Sci U S A* **101**, 18058-18063.
- Franz-Odenaal TA (2011) Induction and patterning of intramembranous bone. *Front Biosci (Landmark Ed)* **16**, 2734-2746.
- Gans C, Northcutt RG (1983) Neural crest and the origin of vertebrates: a new head. *Science* **220**, 268-273.
- Gay L, Crochet PA, Bell DA, Lenormand T (2008) Comparing clines on molecular and phenotypic traits in hybrid zones: a window on tension zone models. *Evolution* **62**, 2789-2806.
- Gerasimov S, Nikolov H, Mihailova V, Auffray J-C, Bonhomme F (1990) Morphometric stepwise discriminant analysis of the five genetically determined European taxa of the genus *Mus*. *Biological Journal of the Linnean Society* **41**, 47-64.
- Gompel N, Prud'homme B (2009) The causes of repeated genetic evolution. *Developmental Biology* **332**, 36-47.
- Green SA, Simoes-Costa M, Bronner ME (2015) Evolution of vertebrates as viewed from the crest. *Nature* **520**, 474-482.
- Hadjidakis DJ, Androulakis, II (2006) Bone remodeling. *Ann N Y Acad Sci* **1092**, 385-396.
- Hardouin EA, Orth A, Teschke M, *et al.* (2015) Eurasian house mouse (*Mus musculus* L.) differentiation at microsatellite loci identifies the Iranian plateau as a phylogeographic hotspot. *BMC Evol Biol* **15**.

- Hay E, Laplantine E, Geoffroy V, *et al.* (2009) N-cadherin interacts with axin and LRP5 to negatively regulate Wnt/beta-catenin signaling, osteoblast function, and bone formation. *Mol Cell Biol* **29**, 953-964.
- Helms JA, Schneider RA (2003) Cranial skeletal biology. *Nature* **423**, 326-331.
- Herring SW (1993) Epigenetic and functional influences on skull growth. In: *The Skull, Volume 1: Development* (eds. Hanken J, Hall BK). University of Chicago Press.
- Heude E, Bellessort B, Fontaine A, *et al.* (2015) Etiology of craniofacial malformations in mouse models of blepharophimosis, ptosis and epicanthus inversus syndrome. *Hum Mol Genet* **24**, 1670-1681.
- Hoekstra HE, Coyne JA (2007) The locus of evolution: evo devo and the genetics of adaptation. *Evolution* **61**, 995-1016.
- Howie BN, Donnelly P, Marchini J (2009) A Flexible and Accurate Genotype Imputation Method for the Next Generation of Genome-Wide Association Studies. *PLoS Genet* **5**, e1000529.
- Hu Z, Yu M, Hu G (2007) NDST-1 modulates BMPR and PTHrP signaling during endochondral bone formation in a gene knockout model. *Bone* **40**, 1462-1474.
- Inman KE, Purcell P, Kume T, Trainor PA (2013) Interaction between Foxc1 and Fgf8 during mammalian jaw patterning and in the pathogenesis of syngnathia. *PLoS Genet* **9**, e1003949.
- Iqbal Z, Cejudo-Martin P, Brouwer Ad, *et al.* (2010) Disruption of the Podosome Adaptor Protein TKS4 (SH3PXD2B) Causes the Skeletal Dysplasia, Eye, and Cardiac Abnormalities of Frank-Ter Haar Syndrome. *The American Journal of Human Genetics* **86**, 254-261.
- Isaac J, Erthal J, Gordon J, *et al.* (2014) DLX3 regulates bone mass by targeting genes supporting osteoblast differentiation and mineral homeostasis in vivo. *Cell Death Differ* **21**, 1365-1376.
- Itoh M, Yoshida Y, Nishida K, *et al.* (2000) Role of Gab1 in heart, placenta, and skin development and growth factor- and cytokine-induced extracellular signal-regulated kinase mitogen-activated protein kinase activation. *Mol Cell Biol* **20**, 3695-3704.
- Jacob F, Monod J (1961) Genetic regulatory mechanisms in the synthesis of proteins. *J Mol Biol* **3**, 318-356.
- Jamniczky H, Campeau S, Barry T, Skelton J, Rogers S (2015) Three-Dimensional Morphometrics for Quantitative Trait Locus Analysis: Tackling Complex Questions with Complex Phenotypes. *Evolutionary Biology*, 1-12.
- Jaubert J, Jaubert F, Martin N, *et al.* (1999) Three new allelic mouse mutations that cause skeletal overgrowth involve the natriuretic peptide receptor C gene (Npr3). *Proc Natl Acad Sci U S A* **96**, 10278-10283.
- Jin W, Chang M, Paul EM, *et al.* (2008) Deubiquitinating enzyme CYLD negatively regulates RANK signaling and osteoclastogenesis in mice. *J Clin Invest* **118**, 1858-1866.
- Karolchik D, Barber GP, Casper J, *et al.* (2014) The UCSC Genome Browser database: 2014 update. *Nucleic Acids Res* **42**, D764-770.

- Kaufman MH, Bard J (1999) *The Anatomical Basis of Mouse Development* Academic Press.
- Kawatani M, Okumura H, Honda K, *et al.* (2008) The identification of an osteoclastogenesis inhibitor through the inhibition of glyoxalase I. *Proc Natl Acad Sci U S A* **105**, 11691-11696.
- Keane TM, Goodstadt L, Danecek P, *et al.* (2011) Mouse genomic variation and its effect on phenotypes and gene regulation. *Nature* **477**, 289-294.
- Kendall DG (1977) The diffusion of shape. *Advances in Applied Probability* **9**, 428-430.
- Kent WJ, Sugnet CW, Furey TS, *et al.* (2002) The human genome browser at UCSC. *Genome Res* **12**, 996-1006.
- Kim H-J, Im S-W, Jargal G, *et al.* (2013) Heritabilities of Facial Measurements and Their Latent Factors in Korean Families. *Genomics & Informatics* **11**, 83-92.
- Kimmel CB, Ullmann B, Walker C, *et al.* (2005) Evolution and development of facial bone morphology in threespine sticklebacks. *Proc Natl Acad Sci U S A* **102**, 5791-5796.
- Kimura M (1983) *The Neutral Theory of Molecular Evolution* Cambridge University Press, Cambridge.
- King MC, Wilson AC (1975) Evolution at two levels in humans and chimpanzees. *Science* **188**, 107-116.
- Klingenberg CP (2010) Evolution and development of shape: integrating quantitative approaches. *Nat Rev Genet* **11**, 623-635.
- Klingenberg CP (2011) MorphoJ: an integrated software package for geometric morphometrics. *Molecular Ecology Resources* **11**, 353-357.
- Klingenberg CP (2015) Analyzing Fluctuating Asymmetry with Geometric Morphometrics: Concepts, Methods, and Applications. *Symmetry* **7**, 843-934.
- Klingenberg CP, Barluenga M, Meyer A (2002) Shape analysis of symmetric structures: quantifying variation among individuals and asymmetry. *Evolution* **56**, 1909-1920.
- Klingenberg CP, Leamy LJ (2001) Quantitative genetics of geometric shape in the mouse mandible. *Evolution* **55**, 2342-2352.
- Klingenberg CP, Leamy LJ, Cheverud JM (2004) Integration and modularity of quantitative trait locus effects on geometric shape in the mouse mandible. *Genetics* **166**, 1909-1921.
- Klingenberg CP, Leamy LJ, Routman EJ, Cheverud JM (2001) Genetic architecture of mandible shape in mice: effects of quantitative trait loci analyzed by geometric morphometrics. *Genetics* **157**, 785-802.
- Klingenberg CP, Navarro N (2012) Development of the mouse mandible. In: *Evolution of the House Mouse* (eds. Macholán M, Baird SJE, Munclinger P, Pialek J), pp. 135-149. Cambridge University Press, Cambridge.
- Koyabu D, Werneburg I, Morimoto N, *et al.* (2014) Mammalian skull heterochrony reveals modular evolution and a link between cranial development and brain size. *Nat Commun* **5**, 3625.

- Kume T, Deng KY, Winfrey V, *et al.* (1998) The forkhead/winged helix gene *Mf1* is disrupted in the pleiotropic mouse mutation congenital hydrocephalus. *Cell* **93**, 985-996.
- Lamichhaney S, Berglund J, Almen MS, *et al.* (2015) Evolution of Darwin's finches and their beaks revealed by genome sequencing. *Nature* **518**, 371-375.
- Lango Allen H, Estrada K, Lettre G, *et al.* (2010) Hundreds of variants clustered in genomic loci and biological pathways affect human height. *Nature* **467**, 832-838.
- Latour Y, Perriat-Sanguinet M, Caminade P, *et al.* (2013) Sexual selection against natural hybrids may contribute to reinforcement in a house mouse hybrid zone. *Proceedings of the Royal Society of London B: Biological Sciences* **281**.
- Laurie CC, Nickerson DA, Anderson AD, *et al.* (2007) Linkage Disequilibrium in Wild Mice. *PLoS Genet* **3**, 1487-1495.
- Lausch E, Hermanns P, Farin HF, *et al.* (2008) *TBX15* Mutations Cause Craniofacial Dysmorphism, Hypoplasia of Scapula and Pelvis, and Short Stature in Cousin Syndrome. *The American Journal of Human Genetics* **83**, 649-655.
- Leamy LJ, Klingenberg CP, Sherratt E, Wolf JB, Cheverud JM (2008) A search for quantitative trait loci exhibiting imprinting effects on mouse mandible size and shape. *Heredity* **101**, 518-526.
- Leamy LJ, Pomp D, Eisen EJ, Cheverud JM (2000) Quantitative trait loci for directional but not fluctuating asymmetry of mandible characters in mice. *Genet Res Camb* **76**, 27-40.
- Leamy LJ, Routman EJ, Cheverud JM (1997) A Search for Quantitative Trait Loci Affecting Asymmetry of Mandibular Characters in Mice. *Evolution* **51**, 957-969.
- Leamy LJ, Routman EJ, Cheverud JM (1999) Quantitative trait loci for early- and late-development skull characters in mice: a test of the genetic independence model of morphological integration. *Am Nat* **153**, 201-214.
- Lekanne Deprez RH, Riegman PH, Groen NA, *et al.* (1995) Cloning and characterization of *MN1*, a gene from chromosome 22q11, which is disrupted by a balanced translocation in a meningioma. *Oncogene* **10**, 1521-1528.
- Li H, Durbin R (2009) Fast and accurate short read alignment with Burrows-Wheeler transform. *Bioinformatics* **25**, 1754-1760.
- Linares GR, Brommage R, Powell DR, *et al.* (2012) *Claudin 18* is a novel negative regulator of bone resorption and osteoclast differentiation. *J Bone Miner Res* **27**, 1553-1565.
- Listgarten J, Lippert C, Kadie CM, *et al.* (2012) Improved linear mixed models for genome-wide association studies. *Nat Meth* **9**, 525-526.
- Liu F, van der Lijn F, Schurmann C, *et al.* (2012) A genome-wide association study identifies five loci influencing facial morphology in Europeans. *PLoS Genet* **8**, e1002932.
- Long F, Ornitz DM (2013) Development of the endochondral skeleton. *Cold Spring Harb Perspect Biol* **5**, a008334.

- Macholán M (2006) A geometric morphometric analysis of the shape of the first upper molar in mice of the genus *Mus* (Muridae, Rodentia). *Journal of Zoology* **270**, 672-681.
- Maga AM, Navarro N, Cunningham ML, Cox TC (2015) Quantitative trait loci affecting the 3D skull shape and size in mouse and prioritization of candidate genes in-silico. *Front Physiol* **6**, 92.
- Mallarino R, Abzhanov A (2012) Paths less traveled: evo-devo approaches to investigating animal morphological evolution. *Annu Rev Cell Dev Biol* **28**, 743-763.
- Mao M, Thedens DR, Chang B, *et al.* (2009) The podosomal-adaptor protein SH3PXD2B is essential for normal postnatal development. *Mamm Genome* **20**, 462-475.
- Mardia KV, Bookstein FL, Moreton IJ (2000) Statistical assessment of bilateral symmetry of shapes. *Biometrika* **87**, 285-300.
- Marie PJ, Hay E (2013) Cadherins and Wnt signalling: a functional link controlling bone formation. *Bonekey Rep* **2**, 330.
- Martin A, Orgogozo V (2013) The Loci of repeated evolution: a catalog of genetic hotspots of phenotypic variation. *Evolution* **67**, 1235-1250.
- Martínez-Abadías N, Esparza M, Sjøvold T, *et al.* (2009) Heritability of human cranial dimensions: comparing the evolvability of different cranial regions. *Journal of Anatomy* **214**, 19-35.
- Masserdotti G, Badaloni A, Green YS, *et al.* (2010) ZFP423 coordinates Notch and bone morphogenetic protein signaling, selectively up-regulating *Hes5* gene expression. *J Biol Chem* **285**, 30814-30824.
- McKenna A, Hanna M, Banks E, *et al.* (2010) The Genome Analysis Toolkit: a MapReduce framework for analyzing next-generation DNA sequencing data. *Genome Res* **20**, 1297-1303.
- Mears AJ, Jordan T, Mirzayans F, *et al.* (1998) Mutations of the forkhead/winged-helix gene, *FKHL7*, in patients with Axenfeld-Rieger anomaly. *Am J Hum Genet* **63**, 1316-1328.
- Meester-Smoor MA, Vermeij M, van Helmond MJ, *et al.* (2005) Targeted disruption of the *Mn1* oncogene results in severe defects in development of membranous bones of the cranial skeleton. *Mol Cell Biol* **25**, 4229-4236.
- Mikula O, Auffray J-C, Macholan M (2010a) Asymmetric size and shape variation in the Central European transect across the house mouse hybrid zone. *Biological Journal of the Linnean Society* **101**, 13-27.
- Mikula O, Auffray JC, Macholan M (2010b) Asymmetric size and shape variation in the Central European transect across the house mouse hybrid zone. *Biological Journal of the Linnean Society* **101**, 13-27.
- Mikula O, Macholán M (2008) There is no heterotic effect upon developmental stability in the ventral side of the skull within the house mouse hybrid zone. *Journal of Evolutionary Biology* **21**, 1055-1067.
- Mirzayans F, Lavy R, Penner-Chea J, Berry FB (2012) Initiation of Early Osteoblast Differentiation Events through the Direct Transcriptional Regulation of *Msx2* by *FOXC1*. *PLoS ONE* **7**.

- Mitteroecker P, Gunz P (2009) Advances in Geometric Morphometrics. *Evolutionary Biology* **36**, 235-247.
- Moller AP (1997) Developmental stability and fitness: a review. *Am Nat* **149**, 916-932.
- Muller GB, Newman SA (2003) Origination of organismal form: The forgotten cause in evolutionary biology. In: *Origination of organismal form: beyond the gene in developmental and evolutionary biology* (eds. Muller GB, Newman SA), pp. 3-10. MIT Press.
- Nunes MDS, Arif S, Schlotterer C, McGregor AP (2013) A Perspective on Micro-Evo-Devo: Progress and Potential. *Genetics* **195**, 625-634.
- Orr HA (1998) The population genetics of adaptation : the distribution of factors fixed during adaptive evolution. *Evolution* **52**, 935-949.
- Orr HA (2005a) The genetic theory of adaptation: a brief history. *Nat Rev Genet* **6**, 119-127.
- Orr HA (2005b) The genetic theory of adaptation: a brief history. *Nat Rev Genet* **6**, 119-127.
- Orr HA, Coyne JA (1992) The genetics of adaptation: a reassessment. *Am Nat* **140**, 725-742.
- Pallares LF, Harr B, Turner LM, Tautz D (2014) Use of a natural hybrid zone for genomewide association mapping of craniofacial traits in the house mouse. *Molecular Ecology* **23**, 5756-5770.
- Pallerla SR, Pan Y, Zhang X, Esko JD, Grobe K (2007) Heparan sulfate Ndst1 gene function variably regulates multiple signaling pathways during mouse development. *Developmental Dynamics* **236**, 556-563.
- Parker CC, Carbonetto P, Sokoloff G, *et al.* (2014) High-Resolution Genetic Mapping of Complex Traits from a Combined Analysis of F2 and Advanced Intercross Mice. *Genetics* **198**, 103-116.
- Paternoster L, Zhurov AI, Toma AM, *et al.* (2012) Genome-wide association study of three-dimensional facial morphology identifies a variant in PAX3 associated with nasion position. *Am J Hum Genet* **90**, 478-485.
- Pavlos NJ, Xu J, Papadimitriou JM, Zheng MH (2001) Molecular cloning of the mouse homologue of Rab3c. *J Mol Endocrinol* **27**, 117-122.
- Payseur BA, Krenz JG, Nachman MW (2004) Differential patterns of introgression across the X chromosome in a hybrid zone between two species of house mice. *Evolution* **58**, 2064-2078.
- Peake NJ, Hobbs AJ, Pinguan-Murphy B, *et al.* (2014) Role of C-type natriuretic peptide signalling in maintaining cartilage and bone function. *Osteoarthritis Cartilage* **22**, 1800-1807.
- Pejchalova K, Krejci P, Wilcox WR (2007) C-natriuretic peptide: an important regulator of cartilage. *Mol Genet Metab* **92**, 210-215.
- Peters T, Ausmeier K, Dildrop R, Ruther U (2002) The mouse Fused toes (Ft) mutation is the result of a 1.6-Mb deletion including the entire Iroquois B gene cluster. *Mamm Genome* **13**, 186-188.
- Poissant J, Davis CS, Malenfant RM, Hogg JT, Coltman DW (2012) QTL mapping for sexually dimorphic fitness-related traits in wild bighorn sheep. *Heredity* **108**, 256-263.

- Price JA, Bowden DW, Wright JT, Pettenati MJ, Hart TC (1998) Identification of a mutation in DLX3 associated with tricho-dento-osseous (TDO) syndrome. *Hum Mol Genet* **7**, 563-569.
- Purcell S, Neale B, Todd-Brown K, *et al.* (2007) PLINK: a toolset for whole-genome association and population-based linkage analysis. *American Journal of Human Genetics* **81**, 559-575.
- R-Core-Team (2013) R: A language and environment for statistical computing. R Foundation for Statistical Computing, Vienna, Austria, Vienna, Austria.
- Raggatt LJ, Partridge NC (2010) Cellular and molecular mechanisms of bone remodeling. *J Biol Chem* **285**, 25103-25108.
- Renaud S, Alibert P, Auffray JC (2009) Mandible shape in hybrid mice. *Naturwissenschaften* **96**, 1043-1050.
- Renaud S, Alibert P, Auffray JC (2012) Modularity as a source of new morphological variation in the mandible of hybrid mice. *BMC Evol Biol* **12**, 141.
- Renaud S, Auffray JC (2010) Adaptation and plasticity in insular evolution of the house mouse mandible. *Journal of Zoological Systematics and Evolutionary Research* **48**, 138-150.
- Renaud S, Auffray JC, de la Porte S (2010) Epigenetic effects on the mouse mandible: common features and discrepancies in remodeling due to muscular dystrophy and response to food consistency. *BMC Evol Biol* **10**, 28.
- Reyment RA (1996) An idiosyncratic history of early morphometrics. In: *Advances in Morphometrics* (eds. Marcus LF, Corti M, Loy A, Naylor GJP, Slice DE). Plenum Press, New York.
- Rice R, Rice DPC, Olsen BR, Thesleff I (2003) Progression of calvarial bone development requires Foxc1 regulation of Msx2 and Alx4. *Developmental Biology* **262**, 75-87.
- Rieseberg LH, Buerkle CA (2002) Genetic mapping in hybrid zones. *Am Nat* **159 Suppl 3**, S36-50.
- Robinson MR, Santure AW, Decauwer I, Sheldon BC, Slate J (2013) Partitioning of genetic variation across the genome using multimarker methods in a wild bird population. *Mol Ecol* **22**, 3963-3980.
- Rockman MV (2012) The QTN program and the alleles that matter for evolution: all that's gold does not glitter. *Evolution* **66**, 1-17.
- Rohlf FJ, Marcus LF (1993) A revolution in morphometrics. *Trends Ecol Evol* **8**, 129-132.
- Santagati F, Rijli FM (2003) Cranial neural crest and the building of the vertebrate head. *Nat Rev Neurosci* **4**, 806-818.
- Schielzeth H, Husby A (2014) Challenges and prospects in genome-wide quantitative trait loci mapping of standing genetic variation in natural populations. *Annals of the New York Academy of Sciences* **1320**, 35-57.
- Schoenebeck JJ, Hutchinson SA, Byers A, *et al.* (2012) Variation of BMP3 Contributes to Dog Breed Skull Diversity. *PLoS Genet* **8**, e1002849.

- Schoenebeck JJ, Ostrander EA (2013) The Genetics of Canine Skull Shape Variation. *Genetics* **193**, 317-+.
- Schunke A, Bromiley P, Tautz D, Thacker N (2012) TINA manual landmarking tool: software for the precise digitization of 3D landmarks. *Frontiers in Zoology* **9**, 6.
- Shi F, Ding S, Zhao S, *et al.* (2014) A piggyBac insertion disrupts Foxl2 expression that mimics BPES syndrome in mice. *Hum Mol Genet* **23**, 3792-3800.
- Shimeld SM, Holland PW (2000) Vertebrate innovations. *Proc Natl Acad Sci U S A* **97**, 4449-4452.
- Shur I, Socher R, Benayahu D (2006) In vivo association of CREMM/CHD9 with promoters in osteogenic cells. *J Cell Physiol* **207**, 374-378.
- Siahsarvie R, Auffray J-C, Darvish J, *et al.* (2012) Patterns of morphological evolution in the mandible of the house mouse *Mus musculus* (Rodentia: Muridae). *Biological Journal of the Linnean Society* **105**, 635-647.
- Singh MK, Petry M, Haenig B, *et al.* (2005) The T-box transcription factor Tbx15 is required for skeletal development. *Mech Dev* **122**, 131-144.
- Slate J (2005) Quantitative trait locus mapping in natural populations: progress, caveats and future directions. *Molecular Ecology* **14**, 363-379.
- Slate J (2013) From Beavis to beak color: a simulation study to examine how much QTL mapping can reveal about the genetic architecture of quantitative traits. *Evolution* **67**, 1251-1262.
- Slate J, Visscher PM, MacGregor S, *et al.* (2002) A genome scan for quantitative trait loci in a wild population of red deer (*Cervus elaphus*). *Genetics* **162**, 1863-1873.
- Stern DL (2000) Perspective: Evolutionary developmental biology and the problem of variation. *Evolution* **54**, 1079-1091.
- Stern DL (2013) The genetic causes of convergent evolution. *Nat Rev Genet* **14**, 751-764.
- Stern DL, Orgogozo V (2008) The loci of evolution: how predictable is genetic evolution? *Evolution* **62**, 2155-2177.
- Stern DL, Orgogozo V (2009) Is Genetic Evolution Predictable? *Science* **323**, 746-751.
- Stratakis CA, Lafferty A, Susan E. Taymans, *et al.* (2000) Anisomastia Associated with Interstitial Duplication of Chromosome 16, Mental Retardation, Obesity, Dysmorphic Facies, and Digital Anomalies: Molecular Mapping of a New Syndrome by Fluorescent in Situ Hybridization and Microsatellites to 16q13 (D16S419-D16S503). *The Journal of Clinical Endocrinology & Metabolism* **85**, 3396-3401.
- Sun J, Ishii M, Ting MC, Maxson R (2013) Foxc1 controls the growth of the murine frontal bone rudiment by direct regulation of a Bmp response threshold of Msx2. *Development* **140**, 1034-1044.
- Sur I, Rozell B, Jaks V, Bergstrom A, Toftgard R (2006) Epidermal and craniofacial defects in mice overexpressing Klf5 in the basal layer of the epidermis. *J Cell Sci* **119**, 3593-3601.

- Sutton AL, Zhang X, Ellison TI, Macdonald PN (2005) The 1,25(OH)₂D₃-regulated transcription factor MN1 stimulates vitamin D receptor-mediated transcription and inhibits osteoblastic cell proliferation. *Mol Endocrinol* **19**, 2234-2244.
- Tautz D, Domazet-Loso T (2011) The evolutionary origin of orphan genes. *Nat Rev Genet* **12**, 692-702.
- Teeter KC, Payseur BA, Harris LW, *et al.* (2008) Genome-wide patterns of gene flow across a house mouse hybrid zone. *Genome Res* **18**, 67-76.
- Thorogood P (1993) Differentiation and morphogenesis of cranial skeletal tissues. In: *The Skull, Volume 1: Development* (eds. Hanken J, Hall BK). University of Chicago Press.
- Turner LM, Harr B (2014) Genome-wide mapping in a house mouse hybrid zone reveals hybrid sterility loci and Dobzhansky-Muller interactions. *Elife* **3**.
- Turner LM, Schwahn DJ, Harr B (2012) Reduced male fertility is common but highly variable in form and severity in a natural house mouse hybrid zone. *Evolution* **66**, 443-458.
- Van der Auwera GA, Carneiro MO, Hartl C, *et al.* (2013) From FastQ data to high confidence variant calls: the Genome Analysis Toolkit best practices pipeline. *Curr Protoc Bioinformatics* **11**, 10 11-11 10 33.
- Vierkotten J, Dildrop R, Peters T, Wang B, Ruther U (2007) Ftm is a novel basal body protein of cilia involved in Shh signalling. *Development* **134**, 2569-2577.
- Visscher PM (2008) Sizing up human height variation. *Nat Genet* **40**, 489-490.
- Wang J, Kalyan S, Steck N, *et al.* (2015) Analysis of intestinal microbiota in hybrid house mice reveals evolutionary divergence in a vertebrate hologenome. *Nat Commun* **6**, 6440.
- Weng TJ, Mao FF, Wang YL, *et al.* (2010) Osteoblastic molecular scaffold Gab1 is required for maintaining bone homeostasis. *J Cell Sci* **123**, 682-689.
- Wilkie AOM, Morris-Kay GM (2001) Genetics of craniofacial development and malformation. *Nat Genet* **2**, 458-468.
- Wilson GR, Sunley J, Smith KR, *et al.* (2014) Mutations in SH3PXD2B cause Borrone dermatocardio-skeletal syndrome. *Eur J Hum Genet* **22**, 741-747.
- Wolf JB, Leamy LJ, Routman EJ, Cheverud JM (2005) Epistatic pleiotropy and the genetic architecture of covariation within early and late-developing skull trait complexes in mice. *Genetics* **171**, 683-694.
- Wongdee K, Pandaranandaka J, Teerapornpuntakit J, *et al.* (2008) Osteoblasts express claudins and tight junction-associated proteins. *Histochem Cell Biol* **130**, 79-90.
- Wood AR, Esko T, Yang J, *et al.* (2014) Defining the role of common variation in the genomic and biological architecture of adult human height. *Nat Genet* **46**, 1173-1186.
- Wray GA (2007) The evolutionary significance of cis-regulatory mutations. *Nat Rev Genet* **8**, 206-216.

- Wray NR, Yang J, Hayes BJ, *et al.* (2013) Pitfalls of predicting complex traits from SNPs. *Nature reviews. Genetics* **14**, 507-515.
- Yalcin B, Nicod J, Bhomra A, *et al.* (2010) Commercially Available Outbred Mice for Genome-Wide Association Studies. *PLoS Genet* **6**, e1001085.
- Yang B, Tian C, Zhang ZG, *et al.* (2011a) Sh3pxd2b mice are a model for craniofacial dysmorphology and otitis media. *PLoS ONE* **6**, e22622.
- Yang H, Ding Y, Hutchins LN, *et al.* (2009) A customized and versatile high-density genotyping array for the mouse. *Nat Methods* **6**, 663-666.
- Yang H, Wang JR, Didion JP, *et al.* (2011b) Subspecific origin and haplotype diversity in the laboratory mouse. *Nat Genet* **43**, 648-655.
- Yang J, Benyamin B, McEvoy BP, *et al.* (2010) Common SNPs explain a large proportion of the heritability for human height. *Nat Genet* **42**, 565-569.
- Yang J, Lee SH, Goddard ME, Visscher PM (2011c) GCTA: a tool for genome-wide complex trait analysis. *Am J Hum Genet* **88**, 76-82.
- Yang J, Manolio TA, Pasquale LR, *et al.* (2011d) Genome partitioning of genetic variation for complex traits using common SNPs. *Nat Genet* **43**, 519-525.
- Zelditch ML, Swiderski DL, Sheets HD (2012) *Geometric Morphometrics for Biologists: A Primer* Elsevier Academic Press, New York, USA.
- Zhang B, Zhang Z, Xia S, *et al.* (2013) KLF5 activates microRNA 200 transcription to maintain epithelial characteristics and prevent induced epithelial-mesenchymal transition in epithelial cells. *Mol Cell Biol* **33**, 4919-4935.
- Zhang S, Cagatay T, Amanai M, *et al.* (2007) Viable mice with compound mutations in the Wnt/Dvl pathway antagonists nkd1 and nkd2. *Mol Cell Biol* **27**, 4454-4464.
- Zhang X, Dowd DR, Moore MC, *et al.* (2009) Meningioma 1 is required for appropriate osteoblast proliferation, motility, differentiation, and function. *J Biol Chem* **284**, 18174-18183.
- Zhao H, Ross FP, Teitelbaum SL (2005) Unoccupied alpha(v)beta3 integrin regulates osteoclast apoptosis by transmitting a positive death signal. *Mol Endocrinol* **19**, 771-780.
- Zhou X, Carbonetto P, Stephens M (2013) Polygenic Modeling with Bayesian Sparse Linear Mixed Models. *PLoS Genet* **9**, e1003264.
- Zhou X, Stephens M (2012) Genome-wide efficient mixed-model analysis for association studies. *Nat Genet* **44**, 821-824.

Curriculum Vitae

| | |
|--------------------------------|--|
| Name | Luisa Fernanda Pallares Amaya |
| Date and place of birth | 22.08.1988 / Ocana, Colombia |
| Nationality | Colombian |
| Place of residence | Rautenbergstraße 55, 24306 Plön, Germany |
| Civil status | Single |
| Education | |
| 1994 –1998 | Primary School Escuela Normal Superior Ocana, Colombia |
| 1999 – 2004 | High School Colegio Nacional Jose Eusebio Caro Ocana, Colombia |
| 2005 – 2009 | Bachelor of Sciences in Biology National University of Colombia Bogota, Colombia |
| 2010 – Aug 2011 | Researcher Evolutionary Ecology Group National University of Colombia Bogota, Colombia |
| Sep 2011 – Dec 2011 | IMPRS rotation period Max Planck Institute for Evolutionary Biology Christian-Albrecht-University of Kiel Plön and Kiel, Germany |
| Since January 2012 | Doctoral Studies Max Planck Institute for Evolutionary Biology Department of Evolutionary Genetics IMPRS for Evolutionary Biology Christian-Albrecht-University of Kiel Plön, Germany |
| Stipends / Awards | |
| 2012 – today | Scholarship for doctoral studies. Awarded by International Max Planck Research School for evolutionary biology –IMPRS |
| 2011 | Young Researcher Grant Awarded by COLCIENCIAS –Colombian Administrative Department of Science, Technology and Innovation |

Affidavit

Hiermit erkläre ich, dass die vorliegende Arbeit

- nach Inhalt und Form meine eigene ist, abgesehen von der Beratung durch meinen Betreuer Prof. Diethard Tautz
- an keiner anderen Stelle im Rahmen eines Prüfungsverfahrens vorgelegen hat, noch nicht veröffentlicht ist und auch nicht zur Veröffentlichung eingereicht wurde
- unter Einhaltung der Regeln guter wissenschaftlicher Praxis der Deutschen Forschungsgemeinschaft entstanden ist.

Plön, den 18.06.2014

Luisa Fernanda Pallares Amaya

